COMPREHENSIVE LIPID PROFILING OF GLIOMA AND BRAIN AROUND TUMOR HETEROGENEITY BY MRM-MS FOR THERAPEUTIC TARGET IDENTIFICATION

by

Stephen Miloro

A Dissertation

Submitted to the Faculty of Purdue University

In Partial Fulfillment of the Requirements for the degree of

Doctor of Philosophy

Department of Agricultural and Biological Engineering

West Lafayette, Indiana

May 2020

THE PURDUE UNIVERSITY GRADUATE SCHOOL
STATEMENT OF COMMITTEE APPROVAL

Dr. Kari Clase, Co-Chair

Department of Agricultural and Biological Engineering

Dr. Jenna Rickus, Co-Chair

Department of Agricultural and Biological Engineering

Dr. Christina Ferreira

Metabolite Profiling Facility, Bindley Bioscience Center

Dr. Emily Dykhuizen

Department of Medicinal Chemistry and Molecular Pharmacology

Dr. Susan Mendrysa

Department of Basic Medical Sciences

Approved by:

Dr. Nathan Mosier

First and foremost, I would like to dedicate this dissertation to my family. My mom Bernadette Miloro, my Dad Stephen Miloro, my brother and sister Andrew and Kristen Miloro, my Uncle Salvatore DiSanto, my Aunt and Uncle Gloria and Ralph D'Ottavio, my Aunt Kimberly Aylward, my Aunt Andrea Miloro, and my Nana Kathleen Miloro. Your continued love and support saw me through this tough Ph.D. journey, and I could not have done it without you.

Second, I would like to dedicate this dissertation to my friends (Cynthia Alvarado, Nicole Vike, Katherine Wehde, Priya Prakash, Kathryn Jacobson, and Ethan Hillman) -You all are my Purdue family and I could not have accomplished this without all of your support.

A special dedication to my grandparents Yolanda (1929-2014) and Ralph D'Ottavio (1931-2010), I could feel your unconditional love around me each day during my Ph.D. journey.

Another special dedication to Dr. Carol Kruse (1953-2015), my mentor prior to coming to Purdue. Your investment in me inspired me to pursue my PhD studying brain cancer and I could not have made it this far without your help. Hope I made you proud.

Lastly, I would like to dedicate this work to my colleagues (Ikenna Okekeogbu, Soo Ha, Yi Li, Rachel Morrison, James Nolan, Mian Yang, Francesca Whitt, Gillian Smith, Emily Kerstiens, Mercy Okezue, and Abigail Ekeigwe). Your encouragement and support throughout made this possible.

ACKNOWLEDGMENTS

First, I would like to acknowledge my committee members (Dr. Kari Clase, Dr. Jenna Rickus, Dr. Christina Ferreira, Dr. Susan Mendrysa, and Dr. Emily Dykhuizen) for their expertise, guidance, and investment throughout my PhD journey. Next, I would like to acknowledge the Agricultural and Biological Engineering Department for your support throughout my time at Purdue. Third, I would like to acknowledge the Biotechnology Innovation Regulatory Science (BIRS) Center for providing funding for my project. Fourth, I would like to acknowledge each of the facilities, cores, and individuals that made major contributions to my project. The Bindley Bioscience Center for providing a space and housing facilities to conduct my lipidomics experiments. The Bindley Metabolomics Core, especially Dr. Christina Ferreira, for their pivotal collaboration and expertise performing lipidomics analysis. The Birck Nanotechnology Center, especially Dr. Tim Kwok, for your insight and guidance using laser capture microdissection technology. I would like to acknowledge three individuals from the Histology Research Laboratory; Victor Bernal-Crespo for his assistance sectioning, staining, and scanning glioma samples, Dr. Agnes Wong for her support tracing and localizing tumor in sectioned tissue, and Dr. Tiffany Lyle for her expertise in histology, which was a vital component, and investment to the project. Lastly, I would like to acknowledge the Indiana University Simon Cancer Tumor bank for providing the human glioma samples analyzed in this project.

TABLE OF CONTENTS

LIST OF TABLES

LIST OF FIGURES

ABSTRACT

Glioma is the most common and deadliest form of brain cancer. The highly aggressive nature of this disease drives progression toward malignancy and patient overall survival average between 12-15 months. Standard treatment protocol has minimally changed over the last decade, consisting of resection surgery, radiation, and TMZ-based chemotherapy. Sadly, this approach has had limited success in bettering patient outcomes, predominantly due to ineffective treatments currently available. Therefore, there is a critical need to identify novel therapeutic targets to improve on current treatments that will increase patient overall survival. Recent studies have shown lipids maintain distinct expression in glioma compared brain, due to metabolic reprogramming, and support tumor growth, progression, and drug resistance. This dissertation utilized multiple reaction monitoring-mass spectrometry to define lipid profiles in glioma and brain around tumor, using three screening methods (M1, M2, and PC) to investigate differences: 1) by glioma grade, 2) by BAT grade, and 3) between glioma and BAT, to elucidate lipids critical to glioma progression that can serve as therapeutic targets. In each study, an integrated workflow combining histological analysis, laser capture microdissection, and MRM-MS characterized lipids expressed specifically in both glioma and BAT tissue.

MRM is a fast, sensitive approach capable of profiling lipids in small sample volumes and evaluated lipid alterations across glioma grades I-IV. With each increase in glioma grade, the disease becomes more aggressive and untreatable, potentially attributed to lipid composition changes. This study identified significant differences in lipid profiles between low- and high-grade glioma. Phosphatidylcholine (PC) and sphingomyelin (SM) lipids were differentially expressed as glioma undergoes malignant transition. Distinctions in PC and SM saturation and chain length relative abundance were shown to be grade specific. Lastly, individual PC and SM were observed to possess strong discriminating power in ROC curve analysis to distinguish between low- and high-grade glioma. Results suggested lipid composition changes as glioma progresses.

BAT profiling by MRM indicated highly distinct lipid composition between BAT exposed to different glioma grades. Low-grade BAT expressed greater relative abundances of carnitines, TAG, and high unsaturated PC compared to high-grade. Conversely, high-grade BAT maintained significantly higher low unsaturated PC vs low-grade. A significant transition from high unsaturated PC to low unsaturated PC average sum relative abundance was observed in low- and

high-grade respectively. ROC analysis also determined strong discriminating power of PC and SM to differentiate between low- and high-grade BAT. This study indicated major PC and SM expression changes in BAT proximal to different grades of glioma.

In the final study, MRM profiling determined glioma and BAT maintain largely similar lipid compositions based on applied MRM-MS methods. Multivariate analysis demonstrated proximal localization of clusters between groups, indicating comparable lipid profiles. Cluster analysis visualized slight distinction in expression of low unsaturated and high unsaturated PC in BAT and glioma respectively. Five PC and SM lipids were significantly different between glioma and BAT however, similarity in overall profiles reduced their discriminating power in ROC analysis. The results of this study indicate BAT molecular changes predate morphological changes, suggesting potential influence of glioma on its surrounding tissue.

Taken together, the applied integrative workflow is a powerful tool to comprehensively profile distinct lipids in glioma and brain around tumor at small sample volumes. Overall, results indicate PC and SM lipid expression are significantly at different stages of progression in glioma and BAT tissue. Studies in Chapters 3-5 will highlight the importance of defining lipid profiles in glioma and the surrounding brain to identify novel therapeutic lipid targets that both specifically target glioma, but also improve overall patient survival.

1 INTRODUCTION

1.1 Objectives

The overall objective of this project is to define lipid profiles in glioma tumors (grades I-IV) and the brain around tumor (BAT) using multiple reaction monitoring (MRM) mass spectrometry to identify lipid and pathway candidates for therapeutic targeting. The studies investigated three specific aims: 1) identify distinct lipids between glioma grades I-IV; 2) characterize differentially expressed lipids in BAT neighboring different glioma grades; and 3) elucidate key lipids between glioma and BAT. The study also aimed to highlight the capabilities of combining pathology and laser capture microdissection (LCM) with MRM-MS to both comprehensibly profile lipid species in a small sample and attribute detected lipids to a specific tissue type. This project incorporated diverse areas of biological expertise, through techniques, instrumentation, and statistical analyses employed. An overview denoting the expertise utilized in this project is demonstrated in Figure 1.1.

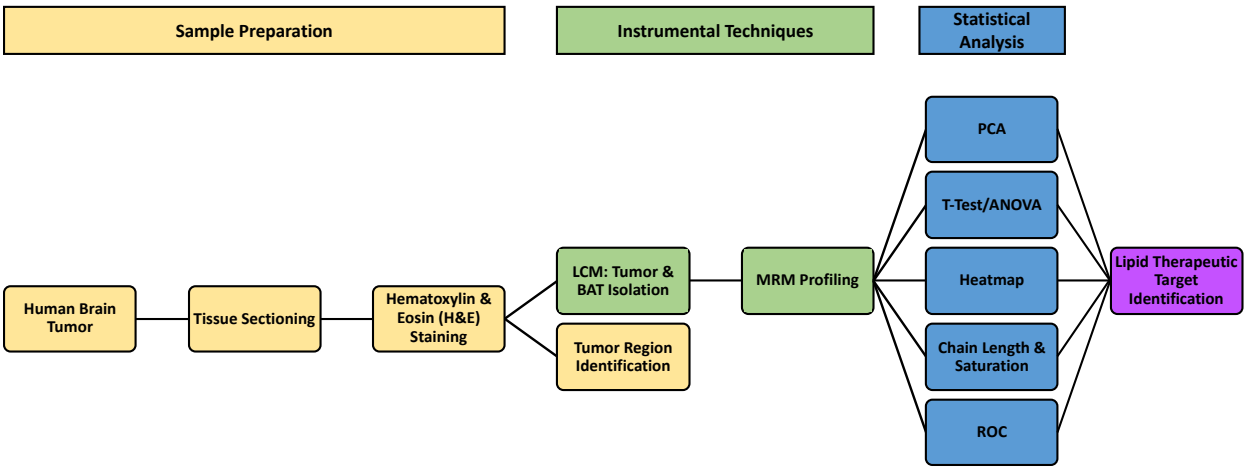

Figure 1.1 Overview of Project

1.2 Motivation

Gliomas are deadliest, most common forms of brain cancer. These tumors of glial lineage, account for approximately 80% of diagnosed malignant brain tumors[1]. In 2019, an estimated 19,000 high grade glioma patients will be newly diagnosed. The standard of care for gliomas traditionally includes maximum bulk tumor resection, followed by radiation treatment and chemotherapy[2]. Temozolomide (TMZ)-based chemotherapy has been the gold standard treatment since its clinical approval in 2005. TMZ is an alkylating agent that seeks to induce DNA damage through guanine nucleotide methylation, leading to tumor cell death[2]. Although clinically approved, TMZ has limited success increasing overall patient survival due to the removal of bulky methyl groups by O^6-methylguanine-DNA methyltransferase (MGMT)[3]. The highly incurable, invasive nature of gliomas has stimulated and emphasis on biomarker-based research to improve patient outcomes.

Most low-grade gliomas progress to high-grade and become highly untreatable. Upon malignant transition, glioma patient survival plummets from an average of 7 years to 1.25 years[4]. With high-grade glioma (HGG) patients having one of the worst survival rates compared to all cancer types, biomarker discovery focused on improving both survival of high-grade patients and preventing glioma progression is of utmost importance. Biomarker research has focused primarily on genetic and protein-based biomarkers in recent years predominantly for diagnostic and prognostic applications. Characterized glioma genetic signatures, utilizing alterations like IDH-mutations, aid in differentiation in glioblastoma (GBM) subtypes and determination of prognostic outlook for each patient[5]. Similarly, intraoperative applications of protein biomarkers like the oncometabolite, 2-hydroxyglutarate (2HG), have assisted tumor margin assessment and diagnosis[6]. Despite the various clinical applications of identified protein and genetic biomarkers, neither has translated to prolonged patient survival. Therefore, alternative biomolecules must be investigated to address the need to identify novel therapeutic targets aimed at promoting clinical success.

Lipids have emerged as promising targets in glioma due to their altered expression in glioma[7]. Studies showed the Warburg effect stimulates biosynthetic pathways driving elevated lipid synthesis and support tumorigenesis[8]. Lipidomic-based biomarker discovery have predominantly sought to define altered lipid profiles in glioma for diagnostic applications. The lipid precursor, N-acetyl aspartate (NAA), has shown early success in differentiating glioma from its surrounding brain tissue, but has limited applications in glioma treatment[9]. To date, there has been a lack of

motivation to target lipids therapeutically even though lipid metabolism is critical to glioma tumorigenesis. The complexity of glioma lipid profiles and their associated pathways has hindered their applicability as targets as they are poorly characterized.

This project utilizes a comprehensive lipid profiling approach, through MRM-MS, to improve on lipid coverage of previous imaging mass spectrometry approaches and address the poor glioma lipid composition definition. MRM-MS' broader lipid coverage employed to investigate differentially expressed lipids in glioma and BAT for lipid target identification. The overall objective of this project is to better define lipid profiles across glioma grades and their surrounding tissue to identify candidate lipid species specific to glioma and are important to low- to high-grade progression to utilize, upon future validation, as therapeutic targets.

1.3 Thesis Overview

This project utilized a combination of pathology-guided LCM isolation and MRM-profiling of glioma (grades I-IV) and BAT tissue to define lipid profiles throughout disease progression and investigate distinct lipid species for therapeutic target identification.

The first chapter introduces background information about glioma, importance of lipids in brain and glioma biology, the role metabolic reprograming in altered lipid composition in glioma, MRM lipid profiling in glioma, and the impact of comprehensive lipid profiling in glioma.

The second chapter details the novel analytical design and workflow of the project and pilot study results validating the applicability of the approach. Pairing LCM with MRM-profiling supports tissue specific attribution of detected lipids through its simple, precise, efficient workflow. Histological analysis tracing tumor regions on hematoxylin and eosin (H&E) stained tissue sections informed LCM isolation of glioma and BAT samples. The simple sample preparation for MRM-profiling, not requiring chromatography, minimized sample loss promoting comprehensive lipid capture. MRM sensitivity permitted small sample, microscale in size, lipid analysis across three distinct methods (embryo and phosphatidylcholine). The chemical-based lipid interrogation improves lipid detection sensitivity by reducing lost lipid information driven by low abundance and poor ionization[10]. Statistics applied to MRM output will also be discussed.

The third chapter discusses MRM-profiling driven investigation of changes in lipid expression across glioma grades I to IV throughout disease progression. Precision glioma grade sample isolation by LCM allows for analysis lipid species from tumor regions of interest and

attribution of lipids detected by MRM to a particular glioma grade. Studies indicate the level of metabolic alterations that occur in glioma increase with tumor grade and lipid compositions parallel this phenomenon. The shifts in lipid profiles as metabolic changes that occur throughout progression are not well understood. This study will better define distinct lipids in each glioma grade with the goal to identify key lipids species relevant to progression-associated tumor behaviors.

The fourth chapter investigates the changes between lipids profiles of BAT subjected to different glioma grades. Lipidomic studies have identified several metabolites that are distinct between glioma and BAT, but glioma grade-related impact on BAT lipid expression remains unclear. Due to proximity to glioma, BAT is exposed to autocrine signaling factors glioma releases to stimulate tumorigenesis. MRM-profiling will elucidate the impact of these interactions on BAT lipid expression and provide a better understanding of role glioma aggressiveness has on influencing molecular profiles of its surrounding tissue.

The fifth chapter will explore differentially expressed lipids between glioma and BAT. MRM was performed on LCM-isolated samples of each tissue type to determine distinct lipids between them. Imaging mass spectrometry (IMS) studies have identified lipid precursor, NAA, as an efficient biomolecule to differentiate tumor and brain. By broadening lipid detection with MRM-MS, we will expand our understanding of distinct lipid species between glioma and non-cancerous brain. Defining these species will not only identify candidate targets, but most importantly promote tumor-specific targeting thereby minimizing toxic side-effects.

The sixth chapter discusses major conclusions of the project, summarizing experimental results. The final chapter will also include future directions and important areas to consider as the project progresses toward the long-term goal of lipid pathway targeted therapeutics to improve patient survival.

1.4 Background

1.4.1 Glioma

Gliomas are the most common form of primary brain tumor theorized to originate from neuroglial stem or brain progenitor cells[11]. Glioma comprise about 30% of all diagnosed primary brain tumors, most of which progress toward malignancy[4]. Glioma are categorized by the World Health

Organization (WHO) in grades by malignancy, from grade I the most benign to grade IV the most malignant. By nature, gliomas are highly aggressive, diffusely invading local brain away from the original tumor lesion. The infiltrative capabilities of glioma, starting as early as grade II but most severely noted in grade IV GBM, makes complete resection impossible while reducing effective treatment options[11]. Surgeons strive to achieve maximal tumor resection as studies have determined >90% resection prolongs patient survival[12]. Gliomas present at any age, with glioma grade I-III most commonly occurring in young children (0-19 years) and GBM occurring mainly in individuals over 50 years old[13]. Incidence of glioblastoma presentation is directly related to age, prominently seen in older patients. Treatment protocol for glioma patients includes surgery, radiation, and alkylating agent-based chemotherapy (TMZ) and has been the consistent treatment approach for almost two decades. Although the standard treatment approach has persisted over time, it has failed to effective treat glioma patients and prolong survival. As most glioma progress toward GBM, these patients have an average survival time post-diagnosis of 12-15 months, and a five-year survival rate of about 5%[2]. The five-year survival rate of GBM (5%) is worse than the 10-year survival rate of patients with invasive breast cancer (83%)[14]. The discrepancy in overall and disease-free survival between glioma and other types of cancer highlights the critical need for better treatments options capable of more than extending patients' lives.

The heterogeneity across glioma grades have been investigated using various proteomic and genomic approaches to characterize molecular profiles to identify novel biomarkers aimed to address the gap in glioma diagnostics and therapeutics. Genetic modifications occur throughout glioma progression and have been applied to diagnose grade based on these parameters. Low grade glioma commonly express mutations to both the tumor suppressor gene TP53 and the metabolic protein isocitrate dehydrogenase (IDH)[15]. GBM has been classified by a combination of growth factor proteins (EGFR, PDGFRA) and epigenetic modifications to methylation status of MGMT and DNA[4]. To date, the Cancer Genome Atlas has sequenced several hundred distinct human GBM tumors to better understand glioma pathobiology. Whole proteome analysis of glioma patient tissue and serum have been conducted for biomarker identification[16]. Several diagnostic and prognostic biomarkers have been identified for potential clinical application, however, still lack as effective therapeutic targets for glioma patients. Lipids are distinctly expressed in glioma due to metabolic protein and genetic alterations noted in systems biology studies[17]. Lipid species and their associated molecular mechanisms driving poor patient outcomes in glioma patients are not

well characterized. Therefore, taking a systems biology approach using lipidomics, will provide a better understanding of key lipids and pathways involved in glioma progression and aid in identification of candidate lipid targets to test for clinical application.

1.4.2 Importance of lipids in healthy brain

First, it is important to understand the role and composition of lipids in healthy brain tissue. Human brains are comprised of approximately 60% lipids, categorizing it as the fattiest organ in the body[18]. The high lipid content maintained in the human brain highlights the relevance of this biomolecule to normal brain function (Figure 1.2). The role of lipids in brain can be grouped in several main categories: membrane, structural, and signaling. The two most abundant lipid classes expressed in these categories are phospholipids and cholesterol[19]. Phospholipids are amphiphilic lipids predominantly found in cell membranes and can be grouped into several subgroups: phosphatidylcholine (PC), phosphatidylethanolamine (PE), phosphatidylinositol (PI), and phosphatidylserine (PS)[18]. PC and PE comprise a majority of phospholipids within lipid bilayer of central nervous system (CNS) cells and work in conjunction with cholesterol to regulate membrane fluidity and integrity[20,21]. Lipid content and composition varies based on type of brain matter. Grey matter consists mainly of unmyelinated neural axons and white matter has mostly myelinated axons. Raman spectroscopy studies have identified grey matter to maintain a phospholipid to cholesterol ratio of 3:1 and a white matter ratio of 2:1[19]. Myelin composition is responsible for this distinction as myelin comprised a larger percentage of cholesterol than that found in grey matter membranes[21,22]. Myelination is responsible for accelerating signal transduction in neurons. Proper neuronal signaling is critical to maintain normal functioning not only in the brain, but across the entire human body. Regulating processes ranging from sensory perception to motor function, it is critical to maintain the brain's lipid composition to prevent dysfunction within the brain.

Alterations in the brain's lipid composition have been identified to drive or present in neurological and neurodegenerative disorders. Abnormalities in cholesterol homeostasis have been detected in Alzheimer's and Huntington's disease, contributing to increase in amyloid-beta plaques and neuronal excitotoxicity respectively[23,24]. Degradation of myelin is the main characteristic of Parkinson's disease induces motor dysfunction and tremors in patients[25]. Lipidomic studies have also connected lipid expression changes in normal brain when transitioning to neoplastic tissue. Lipid composition acts an indicator of current brain states; effective in

distinguishing normal from pathological tissue. Definition of lipids expressed in brain around glioma can characterize the state of non-cancerous brain, identifying differentiating lipid species as well as the impact glioma has on its expression profile.

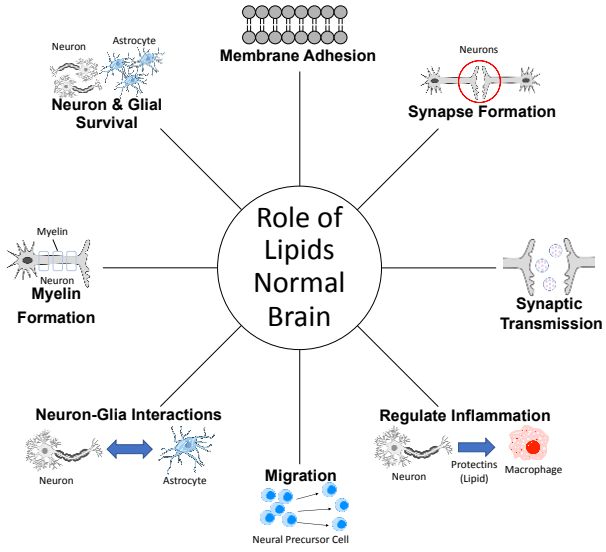

Figure 1.2 Diverse roles of lipids in normal human brain

1.4.3 Importance of lipids in glioma

Gliomas are characterized as both a rapid dividing and treatment resistant tumor, especially as they progress toward malignant stages. Lipids are involved in diverse cellular mechanisms responsible for three fundamental areas of glioma pathobiology: neoplastic transformation, tumorigenic development, and glioma progression (Figure 1.3)[26]. Altered lipid composition in these key areas provides increased adaptability, allowing glioma to meet both metabolic, structural, and proliferative demands to promote survival. Beginning at early grades, glioma undergoes greater levels of cell division compared to surrounding non-cancerous brain[5]. NMR studies have quantified elevated PC species abundance in glioma vs normal brain, which is postulated to address alterations to cell turnover rates and membranes[27]. Gliomas maintain a higher energy demand than normal brain due to their high proliferation rate and utilize lipids as an alternative energy source[28]. Triglycerides (TAG), typically not found in healthy brain, was detected in high grade gliomas and can act as energy storage, similar to peripheral tissues, and consolidate its fatty acids (FA) for energy production through β-oxidation[29,30]. Changes to FA saturation state has also been found to

relate glioma invasiveness[31,32]. Studies determined the most invasive high-grade gliomas maintained the greatest levels of FA unsaturation which increases membrane fluidity[18,32]. A recent study has also linked hyperlipidemia to angiogenesis, another characteristic of high-grade gliomas[33]. High levels of free fatty acids and cholesterol detected within glioma would normally induce lipotoxicity but is prevented through production of lipid droplets (LD)[34]. LD act as storage vessels for excess lipids to be consolidated when nutritional or environmental cues demand. Expression of these structures increase with glioma grade and provide great adaptive flexibility to high grade tumors. Components stored in LD can provide sources of energy through FAs, structural components for membrane synthesis, and most importantly promote treatment resistance.

To date there have been conflicting findings about lipid concentration differences between glioma and normal brain. The metabolic reprogramming needed to meet glioma energetic demands drives glycolysis toward lipogenesis, thereby inducing greater lipid expression. Alternatively, studies have also noted elevation of specific lipid classes in glioma, not total lipid concentration. Comprehensively profiling both glioma and BAT will help to better define the lipid distinctions between tissue types that the field is currently debating.

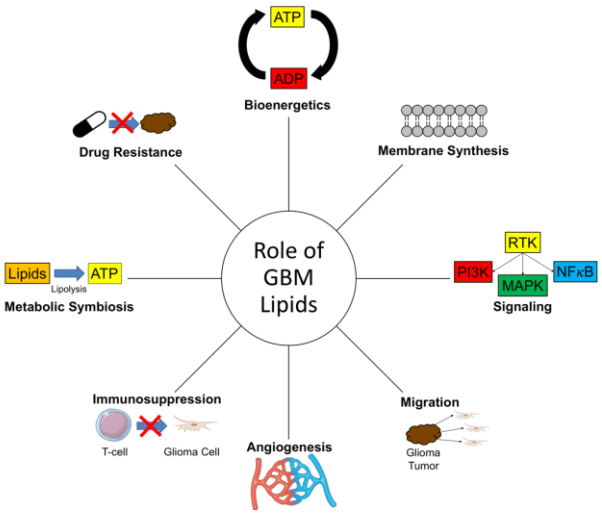

Figure 1.3 Diverse roles of lipids in glioma

1.4.4 Importance of understanding metabolic reprogramming's impact on glioma lipid profiles

The aggressive nature of glioma demands high amounts of energy to support continued tumor growth[28]. Gliomas primarily utilize glucose as a source of energy that is metabolized through a process called the Warburg Effect[35]. As a form of anaerobic glycolysis, glucose is converted into lactate and yields 10% of the ATP produced in oxidative phosphorylation (OXPHOS)[36]. It remains unclear the advantage choosing a metabolic process less efficient at producing energy would be employed in an energy-dependent cancer like glioma, but it indicates glioma relies of other mechanisms for energy production. Glucose is a major source of carbons in glioma and can be redirected into biosynthetic pathways identified to produce nucleic acids and lipids[37]. These alternative pathways utilize glycolytic intermediates as substrates for biosynthesis. Glycolytic intermediates in glioma are more readily available for biosynthesis due to pyruvate kinase M2 (PKM2) glycolysis regulation[38]. The extensive metabolic reprogramming in glioma is not fully understood, however, evidence indicates biosynthetic production of nucleic acids and lipids appears to maximize the utility of glucose. Being metabolized by biosynthesis instead of OXPHOS, glucose can generate energy, nucleic acids for neutralization of reactive oxygen species, and lipids that drive tumorigenic behaviors (Figure 1.3).

The diverse functions of lipids play an important role in glioma development. Upregulated lipogenesis in glioma stimulates elevated and distinct lipid expression from normal brain and suggests glioma's reliance on lipid pathways for survival. Studies have identified several key proteins that regulate lipid synthesis, but the exact molecular mechanisms altering lipid profiles in glioma are not well described[36]. There is a critical need to better understand the molecular mechanisms utilized to reprogram glioma metabolism towards lipogenesis, the resulting lipid produced, and how these lipids contribute to drug-resistance for effective future clinical translation. Developed lipid profiling approaches, like MRM-MS, provide the comprehensive level of analysis necessary to interrogate complex molecular profiles of glioma for lipid pathway characterization.

1.4.5 MRM-profiling in glioma

The extensive lipid composition of glioma induced by metabolic alterations requires a lipidomics approach with great selectivity and sensitivity to define its profile. MRM-MS is a

simple, accelerated strategy formulated to overcome the limitations of other lipidomic approaches. Targeted lipidomic approaches cannot investigate the spectrum of lipid classes comprising human tissues, severely reducing total lipid species discovery[39]. MRM addresses this limitation through its two analysis phases, discovery and screening. The discovery step utilizes both chemical functional groups and molecular features to identify lipids within the samples, applying previously acquired chemical information to make the distinction[10]. Non-reliance on abundance and ionization efficiency to detect lipids, like in other lipidomic methods, MRM is suited for small sample characterization[40]. Additionally, MRM is unique as it does not require chromatographic separation or dilution of samples prior to analysis to capture lipids in the sample. MRM instead interrogates chemical groups of sample lipids by performing precursor (Prec) ion and neutral loss (NL) scans[41]. Upon injection, lipid precursor ions are selected and scanned, sorted by m/z, in Q1 of the triple-quadrupole (QQQ), fragmented in Q2, and undergo a product ion scan determine the neutral loss between Q1 and Q3 (Figure 1.4)[42].

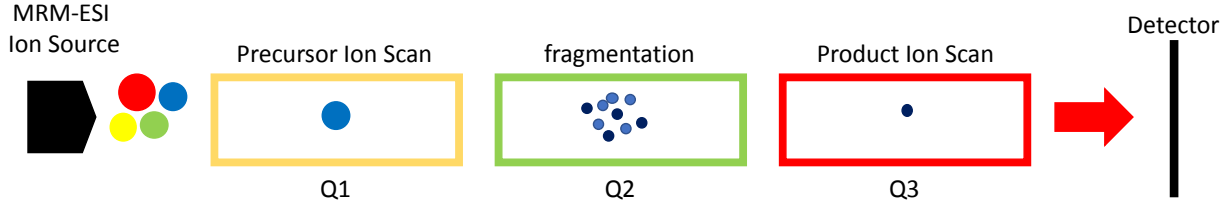

Figure 1.4 MRM lipid profiling through precursor and product ion scans

Precursor and production ion transitions acquired can then be employed during the screening phase. Information from Prec and NL scans are combined and compared to the LIPID MAPS database to inform the MRM screening process[41]. Tailored methods can then be established, using the ion transition output from the discovery step, for the tissue of interest to optimize the screening of its molecular profile[10]. The discovery phase requires a larger number of samples to formulate a new method, as a wide range of lipid classes must be interrogated to determine those best suited for sample profiling. The screening phase is informed by the captured lipid data from the discovery phase, organizing detected ions by molecular features to perform the MRM-profiling. Completion of the screening phase produces an output of all detected lipids from the chosen interrogation method, which is the converted into relative abundances for statistical analysis. Relative abundances are a semi-quantitative metric but has been verified to highly

correlate with absolute abundance. Both univariate and multivariate statistical analyses can be applied, using acquired relative abundances, to determine distinctions between experimental groups. Principal component analysis (PCA), cluster (heatmap) analysis, and receiver operating characteristic (ROC), as well as t-test/ANOVA, are common analyses to investigate differentiate lipid expression in the sample set. Application of MRM-profiling to analyze glioma and BAT lipid composition will accelerate the identification of novel lipid biomarker discovery, and better our understanding of lipid mechanisms involved in glioma presentation. Overcoming the limitations of previously utilized targeted lipidomic methods will provide a more comprehensive profile of lipid expression between tissue types for potential clinical applications upon further validation.

The rapid and sensitive detection capabilities of MRM has supported its application in studies investigating both proteins and lipids in contexts such as the brain, neurodegeneration, and cancer. Maintaining high sensitivity, Chang et al. 2014 applied MRM to quantify low abundance synaptic proteins from human brain[43]. MRM has been utilized for proteomics to detect specific proteins within complex mixtures, for instance human Parkinson's disease brain, containing a milieu of other unwanted proteins for protein biomarker[44]. The broad detection range of MRM has also been employed in lipidomics studies in various cancers, such as ovarian, colon, and endometrial, to identify novel biomarkers aimed at diagnostic applications and better characterizing signal transduction altering lipid composition[45–47]. More recently, MRM was used to investigate pharmacokinetics by quantifying drug concentration of sunitinib, an anti-angiogenic therapy, in murine brain, plasma and brain tumor tissue[48]. Despite MRMs previous applications interrogating human brain, cancer tissue, and lipids, limited studies are available using this approach to profile glioma lipids[49]. Applying MRM to human glioma tissue would expand on previous studies profiling brain tumor lipid composition due to its broad detection range and also through its sensitivity to detect low abundance lipids in complex mixtures.

1.4.6 Impact of comprehensive lipid profiling in glioma

Glioma biomarker discovery has expanded extensively following the application of mass spectrometry (MS) approaches to characterization of molecular profiles. The broad detection range of MS to detect lipids within glioma has established that lipids are differentially expressed in glioma compared to normal brain. However, the reliance of full-scan MS methods on the abundance and ionization efficiency limits the amount of lipid information that can be acquired

from this method[40]. Full-scan MS is less informative when investigating tumor heterogeneity and localization of biomolecules maintained in the sample as tumor regions are not specifically isolated and lipid abundance may not be sufficient for this approach. Electrospray ionization (ESI)-based imaging MS (IMS) overcame the limitations of full-scan MS lipidomic approaches through its capabilities to acquire location-based lipid information, defining tumor region heterogeneity, and detect lower abundance lipids in small glioma samples. Small molecule, lipid and metabolite, spatial information obtained through IMS has aided in the distinction between glioma and brain tissue[50]. IMS has shown promise clinically for diagnostic applications, with great interest in its application to intraoperative tumor border discrimination[51]. Despite overcoming the limitations of full-scan MS methods, IMS proportionate a limited lipid coverage compared to other lipidomics approaches, detecting one to two magnitude lower number of lipid species.

Lipid profiling studies have made great strides over the last four decades, identifying differences in brain and glioma lipid composition began as early as the 1960s. Gopal and colleagues identified gliomas possessed different percentages of fatty acids and phospholipids; gliomas were found to possess a greater percentage of polyunsaturated FAs, lecithin, and lower saturated FA than normal brain[52]. In the late 1990s, Nygren et al. (1997) evaluated cholesterol and cholesterol ester concentration in brain tumor and surrounding tissue by chromatography[22]. It was determined cholesterol was higher in surrounding tissue and brain tumors possessed greater concentration of cholesterol esters. In the 2000s, multinuclear magnetic resonance spectroscopy was applied to non-cancerous brain and gliomas and identified elevated amounts of triglycerides, phospholipids, and cholesterol esters in high grade tumors vs normal brain tissue[29]. More recently, mass spectrometry-based approaches have been implemented for brain tumor lipid profiling, providing more specific lipid species information than previous studies. Imaging mass spectrometry approaches, matrix-assisted laser desorption/ionization (MALDI) and desorption electrospray ionization (DESI), were applied by Eberlin and colleagues to both investigate distinctions in lipid composition between glioma subtypes as well as differentiate between tumor and brain tissue[17,53,54]. Phospholipids, including sphingomyelins and ceramides, were detected by IMS to maintain differential expression in glioma and surround brain matter, both white and grey[55]. To date, lipid profiling studies have established relevant lipid classes to the glioma disease model, and more recently, individual lipid species to help pathologists and surgeons determine tumor border. Although progress has been made in profiling glioma lipids, findings have been geared

mainly toward diagnosis. Looking ahead, using lipids as therapeutic targets would be the next logical application of findings from lipid profiling studies.

The lack of motivation to target lipids may be related to two important aspects, the ability to confidently attribute detected lipids to tumor and the limited lipid coverage capabilities of approaches that can analyze specifically glioma or brain tissue. Development of a workflow that integrates the specific tissue analysis of IMS and the comprehensive lipid characterization of full-scan MS is essential to identify glioma-specific lipids to target. The vital nature of lipids in healthy brain demands precision targeting of glioma-specific lipids to avoid potentially lethal side effects. This project addressed these limitations by combining pathology with LCM to distinctly isolate glioma and BAT for comprehensive MRM-profiling. Glioma tumors maintain an asymmetric shape in the brain; therefore, resected tissue may contain tumor and non-tumor cells. Integrating histological analysis with LCM informs the tissue extraction, localizing tumor and BAT cells that would normally indistinguishable in unstained tissue. Extracted lipids from each individual tissue type can now be comprehensively profiled using MRM and detected lipids are confidently attributed to either glioma or BAT. The more informative output of MRM will provide a better understanding of lipid species differentially expressed in each tissue type and critical lipid pathways contributing to alterations in expression.

1.4.7 Role of lipid chain length and saturation state in glioma

Lipid saturation type has long been understood to be distinct between glioma and healthy brain tissue[31]. In glioma, saturation status has been identified to influence membrane fluidity, supporting tumor invasion and progression. Fatty acids, a major lipid component and expressed at greater abundances in glioma, maintain either saturated or unsaturated compositions and are differentiated by number of double bonds[37,56]. In glioma, unsaturated fatty acids are found at higher levels than surrounding brain[57]. Lipids with fatty acids containing one or more double bond increases cell membrane fluidity, elevating the infiltrative capacity of tumor cells. Polyunsaturated fatty acids were identified to be most prominent in high-grade gliomas, though their role in tumor progression is not yet known[32]. Hindered tumor growth was noted when desaturation reactions in glioma were inhibited, highlighting the importance of unsaturated lipids[58]. Lipid chain length has also been associated with pathology development. Long-chain ceramides positivity correlated with Alzheimer's disease and cystic fibrosis severity[59]. In bladder cancer, long-chain polyunsaturated

phospholipids and TAG were expressed at higher levels than other saturation types[60]. In glioma, studies characterizing lipid chain length profiles and their impact of tumor aggressiveness, to the best of our knowledge, have not been conducted. Based on findings in other pathologies, long-chain lipids appear to be more prominent in disease states. The comprehensive MRM-profiling employed in this project will detect lipids of various saturation states and chain lengths to investigate their relative abundances in both glioma and BAT.

2 ANALYTICAL DESIGN OF NOVEL LIPIDOMICS WORKFLOW COMBINING PATHOLOGY, LASER CAPTURE MICRODISSECTION, AND MULTIPLE REACTION MONITORING FOR GLIOMA AND BAT LIPID PROFILING

2.1 Introduction

Lipids have become increasingly important biomolecule in determination of disease state in the brain, including gliomas. Despite understanding the importance of lipids in glioma biology, there are no clinically approved lipid biomarkers for therapeutic use. Various mass spectrometry-based lipidomics approaches have been applied to profile glioma and its neighboring brain lipidomes and have proven useful in diagnostics. Current findings improving areas of diagnostics, however, have not translated to therapeutics to better glioma patient overall survival. Limitations present in previously utilized MS approaches have not been able to both comprehensively define lipid profile and addressing glioma heterogeneity. Full-scan MS has extensive lipid characterization capabilities but fails to probe for tumor heterogeneity. IMS can investigate tumor heterogeneity but lacks the broader detection capabilities of full-scan MS. In addition, lipids are vital to normal brain functioning, therefore identifying lipids that are distinct to glioma tissue is paramount to avoid toxic side effects during use as targets. Therefore, it is critical to employ a workflow method capable of distinguishing glioma and BAT tissue and comprehensive lipid definition. The workflow in this project integrates several instrumental techniques to address limitations of previous MS approaches. Pathology-guided LCM precisely isolates glioma and BAT tissue and MRM-MS sensitivity captures the broad range of lipids expressed in small samples. This workflow's output will provide detailed characterization of lipids in each tissue type supporting identification glioma-specific lipids and their associated pathways.

2.1.1 Histological Assessment

Initial glioma diagnoses are performed through magnetic resonance imaging (MRI), with final determination being conducted by histology following bulk resection surgery[61]. Pathologists regularly utilize hematoxylin and eosin (H&E) staining to differentiate cellular components and features maintained within resected tissue to confirm a diagnosis[62]. The H&E stain adds contrast to tissue for pathologists to visualize tumor cell nuclear and cytoplasmic elements. Glioma grade

diagnosis is based on the WHO histological criteria (Table 2.1)[61]. Criterion for glioma grading increases in number as the disease progresses and the tissue must possess each feature to establish a final diagnosis. Additionally, the phenotypic guidelines listed in Table 2.1 were utilized to distinguish and trace tumor vs non-tumor boundary outlined in section 2.2.3. Cells containing morphological features, defined in the table below, were designated as tumor and the neighboring cells lacking these criteria were considered BAT. These parameters were implemented to determine tumor border.

Table 2.1 Histological criteria for glioma tumor pathological assessment

WHO Grade	Tumor Type	Histological Criteria
I		
II	Grade 2 Astrocytoma	Nuclear atypia
III	Grade 3 Astrocytoma	Mitoses and nuclear atypia
IV	Grade 4 Astrocytoma	Mitoses, nuclear atypia, microvascular proliferation and/or necrosis

2.1.2 Laser Capture Microdissection

LCM is a powerful isolation tool first developed by the NIH to investigate cell subgroups contained within cell or tissue samples[63]. LCM utilizes a combination of infrared (IR) and ultraviolet (UV) lasers to extract regions of interest within a sample[64]. Application of each laser confers several key advantages to sample capture: 1) speed of extraction, typically held to a few seconds but is proportionate to size of intended isolation; 2) precision, IR laser adheres cells to capture cap while maintaining morphology and UV precisely dissects the region of interest to avoid unwanted contamination; and 3) versatility, the simple isolation protocol can be applied to diverse tissue types and downstream applications[65]. The expedient, non-damaging nature of LCM has supported its integration into MS workflows investigating both lipids and proteins (Table 2.2)[66–70]. Using these technologies in conjunction promotes better characterization of tissue heterogeneity by combining precision sample collection of LCM with the broad detection range and sensitivity of mass spectrometry. Consolidating on these capabilities, this project utilizes LCM

with MRM-MS to investigate glioma and BAT lipid profiles from sectioned human tumor samples, which have not yet been analyzed by this workflow.

Laser capture microdissection functions by applying infrared and/or ultraviolet lasers to sectioned tissue on membrane slides to collect cell populations within the sample. The tissue is first visualized using the LCM microscope connected to a computer, followed by laser control adjustment to parameters suitable for tissue type and research interest. Based on downstream application, laser thickness can be reduced to 7.5μm for single cell dissection or increased to 15μm or 30μm for isolation of a group of cells. Once the region of interest in the tissue is designated on the computer, the LCM cap containing transfer film is placed on the selected tissue area. Upon placement of the LCM cap, IR laser can be applied for begin sample extraction. The IR laser originates from above the membrane slide containing the tissue section, and is critical as photochemical effects on molecular integrity are avoided due to absorption by cap and membrane, and the IR laser melts transfer film on cap that allows cells to adhere for extraction. Following IR laser utilization, the UV laser from beneath the tissue sample is applied. The stronger UV provides more precise dissection, being a narrower beam, reducing dissection and adherence of unwanted cells to the LCM cap. Combining the IR laser to adhere cells of interest to the transfer cap from the membrane slide, and UV laser to dissect only selected cells, LCM provides quick, precise isolation of samples for further downstream molecular profiling applications.

Table 2.2 Review of studies integrating LCM into mass spectrometry molecular profiling

Publications	Tissue Analyzed	LCM Method	Lipid Extraction Method	MS Method	Lipids Screened
Xu et al. 2002	Invasive mammary carcinoma and normal breast epithelium	PixCell II LCM	N/A	MALDI (proteins)	N/A
Hebbar et al. 2014	Drosophila neurons	AutoLPC (Zeiss)	On-Column Extraction (C18)	LC-MS^n	PE, PE-O, PC, PI, PG, Cer, PS, CerPE, LPC, LPE, TAG (~51 lipids)
Dilillo et al. 2017	C57BL/6 Brain	AutoLPC (Zeiss)	N/A	AP MALDI-MSI, MALDI-MS, LC-MS/MS	N/A
Nyalwidhe et al. 2017	Human Pancreatic Beta Cells	ArcturusXT LCM	N/A	LC-MS/MS (proteins)	N/A
Knittelfelder O, Traikov S, Vvedenskaya O, et al. 2018	Murine Liver, Human Plasma	AutoLPC (Zeiss)	MTBE/MeOH	• LC-MS/MS (Orbit trap, proteins [1355 found]) • FT-MS & t-SIM (lipids)	Glycerolipids, PA, PI, PS, PG, PE, PC, PE O-, LPA, LPI, LPC, LPE, Cer, SM, Chol, CE (~200 lipids)

2.1.3 Multiple Reaction Monitoring

As mentioned, MRM is a simple, expedient, and sensitive MS technique able to detect a broad range of lipids within a given sample. Not restricted by abundance to detect lipids present in samples, MRM was capable profiling lipids in samples as few as 16 oocytes, acquiring over 1,500 MRMs across 10 methods[41]. This approach directly injects sample into the ion source, avoiding chromatographic dilution sample loss, and captures lipid information based on Prec and NL scans[10]. Output of Prec and NL scans during the discovery step informs creation of methods to apply during the screening step. Recent MRM-profiling of glioma lipids identified phosphatidylcholine and sphingomyelin MRM transitions to be distinct in glioma tissue leading to the formulation of the PC method utilized in this project[49]. Due to the small sample size and volume, supervised discovery of Prec and NL scans could not be performed and a unique method for this sample set was not created. In lieu of this limitation, two embryo methods (M1 and M2), in addition to the PC method, were employed as glioma taken on a stem-like phenotype, similar to those in embryonic cells, due to the presence of cancer stem cells[71]. The M1 and M2 methods were formulated through the multistep MRM-profiling workflow. The MRM approach consists of two-steps: first, the discovery phase that interrogates functional groups of lipids contained within the

experimental sample, and second, the screening phase that detects selected MRMs based on findings during the discovery phase. Bovine embryos at various stages of embryonic development were evaluated during the discovery phase to identify important MRMs to test for during the following screening phase. Lipid functional group information, using the m/z molecular ion data contained within the LipidMaps database, were consolidated to create a list of MRMs to interrogate for during the discovery phase. About 1,500 MRMs were initially chosen to interrogate the bovine embryos and were comprised of phospholipids, free fatty acids, and triacylglycerol lipid classes. Selected MRMs were divided into 10 methods for multiple scans to be conducted on each individual MRM, to increase confidence in reliability of identified MRMs of interest. MRMs were chosen for the tailored M1 and M2 methods based on ion intensity of transitions. MRMs with absolute ion intensities of transitions greater than the blank were included for the newly formulated methods. At the conclusion of the discovery phase, 383 MRMs maintained absolute intensities compared to the blank, and were combined into the M1 and M2 methods utilized in these studies. Embryonic cells have increased relevancy when considering glioma and disease management due to the presence of glioma stem cells. Embryonic cells, early in development, are totipotent, possessing the ability to divide and differentiate into any cell type in the body. Glioma stem cells, while not maintaining the broad differentiation capacity of embryonic cells, can differentiate into cell types native to the brain being multipotent[72]. The multipotency of glioma stem cells provide glioma increased adaptability to cytotoxic stimuli, like chemotherapy and hypoxia, through maintenance of high therapeutic resistance and differentiation into cell types to combat oxidative stress. Interrogating glioma, which maintains increased stem-like qualities, using M1 and M2 embryonic methods supports the identification of lipids found in embryonic cells, that would not be detected in non-stem cells, that could potentially be specifically targeted therapeutically[41]. Taken together, MRM is uniquely suited for small sample volume analysis, characteristic of LCM isolations, because chemical information and molecular features determine capture of sample lipid information. Lipids screened in each of the three MRM methods are outlined in Appendix A (Table A.1-A.3). Of note, not all lipids in the outlined chain length and saturation parameters for each method were screened and is a limitation in each study. In these studies, lipids from glioma and BAT cells, isolated by pathology-guided LCM, were analyzed using three distinct MRM-profiling methods to define lipid profiles between different tumor grades and tissue types.

2.2 Analytical design

2.2.1 Sample selection

Human glioma samples analyzed in this project were provided by the Indiana University Simon Cancer Tumor Bank. Prior to sample selection, patient gliomas were sorted into groups by WHO tumor grades I-IV. Next, samples were assigned a random number to replace the sample identification information. The blinded samples were then chosen by an impartial third party to guarantee an entirely random and blind selection process. Four numbers, corresponding to a specific sample, were selected from each group, with the exception of grade I due to the possession of one sample at this grade. The random, double-blind nature sample selection ensured sample analyzed would be chosen in a non-biased manner. 13 samples selected are detailed in Table 2.3. Patient clinical and demographic information of selected samples in Appendix A (Table A.4).

Table 2.3 Descriptive Information for Selected Human Glioma Samples

Sample Grade	Sample Name	Pathological Classification
I	M-HBT 364	Dysembbryoplastic neuroepithelial tumour (DNET)
II	M-HBT 203	Mixed Oligoastrocytoma
	M-HBT 237	Oligoastrocytoma
	M-HBT 300	Oligoastrocytoma
	M-HBT 305	Oligoastrocytoma
III	M-HBT 172	Anaplastic Oligodendroglioma
	M-HBT 190	Mixed Oligoastrocytoma
	M-HBT 385	Anaplastic Astrocytoma
	M-HBT 387	Complex Anaplastic Astrocytoma
IV	M-HBT 292	Glioblastoma
	M-HBT 322	Glioblastoma w/large PNET-like components
	M-HBT 319	Glioblastoma w/Oligodendroglial component
	M-HBT 370	Glioblastoma w/ IDH-wildtype

2.2.2 Sample sectioning and staining

13-flash frozen human glioma samples, grades I-IV, were cryosectioned using a Leica cryostat at 10°C at a thickness of 5µm for histological analysis and laser capture microdissection. Sequential tissue sections were cut onto charged glass slides and PEN membrane framed slides (Thermofisher) in preparation for staining and LCM respectively. To reduce potential day-to-day LCM isolation variability, samples from each grade were sectioned onto a single slide, creating 4 groups with up to four tumor sections per slide (Figure 2.1). A total of 26 glioma sections, 13 per slide type, were cut for tissue analysis and extraction. Glioma tissue sectioned on charged glass slides were formalin fixed and stained with hematoxylin and eosin (H&E) using a Leica integrated workstation. Unstained glioma sectioned on PEN membrane slides were stored in a -80°C freezer until LCM sample isolation. Following tumor region identification, described below, samples not containing both glioma and BAT cells underwent a second round of sectioning. Sequential sections were cut at 5µm thick, with adjacent sections cut every 25µm to aid in surveying tumor for each tissue type. Four sections of each sample placed onto the same slide for analysis and isolation.

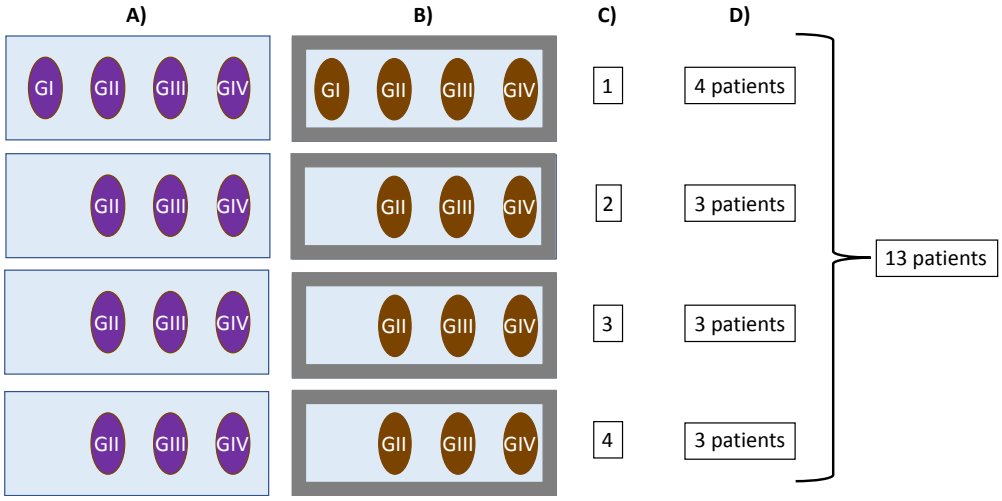

Figure 2.1 Design of sectioned glioma samples for pathology and LCM isolation. A) H&E stained glioma sections on charged glass slides. B) Unstained glioma sections on PEN Membrane Frame Slides. C) Assigned group number. D) Patient samples per group. G = grade.

2.2.3 Tumor region identification

To identify the localization to tumor within sectioned glioma, histological analysis was performed on H&E stained tissue. Tumor region identification followed WHO histological criteria applied

during patient diagnosis (Table 2.1). Following H&E staining in the Leica CV5030 workstation, coverslips (Leica 24mm x 50mm with Leica Surgipath MM24 mounting medium) were placed onto glass slides to prepare for digital scanning. H&E stained sections were scanned using the Aperio Versa slide scanner (Leica Biosystems, CA) at a 40x magnification for histological analysis. Tumor and brain around tumor localization were identified and traced using Aperio Imageworks software by a licensed pathologist (Figure 2.2).

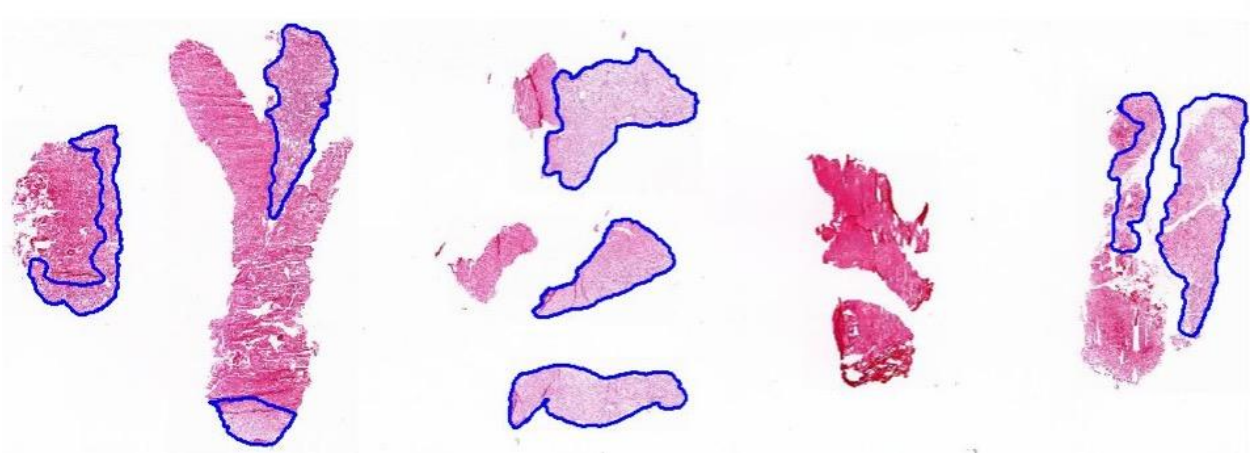

Figure 2.2 Pathological assessment of H&E stained glioma for tumor region identification. Areas outlined in blue indicate tumor regions in scanned H&E stained glioma sections.

2.2.4 Laser capture microdissection: glioma and BAT isolation

Unstained tissue slides were removed from -80°C freezer and dried using a desiccator for 15 minutes to remove moisture from the sectioned samples prior to LCM isolation. Sample collection was conducted over 4 isolation periods, capturing glioma and BAT tissue from one group per session to avoid heat-driven sample degradation. Sample isolations were performed using the ArcturusXT^{TM} Laser Capture Microdissection System (Thermofisher, USA). Tissue was captured using IR and UV lasers, guided through comparison of microscopy scanned pathology slides and LCM microscope images (Figure 2.3). Samples collected were measured, using the LCM software measurement tool, to be approximately 400µm x 950µm ± 30µm, in each direction, in area. Laser dissected samples were captured onto CapSure® LCM Caps (Thermofisher, USA). Sample caps were placed in 0.5µl microfuge tubes containing 100µl of ultra-pure water (UP-H_2O) and stored

on ice until all the samples were collected within the group (Figure 2.4). Samples were stored in a -80°C freezer following isolation until all experimental samples were collected and prepared for lipid extraction. Glioma and BAT samples collected and analyzed were evaluated using the same pathology grading standards, and the grade label used in each project matched these parameters. This approach contained several limitations of note. First, lack of a coverslip reduced optimal visualization of distinct morphological characteristics of cells within the section. Pairing LCM with histological analysis, tracing of tumor region, performed by a licensed pathologist was utilized to address this drawback. Second, LCM requires considerable time to isolate samples. To prevent temperature-driven tissue degradation, samples were collected in smaller groups, limiting time exposed to ambient temperatures, preserving molecular composition of the tissue.

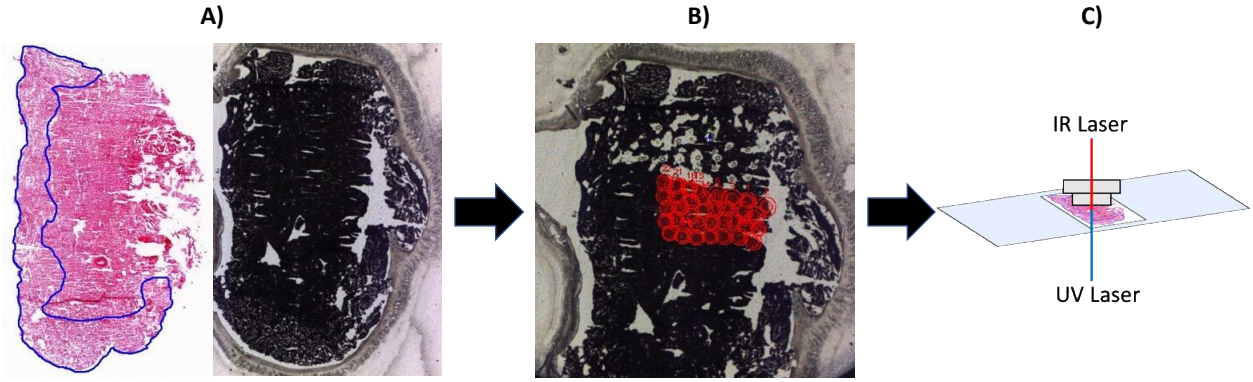

Figure 2.3 Pathology-guided isolation of tissue by LCM. A) Pathology (left) and LCM (right) microscope images used for guided sample isolation. B) Region selected for LCM extraction. C) Diagram representing combined IR and UV laser-based sample isolation.

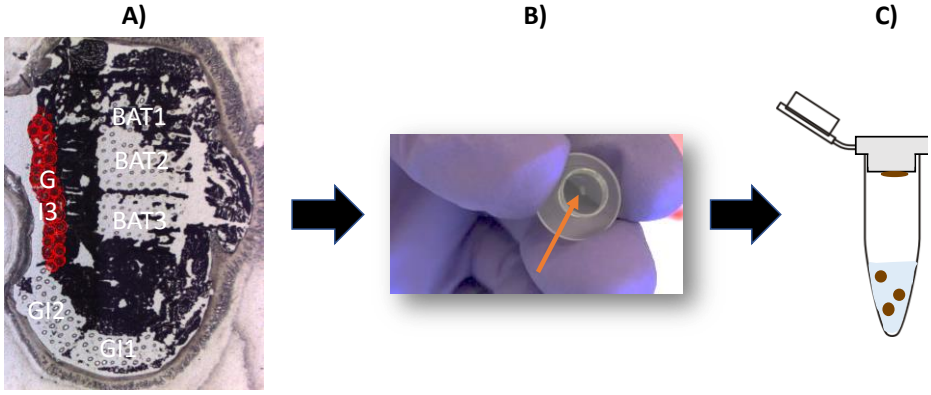

Figure 2.4 Lipid collection from LCM-isolated glioma and BAT tissue. A) Example grade I tumor section post-LCM glioma and BAT sample isolation. B) Image of small sample volume collected for analysis. C) Example of lipid release into solution by UP-H_2O driven cell lysis.

2.2.5 Lipid extraction

59 LCM isolated samples were removed from the -80°C freezer and underwent lipid extraction following the Bligh-Dyer protocol that had been adapted for small sample volumes[73]. Lipids were initially collected from cells by inverting microfuge tubes containing 100µl UP-H_2O, allowing the UP-H_2O to contact the sample causing cell lysis by difference in osmolarity pressure (Figure 2.4). The solution was then transferred to a separate extraction tube. The sample cap was washed a second time with 225µl methanol to collect any residual lipids in the sample and in the original microfuge tube. Following the transfer to the extraction tube, 125µl chloroform was added to the solution and vortexed for 10 seconds to mix and form a 1-phase solution. Additional methanol, in 50µl increments, were added to the UP-H_2O-methanol-chloroform solution until a single phase was present. The extraction tube was incubated at 4°C for 15 minutes to allow the lipids to go into solution. 125µl UP-H_2O and 125µl chloroform was then added to the extraction tube to initiate a biphasic solution. The biphasic solution underwent centrifugation at 16,000 x *g* for 10 minutes at room temperature drive phase separation. In the biphasic solution, the upper phase is the polar phase, the lower phase is the organic phase containing lipids, and the layer between phases contains proteins. Solution for both phases were collected, avoiding the intermediate protein layer, and transferred to a new microtube. Solvent in the microtubes were vacuum dried by speedvac with a nitrogen stream. Dried lipid extracts were then stored in a -80°C freezer until all lipid extraction was completed in all samples. Lipid extraction was conducted over three sessions, randomly assigning samples to groups for extraction, to avoid potential errors impacting samples from a single group or tumor grade (Figure 2.5).

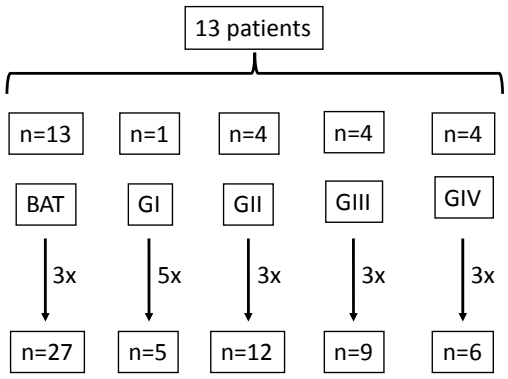

Figure 2.5 Outline of lipid extracted samples for MRM-profiling

2.2.6 MRM-MS profiling

Dried lipid extracts were resuspended 30µl of internal standard solvent containing acetonitrile: methanol: ammonium acetate, at 3: 6.65: 0.35 v/v/v, to prepare for injection. Samples were injected for MRM-profiling into the Agilent 6460 triple quadrupole (QQQ) mass spectrometer (Agilent Technologies, CA) with a jet stream electrospray ionization source equipped. Samples were sent directly to the ESI ionization source using the micro-autosampler (G1377A) to avoid need for chromatographic separation.

Three previously established lipid screening methods were utilized to profile samples lipids: M1, M2, and PC. M1 and M2 methods were formulated to evaluate embryonic samples and the PC method was generated to investigate GBM lipid composition specifically[49]. The discovery step was bypassed due to small sample volume preventing the establishment of new screening methods. Each sample (n=59) was interrogated using these three screening methods and scanned for lipids described in Table 2.4. Several limitations were experienced using MRM-MS. The discovery phase was not performed in these studies due to limited sample volume. Utilizing relevant, previously tailored methods on extracted lipids was applied to address this drawback. Additionally, isomers of detected lipids were not interrogated through this method. Previous studies have combined liquid chromatography (LC) with ion mobility spectrometry to determine lipid isomers, but applying to the workflow could result in loss of sample which is significant due to the small sample volume analyzed in these studies[74]. It is important to note, comparisons of sample lipid compositions within the three projects were based on 583 lipids included in each of the three applied screening methods. Conclusions were made based on relative abundances of these lipids and were not an interrogation of all lipid species contained within the assessed lipid classes.

Table 2.4 Screening methods applied for MRM-profiling of glioma and BAT lipids

Screening Method	Lipid Classes Detected
Method 1 (M1)	Phosphocholines, Carnitines, Sphingomyelins, Triglycerides, Cholesterols
Method 2 (M2)	Free Fatty Acids, Phosphoinositols, Cholesterol Esters, Campesteryl ester, Phosphoglycerols, Phosphoserines, Phosphoethanolamines,
Method 3 (PC)	Phosphocholines, Sphingomyelins

2.2.7 Data processing and statistics analysis

Raw MRM-profiling screening step data output for each method was converted Excel format using an in-house script for relative abundance calculations. Initial calculations determined lipids with ion intensities greater than 1.3 times the blank. Lipids below this threshold were filtered out of the data. Ion intensity comparison between the blank and experimental samples were calculated by taking the maximum value of each lipid and dividing it by the blank ion count for the lipid. Lipid relative abundance was calculated by dividing the ion intensity for the individual lipid in a single sample by the sum ion intensity of all lipids in that sample. Sample relative abundances were then sorted, based on tissue type and tumor grade, to investigate comparisons of interest. MetaboAnalyst 4.0 (www.metaboanalyst.ca), a web-based metabolomics suite with comprehensive data analysis capabilities including statistical, functional, and visual interpretations of omics datasets, was utilized to process data[75].

The data was auto-scaled, more specifically mean-centered and divided by the standard deviation of each variable, prior to statistical testing Several statistical and visualization analyses were performed to examine the data. Principal component analysis (PCA) is a multivariate approach applied to visualize and discriminate groups within the dataset to identify overall lipid profile differences[76]. Partial least squares discriminant analysis (PLS-DA) was utilized to both calculate variance of important in projection (VIP) for each lipid species to determine which lipids were most important to the model and visualize relative abundance differences between groups. Lipids with a VIP score >1.0 were considered important to the model and were applied to further sort the dataset for better PCA discrimination. Significant differences in lipid relative abundance was determined by t-test or ANOVA with $\alpha = 0.05$. Discrimination of lipid profiles was visualized in a heatmap through cluster analysis; the number of lipids included in the heatmap was adjusted to identify the best group clustering. Receiver operating characteristic (ROC) was performed to determined lipids capable of differentiating between tissue types. Lipids that maintained area under the curve (AUC) of >0.8 were considered and selected to test for tissue type attribution testing.

For lipid chain length and saturation analysis, lipids were first sorted based on size of molecule and saturation type. Lipids were divided into three chain length groups, short, medium, and long. To determine chain length group, the number of carbons in the largest and smallest lipids were subtracted and divided by three to evenly divide groups. Saturation groups were also divided into three groups: saturated, low unsaturated, and high unsaturated. Saturated lipids contained no

double bonds, low unsaturated lipid maintained 1-2 double bonds, and high unsaturated lipids had 3+ double bonds. Following sorting based on these guidelines, the sum relative abundance of lipid in each sample were calculated and then averaged for the group being compared. Statistical analyses were performed using JMP® Pro 14. Equal variance was calculated using Bartlett's test. Multiple comparison testing was performed using the non-parametric Dunn's test ($\alpha = 0.05$).

2.3 Pilot study

2.3.1 Pilot study parameters

A pilot study was completed to validate the applicability of this workflow to detect differentially expressed lipids in small volume samples. Implementing techniques described in the analytical design sections above, MRM-profiling was performed on glioma (n = 3) and BAT (n = 3) samples isolated by LCM from grade I glioma sections. Lipids were screened using the M2 embryo method and data was analyzed using MetaboAnalyst 4.0. PCA and cluster analysis were employed to identify distinctions between glioma and BAT. Total MRM signal was monitored to establish if adequate lipid signal was acquired based on the amount of tissue isolated by LCM. Ideal lipid signal is greater than 1×10^5, and larger sample volumes can be isolated to address potential low signal.

2.3.2 Principal component analysis demonstrated distinct lipid profiles between grade I glioma and brain around tumor tissue

MRM-profiling of triplicate grade I glioma and BAT samples identified distinct clusters in the PCA plot (Figure 2.6). The multivariate analysis noted discrimination of tissue types, based on differential expression free fatty acids and species within the phosphatidylserine lipid class, scanned for during the screening step. Several lipid species distant clustering of grade I glioma and BAT included free fatty acids tetratriacontanoic acid (C34:0), dodecanoic acid (C12:0), and dotriacontanoic acid (C32:0); and phosphatidylserines PSp 40:6, PSo 20:0, and PS 14:1. The PCA plot also showed that distinctions can be made in small sample volumes by multivariate analysis, providing initial support for this workflow.

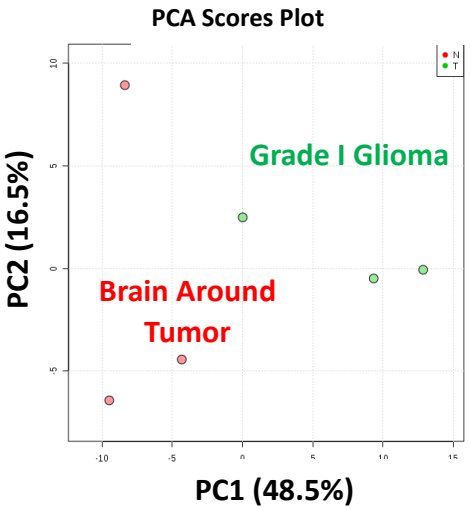

Figure 2.6Principal component analysis showed discrimination of grade I glioma and BAT clusters indicating distinct lipid profiles, according to PC1 and PC2.

2.3.3 Cluster heatmap analysis indicated separate clusters of grade I glioma and brain around tumor based on difference in top 50 lipids.

Cluster analysis identified glioma and BAT maintained distinct lipid profiles. Top 50 lipids visualized in the heatmap to cluster glioma and BAT groups and showed the tissue types could be distinguished based on three classes: free fatty acids, cholesterol esters, and phosphatidylserines. Brain around tumor possessed higher relative abundances of free fatty acids like acids tetratriacontanoic acid (C34:0), dodecanoic acid (C12:0), and dotriacontanoic acid (C32:0) and cholesterol esters species compared to grade I glioma. Additionally, grade I glioma expressed phosphatidylserine species PSp 40:6, PSo 20:0, and PS 14:1 at greater relative abundances. Successful clustering noted in the heatmap validated the capability of the workflow to detect a broad range of lipid species across several lipid classes in small volume samples and apply captured lipid profiles to distinguish between glioma and brain around tumor.

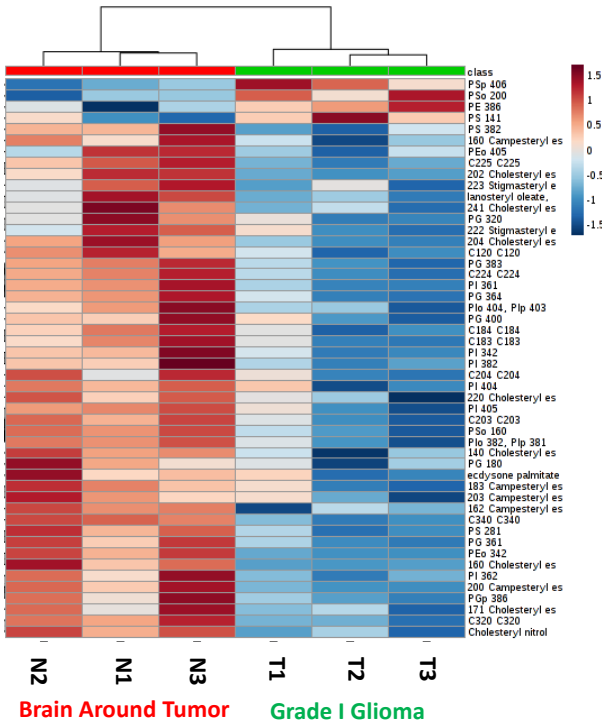

Figure 2.7 Heatmap cluster analysis demonstrates BAT have elevated relative abundances of free fatty acids and cholesterol-related lipids compared to grade I glioma. Grade I glioma maintained greater phosphatidylserine relative abundance.

2.4 Discussion

With the lack of improvement in glioma patient overall survival over the last decade, it is critical to find new approaches to identify new glioma biomarkers for therapeutic target identification. Doing so would provide valuable insight into potential formulation of novel treatment strategies or the repurposing of current FDA approved drugs toward better patient outcomes. Previous studies have shown differences in glioma and non-cancerous brain lipid composition through IMS methods, and have translated into improvements to diagnostics, not treatment[50,77]. Lipids are a highly complex, diverse biomolecule, despite having few structural components[78]. Maintenance of lipid composition in both healthy brain and glioma are essential to their functioning and survival, therefore, for clinically safe and effective application of lipid targeted therapies, comprehensive lipid profiling of both tissue types is required.

With our workflow, we hypothesized that we could profile a broad range of lipids using MRM-MS from small sample volume by LCM, through pathology-informed isolation, to interrogate heterogeneity between glioma tumor and neighboring brain. First, we have

demonstrated histological analysis can be applied to LCM to isolate discrete regions within sectioned glioma tissue. Sequential sections, 5μm apart, maintain a highly similar morphology, thus pathology-traced tumor regions are representative of that in unstained tissue.[54] Next, we established a sample dehydration process for LCM capable with lipidomics. Dehydration of samples is vital for successful LCM collection; proteomics and genomics workflows permit the use of ethanol for drying tissue, but not with lipidomics as lipids would be lost[79]. Desiccator-based dehydration was able to both adequately dry the tissue and preserve the lipids in the sample. Most notably, we verified LCM can be integrated with MRM-profiling to screen for lipids in small sample volumes. Consistent with previous lipidomics studies utilizing LCM, lipids were preserved in isolated tissue[67,70]. IR and UV laser pulses were non-damaging to the tissue morphology and molecular features. High ion signal was also detected during the screen step, indicating adequate sample was collected and MRM-MS is compatible with this workflow.

Our pilot study identified distinctions between grade I glioma and BAT samples using the M2 screening method. Metabolic reprogramming in glioma supports aberrant proliferation, concurrent with elevated lipid metabolism. Production of membrane lipids is important throughout proliferation to maintain membrane biosynthesis[26,80]. Grade I glioma maintained phosphatidylserine (PS), the most abundance anionic cell membrane lipid, a potential indicator of increased membrane synthesis[81]. PS are predominantly localized on the inner leaflet of the cell membrane in normal cells and translocate extracellularly when under oxidative stress[69]. Glioma, and other cancers, more commonly express PS on the outer leaflet of the membrane due to low flippase activity[82]. Recent studies have begun investigating PS as a potential imaging and therapeutic biomarker of this lipid class in glioma mouse models[81,83]. Free fatty acids were also found to maintain increased relative abundance in BAT compared to grade I glioma. This directly contrasts previous studies that have demonstrated unsaturated fatty acids were elevated in high grade gliomas[31,32]. Fatty acids are essential lipid building blocks; therefore, the decrease in free fatty acids could be explained by increased utilization of free FAs in lipid metabolism. The turnover rate of FAs in glioma could potential describe the lower expression compared to BAT.

This study validated the integration of diverse biological techniques to molecularly profile glioma and brain around tumor tissue for lipid abundance changes. Application of this workflow has potential to define differentially expressed lipids in glioma for therapeutic target identification. Current treatments fail to improve patient quality of life and overall survival, thus, there is a critical

need to identify lipid biomarkers to serve as targets. Our approach combines comprehensive lipid analysis with the capability to investigate tissue heterogeneity; two important features to elucidate glioma-specific lipids to further validate for clinical application.

2.5 Conclusions

The project's workflow supports the interrogation of lipid heterogeneity between glioma and BAT through the combination of diverse instrumental techniques. The pilot study validated the applicability of our integrated workflow to characterize glioma and BAT lipid profiles and perform statistical analysis to identify differentially expressed lipids. Preliminary data indicated, glioma and BAT groups maintained distinct lipid composition, noted by cluster localization differences on the PCA plot (Figure 2.6). Additionally, the two tissue types in the cluster analysis were clearly differentiated from one another, visually represented in the heatmap (Figure 2.7). PS, free fatty acids, and cholesterol esters were important lipids to distinguish between glioma and BAT. Initial findings highlight the potential importance of membrane-related lipids to the glioma disease state with elevated PS relative abundance. Lipid profiles will be further investigated, using the workflow established in the pilot study, in 13 patient samples across tumor grades I-IV to identify the extent of their alterations as glioma progresses towards malignancy. Changes to BAT lipid composition will also be examined to elucidate the influence of tumor grade on lipid expression. Lastly, this approach will be utilized to distinguish between glioma and BAT tissue, to discover glioma-specific lipids for future validation as a therapeutic target.

3 GLIOMA GRADE LIPID PROFILE ANALYSIS USING MULTIPLE REACTION MONITORING MASS SPECTROMETRY

3.1 Introduction

Glioma is a rapidly progressing form of brain cancer. The aggressiveness of this tumor increases with each grade, noted by aberrant proliferation, diffuse infiltration, and drug resistance. Migration of glioma cells from the original lesion makes complete tumor resection impossible, raising the likelihood of further progression and recurrence. Additionally, targeted radiotherapy stereotactically localized at the tumor lesion site fails to impact invading neoplastic cells in deeper in the brain. The invasiveness of glioma has been identified as early as grade II tumors; an attribute commonly attributed to higher grade tumors[84]. Taken together with the propensity of low-grade gliomas to undergo malignant transformation, failure to resect and treat glioma at early stages inclines patients toward eventual presentation of the deadliest form of glioma, GBM. Targeting glioma at lower grades is an appealing strategy as the tumor does not possess many of the attributes which make higher grade gliomas largely untreatable. Low grade glioma patients live, on average, 7 years after diagnosis compared to 15 months with GBM patients. Maintaining glioma at less aggressive grades has the potential to better both response to treatment and patient overall survival. However, characterization of low-grade glioma molecular profiles remains largely undefined. Rapid progression of gliomas has limited the availability of datasets investigating lower grade gliomas, like grades II and III, as patients predominantly present with GBM the most common high-grade glioma[85]. Therefore, it is critical to address the gap by profiling lipids across all glioma grades to identify lipids vital to the progression progress and use as potential targets to prevent malignant transition, improving patient outcomes.

In this research, tissue from glioma grades I-IV were isolated to define lipid profiles throughout stages of the disease to identify key lipid classes driving malignant progression. Throughout progression, cancer cells reprogram their metabolism toward lipid biosynthesis to support proliferation, migration, and metastasis[86]. Lipid concentration was found to increase with tumor grade when quantified by proton magnetic resonance spectroscopy highlighting the importance of this biomolecule to disease pathology[87]. Despite this understanding, the diverse glioma lipidome remains to be unutilized therapeutically in the clinic. This can be attributed to

multiple factors including lack of comprehensive definition of glioma lipids, their associated synthesis pathways, and glioma-specific lipid biomarkers to serve as targets.

Lipidomic approaches using imaging mass spectrometry have recently been utilized to characterize glioma lipid composition for subtype discrimination, noting distinctions in sulfatides, PS, and PI lipid classes[51,88]. The capability of IMS to interrogate the lipid distribution in a heterogeneous sample, like glioma, providing relevant tumor-specific molecular information to support lipid biomarker identification. IMS has made great strides in areas of diagnostics and intraoperative applications through its rapid, non-damaging classification of tissue, while also providing the groundwork for future mass spectrometry-based lipidomic approaches to investigate glioma lipids[6]. This project seeks to build off of these findings by applying a MS approach with a broader detection range to more expansively define distinct lipid species within each grade of glioma, while also probe for heterogeneity in glioma tissue.

To analyze lipids across grades of glioma, laser capture microdissection (LCM) was integrated with multiple reaction monitoring-mass spectrometry (MRM-MS) to better understand and profile glioma lipid heterogeneity. LCM has previously been combined with liquid chromatography-mass spectrometry (LC-MS) to perform lipidomics on both brain and liver tissue[67,70]. Application of LCM supports specific acquisition of glioma tissue within sectioned tissue. Glioma grows asymmetrically in the brain, therefore, resected tissue commonly maintains a level of non-cancerous brain[89]. The non-damaging, precision excision of samples will preserve molecular features in the tissue while isolating regions of interest for analysis. MRM-MS is a rapid profiling approach suited for comprehensive lipid analysis in small sample volume. Detection relies on chemical components and molecular features of the molecular, rather than abundance, supporting MRM-MS application possible with just a few to several hundred cells[41]. MRM can profile lipids of most classes through established methods tailored for a specific tissue type to identify lipids implicated in glioma progression. This is critical as lipid metabolism and species produced throughout glioma malignant transition is not well understood.

In this study, MRM-MS was used to comprehensively define lipid profiles across glioma grades, broadening the range of detected lipids, to better understand lipid composition at each stage of progression. Results revealed distinctions in lipid profiles between low- and high-grade glioma, indicating several lipids species potentially promoting disease progression.

3.2 Methods

The methods employed for sample selection, histological analysis, LCM, lipid extraction, MRM-profiling, and data processing for glioma samples in this experiment are outlined in Section 2.2 Analytical design. A total of 32 tumor samples were analyzed from glioma grades I-IV: grade I (n=5), grade II (n =12), grade III (n = 9), and grade IV (n = 6). Sample information is provided in Table 2.3. Glioma samples and lipids were extracted and profiled concurrently with BAT lipids, which are discussed in Chapter 4. Following lipid data acquisition, relative abundances from tumor samples were sorted separately from BAT, and analyzed by Metaboanalyst 4.0 (https://www.metaboanalyst.ca/). Three methods were applied to profile lipids, M1 and PC are detailed in Results below. The M2 method results are included in Appendix B.

3.3 Results

3.3.1 Lipid profiles by glioma grade

Principal component analysis (PCA)

Distinct clusters between glioma grades lipid composition profiled by MRM were indicated in PCA plots filtered for lipids with VIP scores ≥ 1 (Figure 3.1). PC method showed greater discrimination of tumor grade clusters compared to the two embryo methods M1 and M2 (Figure 3.1B). Grade I glioma clusters (red) in both methods localized separately to higher grade groups indicating differential lipid expression. Cluster separation between grade I and grade IV groups were also strong in each method demonstrated by separate areas of the plot. Distinctions, albeit slight, between grade II and grade III glioma were noted using the PC method indicated by the shift in the plot. There was a notable trend of small glioma grade cluster localization shifts in the PC method plot. Slight shifts in localization of the grade clusters suggests more specific, rather than general, changes to the lipid profile. Overall, PCA plots demonstrate PC and SM lipids detected using the PC screening method were effective lipid classes to discriminate changes in glioma grade lipid profiles.

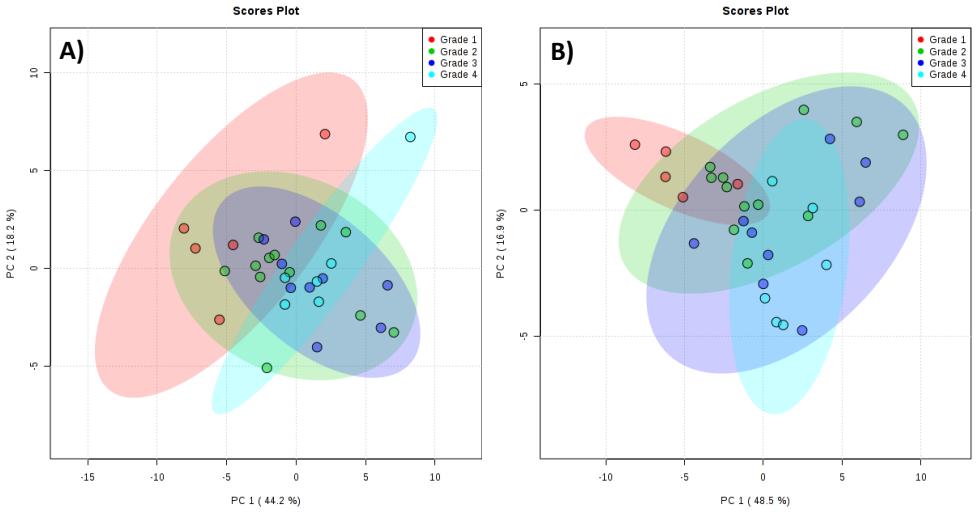

C)

Profiling Method	PC1 (%)	PC2 (%)
M1 Method	44.2	18.2
PC Method	48.5	16.9

Figure 3.1 PCA plots indicated distinctions in glioma lipid profiles according to PC1 and PC2 in two MRM screening methods. A) M1 method. B) PC method C) PC1 and PC2 scores for both screening methods.

Analysis of variance (ANOVA)

ANOVA analysis determined three significantly different lipids in M1 method and ten lipids in PC method between grades of glioma (Table 3.1). PC and SM lipids, across both methods, comprised the majority of differentially expressed lipids in tested tumor samples. High unsaturated PC species, PC 36:5 and PC 38:5, were significantly greater in grade I tumor samples compared to other grades, a trend that was noted in both methods. Several grade-specific lipids were identified in the samples. PC 34:2, PC 36:3, and SM d16:1/24:0 maintained significantly higher relative abundances in grade IV samples compared to the three lower grades. PC 36:1 and SM d 18:0/22:0 relative abundances was significantly greater in grade III samples vs other grades. Lastly, grade II possessed significantly higher SM d18:0/18:0 relative abundance to other grades. Greater expression of several PC and SM species in grade III and IV samples indicate potential critical lipids species to high grade tumor progression. Conversely, greater PC 36:5, PC 38:5, and SM d18:0/18:0 expression in grades I and II highlight species that are distinct to low grade glioma and could potentially serve as targets to disrupt progression. Significant lipids shared between M1 and PC methods are further described in Appendix B Figure B.3.

Table 3.1 ANOVA computation of lipids with significantly different relative abundances between glioma grades.

Lipid Species	f.value	p.value	-log10(p)	FDR	Fisher's LSD
M1					
PC 38:5	13.637	1.14E-05	4.9425	0.0010845	Grade 1 - Grade 2; Grade 1 - Grade 3; Grade 1 - Grade 4
PC 36:5	10.995	6.06E-05	4.2177	0.0028776	Grade 1 - Grade 2; Grade 1 - Grade 3; Grade 1 - Grade 4
O-17-carboxyheptadecanoylcarnitine	9.2628	0.00020327	3.6919	0.0064369	Grade 1 - Grade 2; Grade 1 - Grade 3; Grade 1 - Grade 4
PC					
PC 38:5	52.306	1.34E-11	10.874	1.35E-09	Grade 1 - Grade 2; Grade 1 - Grade 3; Grade 1 - Grade 4
PC 36:5	21.905	1.66E-07	6.7793	8.39E-06	Grade 1 - Grade 2; Grade 1 - Grade 3; Grade 1 - Grade 4
PC 36:2	12.86	1.83E-05	4.7381	0.00061531	Grade 2 - Grade 1; Grade 3 - Grade 1; Grade 4 - Grade 1; Grade 3 - Grade 2; Grade 4 - Grade 2
SM d16:1/24:0	12.062	3.02E-05	4.5207	0.00076135	Grade 4 - Grade 1; Grade 3 - Grade 2; Grade 4 - Grade 2; Grade 4 - Grade 3
SM d18:0/22:0	10.991	6.07E-05	4.2166	0.0012267	Grade 3 - Grade 1; Grade 4 - Grade 1; Grade 3 - Grade 2; Grade 3 - Grade 4
PC 36:1	10.463	8.69E-05	4.0608	0.0014633	Grade 2 - Grade 1; Grade 3 - Grade 1; Grade 3 - Grade 2; Grade 3 - Grade 4
PC 36:3	9.6165	0.00015742	3.8029	0.0022714	Grade 3 - Grade 1; Grade 4 - Grade 1; Grade 4 - Grade 2; Grade 4 - Grade 3
SM d18:0/18:0	8.7164	0.00030444	3.5165	0.0035485	Grade 2 - Grade 1; Grade 2 - Grade 3; Grade 2 - Grade 4
PC 36:8	8.6659	0.0003162	3.5	0.0035485	Grade 1 - Grade 2; Grade 1 - Grade 3; Grade 4 - Grade 2
PC 34:2	5.6289	0.00378	2.4225	0.038178	Grade 4 - Grade 1; Grade 4 - Grade 2; Grade 4 - Grade 3

Cluster analysis (Heatmap)

Cluster analysis visualized distinctions between glioma grade groups (Figure 3.2). The heatmap for M1 of the top 13 indicated separation between lower two grades (I & II) and higher grades (III & IV) based two factors, carnitines and differences in PC saturation. Most grade I and II samples possessed greater relative abundances of carnitine and high unsaturated PC lipids species, clustering to the right of the plot, compared to grades III and IV. Conversely, distinction between higher grade samples was determined by greater expression of low unsaturated PC 36:1 and saturated SM d18:0/22:0. Grades III and IV, clustered to the left of the plot expressed low relative abundance of carnitine and high unsaturated PC species which distinguished them from the lower grades. The PC heatmap was separated into three clusters based off the top 5 lipids displayed. Grade I, clustered together in the center, maintained consistently higher relative abundance of PC 36:5 and PC 38:5. Grade II expressed low levels of each of the five lipids in the plot and clustered to the right. Grades III and IV had greater relative abundances for PC and SM species PC 36:2,

SM d16:1/24:0, and SM d18:0/22:0, clustering both grades to the left. Taken together, PC and SM lipid species can aid in distinguishing lower-grade and higher-grade gliomas.

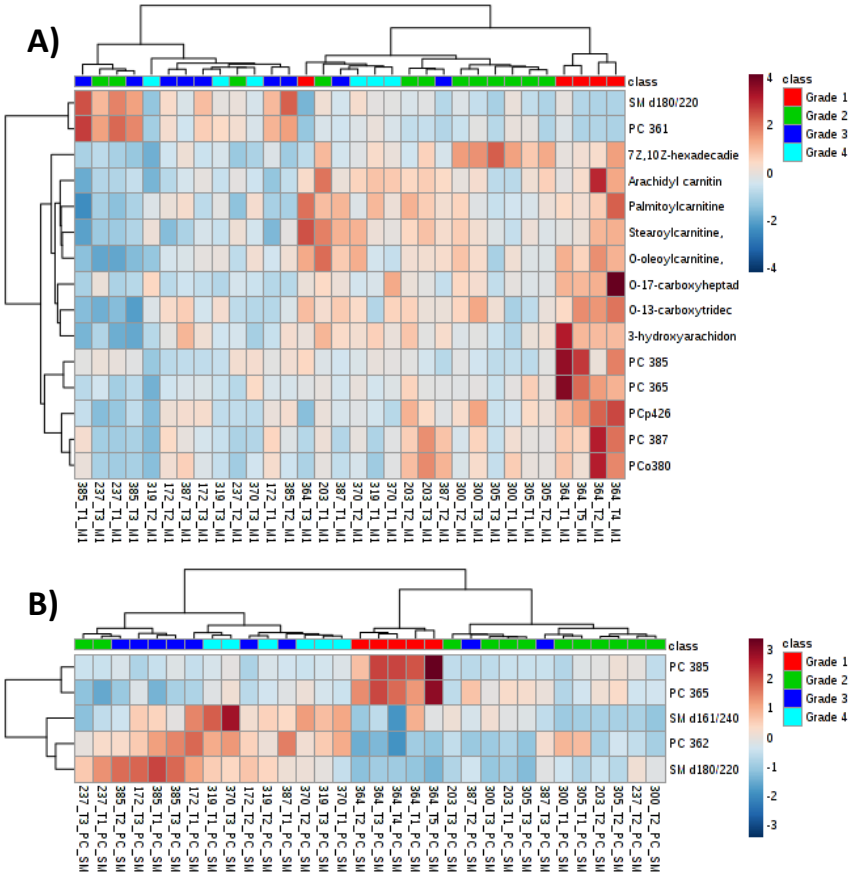

Figure 3.2 Heatmap cluster analysis indicated PC and SM lipids distinguished between lower grade (I & II) and higher grade (III & IV) gliomas. A: M1 method. B: PC method.

3.3.2 Low grade vs high grade lipid profiles

PCA

Principal component analysis of low- and high-grade glioma lipids, with a VIP score ≥1, indicated discrimination between tissue type lipid profiles in the PC method (Figure 3.3). The M1 method, comprised of mainly of PC, SM, TAG, and carnitines, showed negligible separate between tumor grades, suggesting embryo method lipids were unable to differentiate between groups. The PC method, comprised entirely of PC and SM species, demonstrated a trend of discrimination between low- and high-grade glioma groups based on lipids in these two classes (Figure 3.3B). Proximity, but not overlap, of points on the PC method PCA plot suggests comparable lipid profile with the

exception of a few lipid species. Similar lipid profiles were noted between grades II and grade III tissue, based on lipids included in the PC method, when comparing samples by grade, and could account for the similar localization of groups in the PC PCA plot.

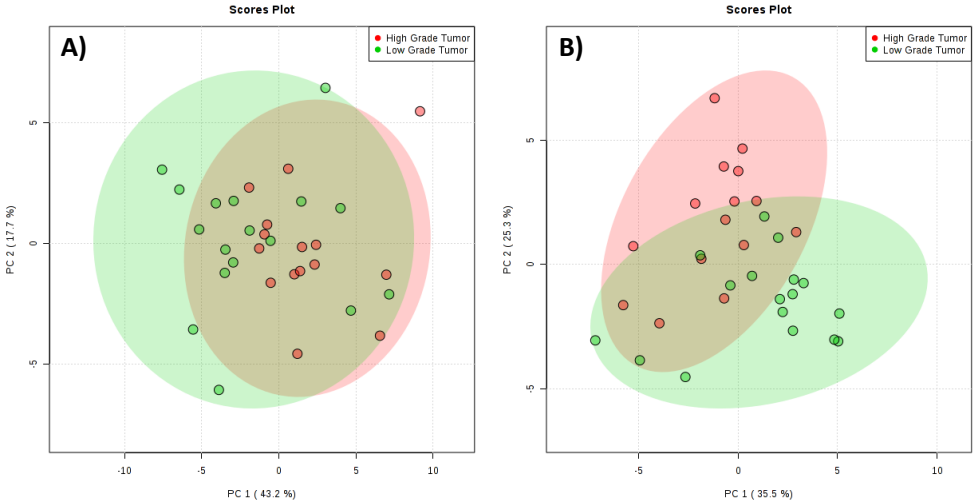

C)

Profiling Method	**PC1** (%)	**PC2** (%)
M1 Method	43.1	17.1
PC Method	35.5	25.3

Figure 3.3 PCA plot revealed low- and high-grade glioma discrimination trend using PC and SM detected in the PC screening method. A) M1 method. B) PC method. C) PC1 and PC2 scores for both screening methods.

T-test

T-test analysis of lipid relative abundance distinctions between low- and high-grade glioma samples revealed four significantly differentially expressed lipids (Table 3.2). Significant lipids consisted entirely of PC and SM class lipids, similar to that seen in by grade analysis (Table 3.1). Each of the four lipids were significantly higher in high-grade samples compare to low grade. Differentially expressed PC lipids shared similar composition, having the same number of carbons and are both unsaturated. Significant SM species also shared similar structural features, being both saturated and long chain SMs. Taken together, unsaturated PC lipids and long, saturated SM highlight distinct lipids species as glioma transitions from low to high grade, indicating lipid species and their compositional features that could be indicative of malignant glioma.

Table 3.2 Significant PC method screened lipids between low- and high-grade glioma

Lipid Species	t.stat	p.value	-log10(p)	FDR
PC 36:2	5.1283	1.62E-05	4.79	0.0016379
SM d16:1/24:0	4.4889	9.82E-05	4.0079	0.0038268
SM d18:0/22:0	4.4366	0.00011367	3.9444	0.0038268
PC 36:3	3.7143	0.00083184	3.08	0.021004

Cluster analysis (Heatmap)

Cluster analysis identified distinctions between low- and high-grade tumor groups in both M1 and PC MRM-screening methods (Figure 3.4). Discrimination between tumor groups in the M1 method was driven by differential expression of two lipid classes, phosphatidylcholines and carnitines (Figure 3.4A). The top 5 distinguishing lipids indicated PC and carnitine species maintained higher relative abundance in low-grade tumor compared to high-grade tumor. As tumor progresses, a diminished expression pattern was noted for these lipids; suggesting several outcomes, the species are being converted into different lipid species not screened for in this method and/or lipid biosynthesis is altered to produce different lipid species or classes. Low- and high-grade tumor groups were also discriminated in the PC screening method due to relative abundances distinctions of two lipid classes, PC and SM (Figure 3.4B). Top 5 lipids used to cluster glioma groups maintained higher relative abundances in high-grade tumors vs low-grade. PC lipids differentially expressed in high-grade tumors were all classified as unsaturated (one or more double bonds) and maintained identical 36-carbon chain length structure. Additionally, differentially expressed SM species possessed similar structural features. The SM species were classified as saturated and long-chain length lipids, based on the chain length parameters set in this study. Taken together, the result highlight PC and SM species maintain distinct relative abundance between low- and high-grade gliomas. Even further, alterations to lipid chain length and saturation could also be a factor during high grade glioma transition.

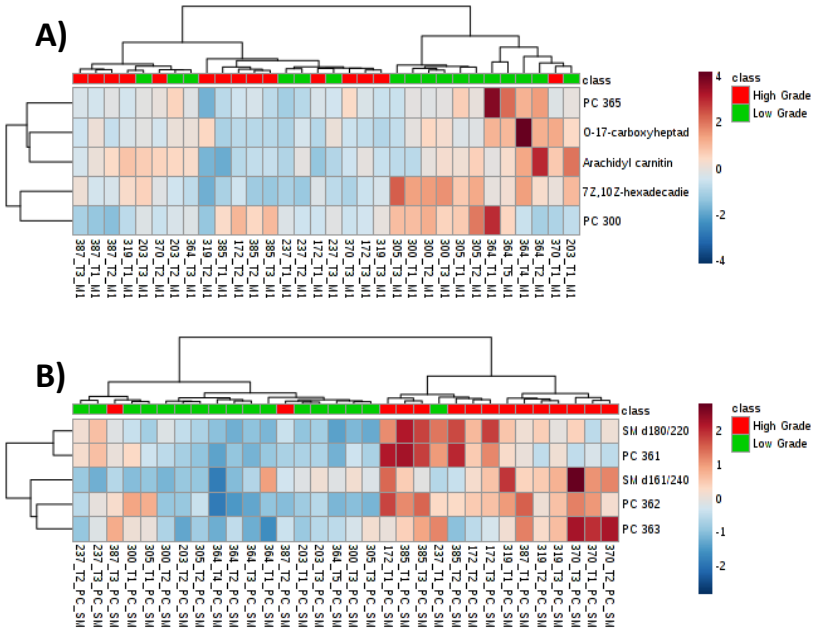

Figure 3.4 Heatmap analysis showed distinctions between low- and high-grade gliomas clusters by differential expression of PC, SM, and carnitine lipid species. A) M1 method. B) PC method.

Lipid chain length and saturation analysis

Lipid chain length and saturation analysis identified distinction between low- and high-grade glioma based on these chemical features. Of note, PC and SM lipid classes were the only lipid classes found to be maintained at significantly different average sum relative abundances between tumor groups. PC lipids showed a shift in saturation status as the disease progressed from low- and high-grade. Low-grade glioma expressed significantly higher saturated average sum PC relative abundance (Figure 3.5A, $p \leq 0.05$). Additionally, high-grade gliomas were comprised of significantly greater low unsaturated average sum PC relative abundance (Figure 3.5B, $p \leq 0.05$), determined by the non-parametric Dunn's test. High-grade gliomas also maintained significantly higher of two types of SM. Low unsaturated SM were found to have a significantly greater expression in high-grade vs low-grade glioma (Figure 3.5C, $p \leq 0.05$). Lastly, long-chain SM were the most differentially expressed lipid subtype between low- and high-grade gliomas of all the lipids sampled (Figure 3.5D, $p < 0.0001$). In summary, PC and SM saturation state and chain length were important chemical features to consider when classifying progression of glioma as distinctions in relative abundances were identified.

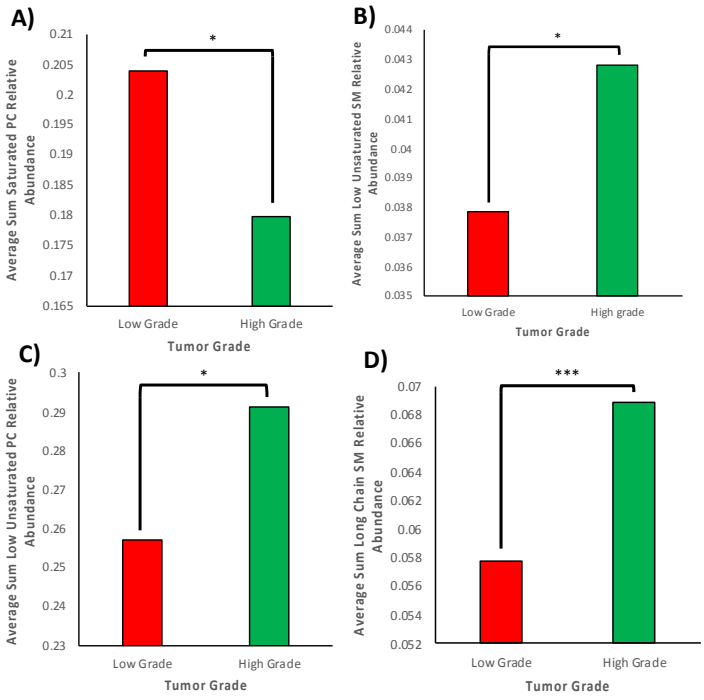

Figure 3.5 Chain length and saturation analysis identified significantly different PC and SM relative abundances between low- and high-grade glioma. A) Saturated PC, B) low unsaturated SM, C) low unsaturated PC, D) long chain SM. *p≤ 0.05, ***p≤ 0.0001

Receiver operating characteristic (ROC)

To determine the diagnostic ability of MRM-profiled lipids to distinguish between low- and high-grade glioma, ROC curve analysis was performed (Figure 3.6). Across both methods, five lipids were identified to maintain an area under the curve (AUC) ≥ 0.8. The AUC above 0.8 is a threshold standard set to be considered potentially clinically applicable upon further validation. Each of the five lipids had greater relative abundances in high grade tumors. Three PC lipids, PC(36:1), PC(36:2), and PC(36:3), possessed an AUC ≥ 0.8; sharing similar chemical characteristics as each are 36-carbons in length and are unsaturated (Figure 3A-C). Additionally, two SM species, SM d(16:1/24:0) and SM d(18:0/22:0) were identified with AUC ≥ 0.8. Both SM species were saturated and long chain in structure. Four of the five lipids with an AUC ≥ 0.8 maintained significantly different relative abundances, with the exception of PC(36:1). To conclude, ROC curve analysis showed discrimination between low- and high-grade glioma based on higher relative abundance of five PC and SM species.

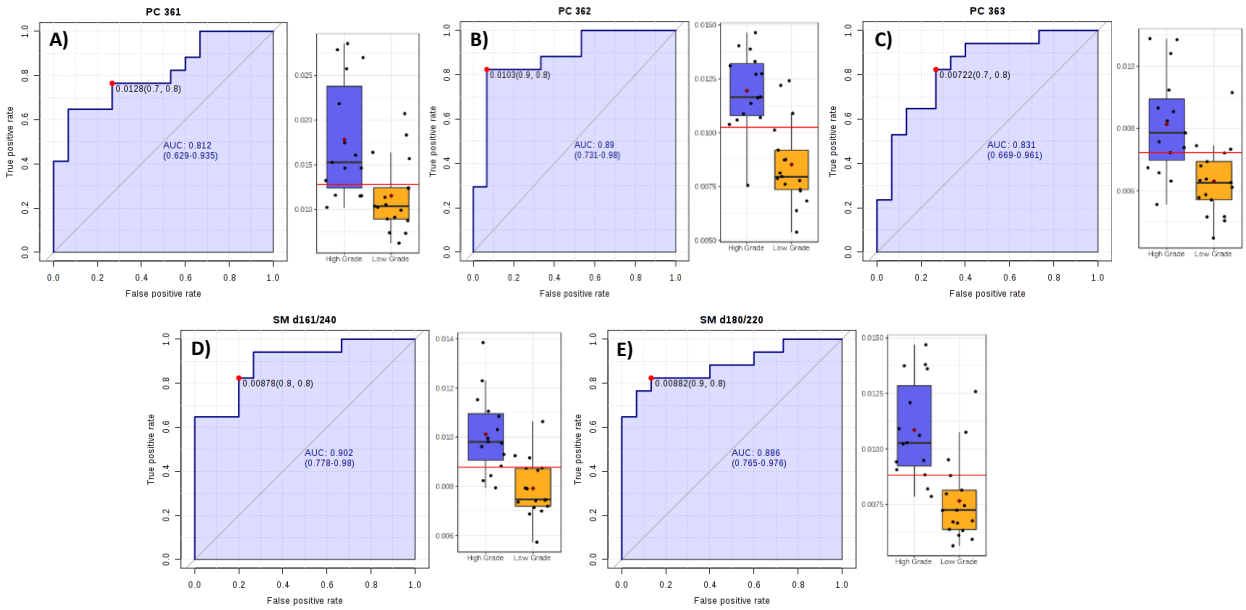

Figure 3.6 Univariate ROC curves for PC method screened lipids identified differential expression of PC(36:1, 36:2, and 36:3) and SM(d16:1/24:0 and d18:0/22:0) between low- and high-grade glioma groups.

The capacity of the five PC method screened lipids with AUC ≥ 0.8 to distinguish between tumor groups was evaluated and showed strong discrimination power (Figure 3.7). This analysis is performed by testing lipids with AUC ≥ 0.8 together in the model, and through use the combination of lipids species, determine the ability of the lipids to distinguish between glioma groups. The tester analysis combining lipid information yielded an AUC of 0.932. Utilization of these five lipid species highlighted their sensitivity in distinguishing tissue types as each was differentially expressed in high-grade glioma tissue.

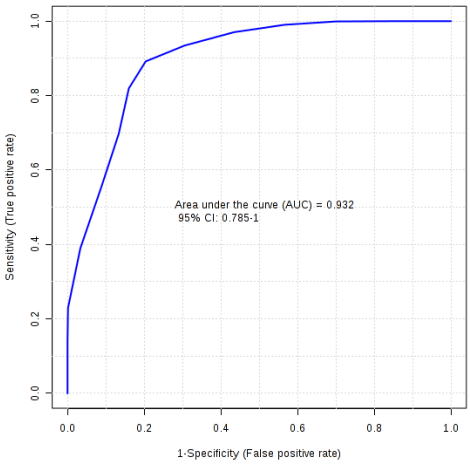

Figure 3.7 Strong discrimination power of most differentially expressed lipids to distinguish between glioma groups.

3.3.3 Glioma grade 2 vs grade 3

PCA

Principal component analysis identified a trend of discrimination between grade II and III clusters (Figure 3.8). Twenty-six lipids possessed a VIP score ≥ 1 in this model and were considered in the plot. M1 and PC methods displayed a slight shift in point localization on the plot suggesting a change in lipid profiles between glioma grades. Clusters were proximal to one another indicating the distinctions in lipid composition were isolated to specific lipid species rather than more general expression. To conclude, multivariate analysis showed more minute changes to lipid species expression were present between grade II and III glioma.

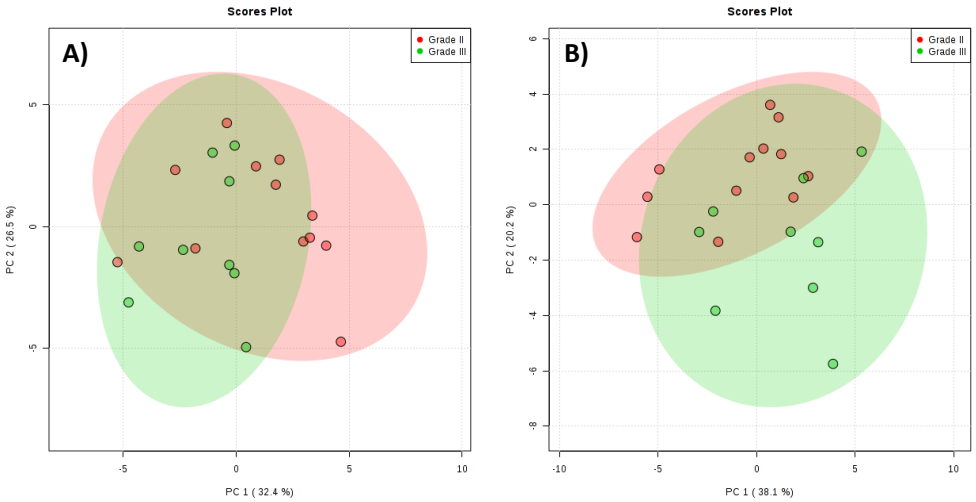

C)

Profiling Method	**PC1** (%)	**PC2** (%)
M1 Method	32.4	26.5
PC Method	38.1	20.2

Figure 3.8 Discrimination of grade II and grade III glioma by M1 and PC screening methods in PCA plot. A) M1 method, B) PC method, C) PC1 and PC2 scores for both screening methods.

Cluster analysis (Heatmap)

Cluster analysis identified distinctions between grade II and grade III glioma groups in both M1 and PC screening methods (Figure 3.9). M1 method discriminated gliomas grades with differential expression of three lipid classes: PC, SM, and carnitines. The heatmap of the top 12 lipids demonstrated grade II gliomas were clustered together based on increased relative abundance of carnitine species and low unsaturated PC relative abundance (Figure 3.9A). Grade III glioma clustered based on elevated relative abundance of unsaturated PC species PC(36:8) and PCo(34:1 and 36:1) and low relative abundance of carnitine species. Discrimination between grades II and III was noted in the PC heatmap based on differential expression of PC and SM species (Figure 3.9B). Grade II glioma clustered together due to elevated relative abundance of medium chain SM, which contain between 17 to 21 carbons in their structure. Grade III glioma were distinguished by higher relative abundance of low unsaturated PC(36:1, 36:2, and 38:2) and long chain SM(d18:1/24:0, d16:1/24:0, d18:1/24115z, and d18:0/22:0). Taken together, grade II and grade III were distinctly clustered based on differential expression of low unsaturated PC and long chain SM lipids.

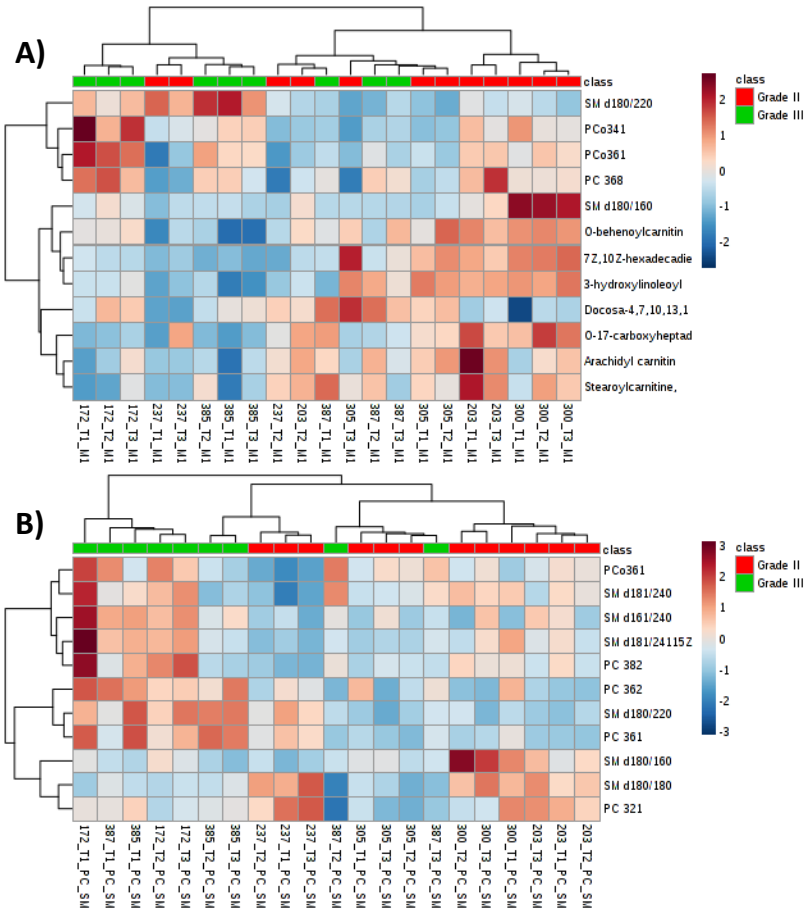

Figure 3.9 Heatmap analysis demonstrated distinct grade II and II clusters based on differential expression of PC, SM, and carnitines across two MRM-profiling methods. A) M1 method, B) PC method.

Receiver operating characteristic (ROC)

ROC curve analysis evaluated discriminating capacity of MRM-profiled lipids and identify lipids with an AUC ≥ 0.8. Six lipids were determined to be above the standard AUC threshold indicating applicability to differentiating glioma grades in this model (Figure 3.10). Five of six species expressed greater relative abundances in grade III glioma compared to grade II. Discrimination between glioma grades was based on differential expression of lipids in PC and SM classes. Two unsaturated PC(36:1 and 36:2) species were identified as discriminant. Additionally, four SM were found to be strong discriminating factors. Long chain SM(d18:1/24:0, d16:1/24:0, d18:1/24115z, and d18:0/22:0) were discriminant lipids with higher expression in grade III tumors. SM(d18:0/18:0), classified as a medium chain SM, was the only lipid expressed higher in grade II. In summary, low unsaturated PC and long-chain SM were discriminant species to identify grade III vs grade II, indicating a shift in PC and lipid structure between grades.

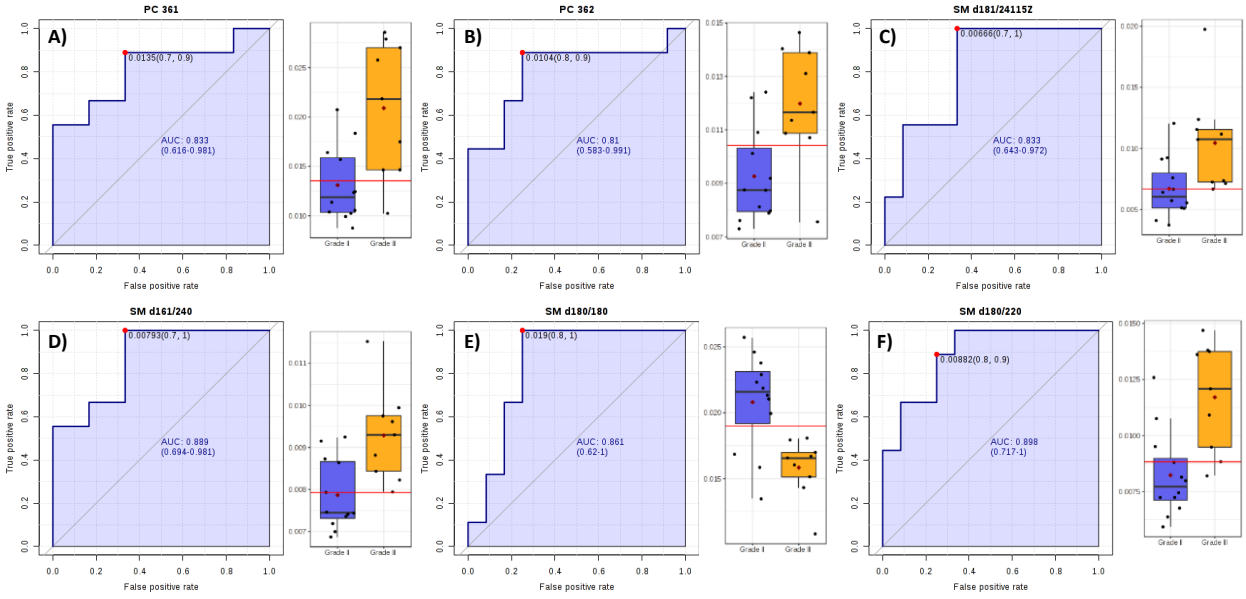

Figure 3.10 Individual ROC curves of PC and SM species with distinct relative abundances that discriminate between grade II and III glioma.

The combined discriminating capacity of lipids with AUC ≥ 0.8 to discern different tumor grades was also evaluated. Combining lipid information of these six lipids possessed strong distinguishing ability, achieving an AUC score of 0.987. Applying the combination of six lipids to sample

prediction yielded no incorrect labeling of glioma grade highlighting the high accuracy when discriminating between groups.

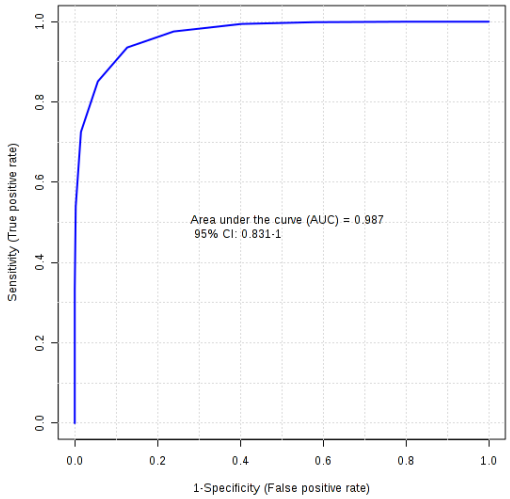

Figure 3.11 Strong discriminating capacity of PC and SM species with AUC ≥ 0.8 to correctly label between glioma grades II and III.

3.4 Discussion

Due to the importance of lipids to supporting glioma growth, driven by metabolic reprogramming toward lipid biosynthesis, it is critical to investigate changes in lipid profiles as the disease progresses. In this study, 32 glioma samples across all four grades were screened by three MRM-profiling methods, M1 and M2 (embryo) and PC (phosphatidylcholine and sphingomyelin), to detect distinctions in lipid composition through malignant transition. Profiling data was processed to analyze lipid differences between individual grades, low- and high-grade, and grade II and III that are relevant to glioma progression. Significant distinctions in lipid profiles as glioma progresses to higher grades were observed.

Lipid profiles between individual glioma grades were observed to express significantly different compositions of phospholipid species. Phospholipids are integral structural components of cell membranes and have been linked to cellular processes like signaling and proliferation[90]. Literature has also identified altered expression of phospholipids in glioma tumors[91]. Phosphatidylcholine, a class of phospholipid comprised of a choline head group, glycerolphosphoric acid, and fatty acids, species were observed to effectively differentiate between glioma grades[92]. Constantin and colleagues determined choline metabolites within the PC

synthesis pathway were effective in distinguishing between low grade glioma and higher grades III and IV, noting a grade-related increase in level of these species[93]. Elevated total phosphatidylcholine and associated metabolites, due to aberrant phospholipid metabolism, were identified to be hallmarks of cancer cell molecular profiles. Increased expression of choline-containing phospholipids has been purported to be connected to malignant transformation in cancer[94]. Studies targeting phosphatidylcholine-specific phospholipase C (PC-PLC) produced lower total PC content, loss of mesenchymal phenotype, and diminished migration in cancer cells[95]. Previous studies demonstrating the importance of PC lipids to aggressive cancer phenotypes warrants further characterization of phospholipid metabolism for therapeutic application.

Multivariate analysis indicated slight shifts in glioma grade clusters suggesting subtler changes to lipid profiles occur during disease progression. Grade I glioma clustered most discriminately from other grades due to expression of grade-specific lipids PC(36:5 and 38:5). Being the most benign form of glioma and least likely to progress, patient outcomes are favorable when presenting with this tumor[4,12]. Relative abundances of PC(36:5 and 38:5) were observed to decrease with each increase in tumor grade. Diminished relative abundance of these two PC species differs from the trend denoted in literature that PC concentration is greater in malignant glioma stages, as this perspective does not account for alterations to individual species within this lipid class. Instead, our findings support the trend that changes to PC species distinct between glioma grades is concurrent with increase in total PC concentration. This study identified several unsaturated, grade-specific PC species highlighting these alterations (Table 3.1). Elevated levels of unsaturated membrane phospholipids, like PC, were identified to promote membrane fluidity and tumor invasion, an acknowledged aggressive characteristic of glioma[32,96]. Increased expression of unsaturated PCs in glioma are maintained due to aberrant levels of unsaturated free fatty acids present in malignant glioma cells[31,97]. Acetyl-CoA carboxylase (ACC) and fatty acid synthease (FAS) regulate fatty acid synthesis and are overexpressed in GBM tumor, driving aberrant FA synthesis[98]. Targeted inhibition of these proteins was observed to hinder cancer cell growth, effectively lowering available free fatty acids[99]. As high-grade glioma in this study maintained differential expression of unsaturated PC species, focusing on altering lipid saturation status presents as an appealing strategy to impede glioma progression and invasion in the brain.

Shift in lipid saturation indicates cells are adapting to current microenvironmental as well as intracellular conditions. In the context of cancer, altering lipid saturation incurs benefits in aspects of drug and oxidative stress resistance as well as cell motility[86]. Due to gliomas high metabolic demands and proliferation rate, elevated levels of reactive oxygen species (ROS) are produced. Accumulation of ROS can result in oxidative-stress induced cell death, therefore, cancer cells alter FA saturation to limit this outcome[100]. Cancer increases resistance to oxidative stress, induced by factors such as hypoxia, lipid peroxidation, and metabolic reprogramming, by increasing levels of saturated and monounsaturated fatty acids[101]. These two FA saturation types provide greater resistance to ROS-induced stress than poly-unsaturated FAs, and cancer increases de novo fatty acid synthesis if conditions are suitable to adapt to cytotoxic conditions. Cancer also becomes more drug resistant by modulating membrane lipid saturation[101]. Increasing membrane saturated fatty acid concentration alters membrane dynamics; reducing the fluidity of the membrane by more densely packing lipids decreases drug uptake, thereby diminishing treatment efficacy. Lipid unsaturation in cancer promotes increased membrane fluidity allowing for greater mobility[102]. Therefore, migrating cancer cells will likely express greater concentration of poly-unsaturated lipids within the membrane compared to non-migratory cancer cells. Altering lipid saturation provides glioma with flexibility to adapt to traditionally cytotoxic stressors, allowing cancer to survive the suboptimal condition and eventually further progress the disease by migrating deeper into tissue. Modulating lipid saturation state could be an attractive aspect to explore as a therapeutic target as maintaining proper lipid saturation type is crucial for glioma survival.

Analysis also detected differential expression of sphingomyelin species between grades. Similar to PC lipids, SM are responsible for modulating membrane fluidity and structure, but also are a component of lipid rafts[103]. Lipid rafts are microdomains that coordinate signal transduction in the membrane and increased expression were found in tumors[104,105]. SM species contained in lipid rafts are predominantly classified as long-chain and saturated[106]. Our results observed saturated, long-chain SM maintain greater relative abundances in high-grade glioma, suggesting potentially greater lipid raft expression in malignant glioma. Glioma tumors have highly deregulated signaling pathways that support growth, and elevated lipid raft expression could be promoting this pro-tumorigenic behavior[107]. Receptor-mediated signaling initiated at lipid rafts have been implicated to stimulate both ACC and FAS for production of fatty acids later used to generate phospholipids[7,105,108]. Therapeutics targeting lipid rafts are currently in development;

simvastatin, a cholesterol-lowering drug, treated glioma cells targeting this microdomain suppressed tumor migration[109,110]. Cholesterol is important not only to normal brain functioning and composition, but for glioma as well. In healthy brain, cholesterol is predominantly localized within both brain neural and glial cell plasma membranes and as a structural component of neuron myelin sheaths[24]. Glioma maintain high demand for cholesterol sustain oncogenic processes such as elevated proliferation, survival, and cell signaling[108]. As a membrane component, cholesterol supports formation of lipid rafts previously identified to be critical for driving tumorigenesis[111]. Studies have identified elevated lipid raft expression in several cancer types, highlighting a viable therapeutic target to consider. Current statin trials postulate reducing the available cholesterol within glioma cells will decrease lipid rapid formation, thereby hindering various oncogenic signaling initiated at these sites and inhibit further tumor growth[110]. In-vitro studies have shown treating glioma cells with simvastatin, a clinically approved statin capable of crossing the blood brain barrier, reduced proliferation and migration, while also inducing apoptosis[112]. Modulating cholesterol within glioma produced anti-tumor effects, highlighting a vulnerability to target. Further research has discovered glioma relies on exogenous sources of cholesterol to satisfy demands, due to their inability to perform de novo cholesterol synthesis, implicating the surrounding brain in supporting tumor growth[113,114]. In this study, broader lipid profiling of both glioma and surrounding brain will elucidate additional lipid classes, supplemental to cholesterol, that are potentially provided by brain around tumor to support tumor growth. Profiling lipid classes such as phospholipids and sphingolipids, two components of lipid rafts, will highlight potential novel biomarkers to target and dysregulate oncogenic signaling that supports tumorigenesis in glioma. Further investigation into effective targeted approaches to disrupt lipid rafts is needed, and our results highlight long-chain SM as an additional lipid classes to consider as targets.

This study demonstrated that membrane lipids PC and SM were differentially expressed across glioma grades. Distinct lipids detected by MRM-profiling improved the understanding of lipid profile changes throughout glioma progression. Better definition of glioma lipid composition at each glioma grade elucidates potential therapeutic biomarkers to target and hinder malignant transition. Preventing high-grade progression can improve overall survival and clinical outcomes for glioma patients, which are aspects that current therapeutics fail to achieve. MRM-profiling provides both the sensitivity and comprehensive lipid analysis needed to identify targetable lipid

pathways. This study introduces several lipids species to investigate further for therapeutic application.

3.5 Conclusions

MRM-profiling identified differential expression of PC and SM species throughout glioma progression. Subtle, rather than general, changes to lipid composition were observed between tumor grades. 11 individual PC and SM species were found to be significantly different between grades, 8 of which were grade specific (Table 3.1). PC and SM saturation and chain length differences were also identified, with high grade possessing greater low unsaturated PC and long-chain SM (Figure 3.5). Lastly, ROC curve analysis indicated significant PC and SM maintained strong discriminating power to distinguish between low- and high-grade groups and also grade II and grade III. In summary, MRM-profiling elucidated phospholipids PC and SM, especially those with unsaturated composition, as critical lipid species during glioma progression. This study provided insight into critical lipids to further investigate to validate for therapeutic application.

4 BRAIN AROUND TUMOR LIPID PROFILE ANALYSIS USING MULTIPLE REACTION MONITORING MASS SPECTROMETRY

4.1 Introduction

With increased understanding of the importance of lipids in glioma and the impact changes in composition has throughout disease progression, emphasis must be focused on the influence of tumors on surrounding non-cancerous brain, also reliant on lipids for proper functioning. Studies have found healthy brain parenchyma surrounding tumor becomes compromised due to the aggressive nature of glioma[115]. Additionally, patient assessments determined between 86-89% of those with primary brain tumor displayed impairments to neurocognitive functioning (NCF)[116]. Increased intracranial pressure, caused by hydrocephalus, has been observed to negatively impact cognitive processes; however, improvement to Karnofsky Performance Score (KPS), a patient impairment test, was noted following ventriculoperitoneal shunt surgery[117]. Alleviation of intracranial pressure failed to completely restore cognitive deficits in patients suggesting additional factors contributing to patient deficits.

Brain lipid composition maintenance, especially phospholipid and cholesterol species, is essential for normal brain functioning[21,118]. Dysregulation of these lipid classes in the brain have been implicated in neurodegenerative and neuropathological disease development[119,120]. Motor and cognitive impairments, characteristic of neurodegenerative diseases like Parkinson's and Alzheimer's diseases, are comparable to symptoms present in glioma patients. However, unlike these diseases, there is limited evidence defining the contribution of lipid profile alteration in brain surrounding tumor, compromised by glioma-related factors, to NCF and disease development. Proximity to tumor exposes non-cancerous cells to paracrine and autocrine signaling factors identified to support cancer proliferation, motility, and invasion[121]. In a study comparing molecular characteristics of normal and breast cancer tissues, non-cancerous myoepithelial cells within the tumor microenvironment exhibited significantly different gene expression patterns to normal breast cells[122]. Another study identified glioma cells manipulate astrocytes to release matrix modifying factors to facilitate invasion[123]. Evidence suggests glioma not only influences surrounding brain leading to cognitive impairments, it also manipulates molecular expression to support tumorigenesis. Therefore, it is critical to investigate brain around tumor lipid profiles

throughout glioma progression to identify both the impact of tumor grade on BAT lipid expression and species that potentially could contribute to tumor growth.

In this study, glioma grade-related influence of brain around tumor lipid composition was evaluated by MRM-profiling. Previous lipidomics studies have evaluated brain surrounding glioma for diagnostic purposes, using lipids to differentiate from glioma, and not to discover glioma manipulation of lipid composition[9,54]. Weiss et al. 2016 demonstrated glioma are unable to produce cholesterol through *de novo* synthesis and rely on an exogenous source for cholesterol to meet metabolic demands[113]. Healthy brain possesses two methods to generate cholesterol, *de novo* synthesis and preformed cholesterol uptake, highlighting a lipid metabolism mechanism glioma can control to acquire essential lipids[119]. Taken together, it is critical to further investigate lipid profiles in BAT exposed to glioma of all grades to elucidate additional lipid pathways that are manipulated by tumor to support growth. This study evaluates twenty-seven BAT samples from glioma grades I-IV isolated by laser capture microdissection. MRM-MS was used to profile expression changes and determine grade-related differences in BAT lipid composition.

4.2 Methods

Brain around tumor were profiled using selection, tissue isolation, lipid extraction and analysis, and statistical processing methods described in Analytical Design section 2.2. In this study, 27 BAT samples neighboring glioma grades I-IV were analyzed: BAT grade I (n = 3), BAT grade II (n = 9), BAT grade III (n = 6), and BAT grade IV (n = 9). Information regarding tumor influencing BAT lipid profiles are provided in Table 2.3. Brain around tumor samples were processed and profiled simultaneously with tumor samples, previously described in Chapter 3, to maintain consistent experimental conditions during analysis. Captured lipid composition data from three screen methods (M1, M2, and PC) were converted into relative abundances, following MRM-profiling, and statistical analysis was performed using Metaboanalyst 4.0 (https://www.metaboanalyst.ca/). Results will focus on data output from M1 and PC screening methods, M2 data is outlined in the Appendix C.

4.3 Results

4.3.1 Brain around tumor by grade

Principal Component Analysis (PCA)

Multivariate analysis identified distinct clusters between BAT grades based on lipid composition profiled by MRM-MS (Figure 4.1). Lipids included in this plot had a VIP score ≥ 1.0. Strong discrimination between BAT group clusters were noted in both M1 (embryo) and PC (phosphatidylcholine and sphingomyelin) screening methods. Distinct cluster localization of BAT groups using the M1 method was influenced by differential expression of carnitine, TAG, and PC lipid species (Figure 4.1A). BAT grade clusters were distinguished in the PC PCA plot due changes in PC and SM chain length and saturation (Figure 4.1B). Complete separation of BAT clusters was not noted in the plots; however, localization shifts in points as the glioma progressed was observed. Clusters in adjacent BAT grades were largely separate from one another indicating a significant change in lipid composition. Overall, M1 and PC PCA plots identified distinctions in lipid profiles in BAT tissue suggesting proximity to microenvironments of different glioma grades has a role in their lipid expression patterns.

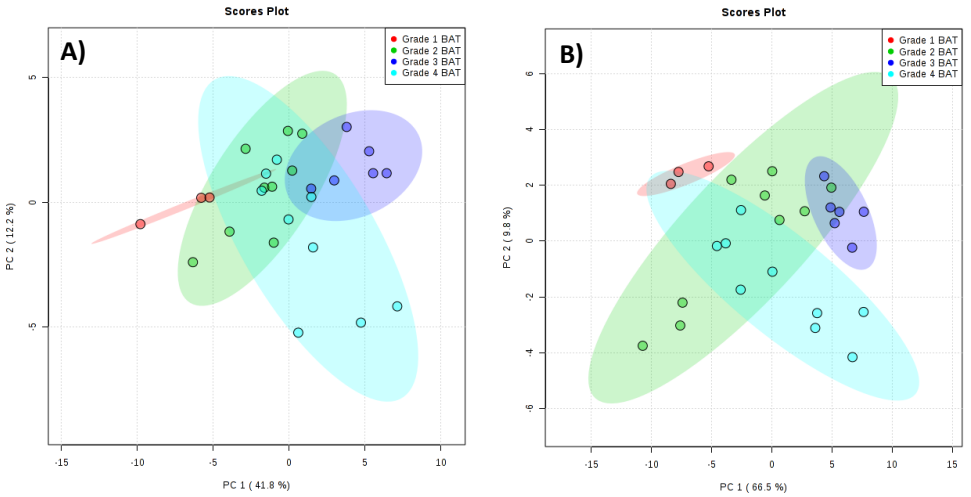

C)

Profiling Method	**PC1** (%)	**PC2** (%)
M1 Method	41.8	66.5
PC Method	12.2	9.8

Figure 4.1 PCA plot indicated discrimination in BAT grade lipid compositions in two screening methods according to PC1 and PC2. A) M1 method, B) PC method, C) PC1 and PC2 scores for both screening methods.

ANOVA

Significance testing by ANOVA determined significant differences in individual expression between BAT grades in both M1 and PC methods. The M1 screening method identified 40 significantly different lipids species between BAT groups; table detailing level of significance and comparison of groups with differential expression using Fisher's LSD noted in the Appendix Table B.1. Additionally, the PC screening method detected 75 individual lipid species with significant differences between BAT grades Appendix Table B.2. Significant lipid species in the M1 method included PC, SM, carnitines, and triglycerides. PC method lipids with significantly different expression were predominantly unsaturated PC, as well as short and long chain SM. ANOVA highlighted notable lipid composition changes BAT undergoes while under the influence of different glioma grades. Significant lipids shared between M1 and PC methods are further described in Appendix C Figure C.3.

Cluster analysis (Heatmap)

Cluster analysis demonstrated distinct grouping of each BAT grade across M1 and PC screening methods (Figure 4.2). The M1 heatmap clustered groups based on differential expression of PC, SM, carnitine, and TAG class lipids (Figure 4.2A). Lower BAT grades (I and II) were grouped based on elevated relative abundance of carnitine and TAG lipids, especially grade I BAT. BAT exposed to higher grade glioma (III and IV), lower expression of lipids in these classes were observed. Grade III BAT were distinguished by increased expression of low unsaturated PCs and long chain SMs. Grade IV BAT lipid expression patterns were mixed, maintaining an intermediate level of lipids used to differentiate between lower and higher-grade BAT groups. Similar trends in group clustering were noted in the PC heatmap (Figure 4.2B). Grade I BAT was distinguished by high relative abundance of PC(30:0, 36:5, 38:5) in addition to high unsaturated PC lipids which clustered grade II BAT. Grade III BAT clustered due to elevated low unsaturated PC and long chain SM species. Comparable to M1, grade IV maintained intermediate levels of both low and high unsaturated PCs. Overall, heatmaps display distinct lipid profiles between BAT grades.

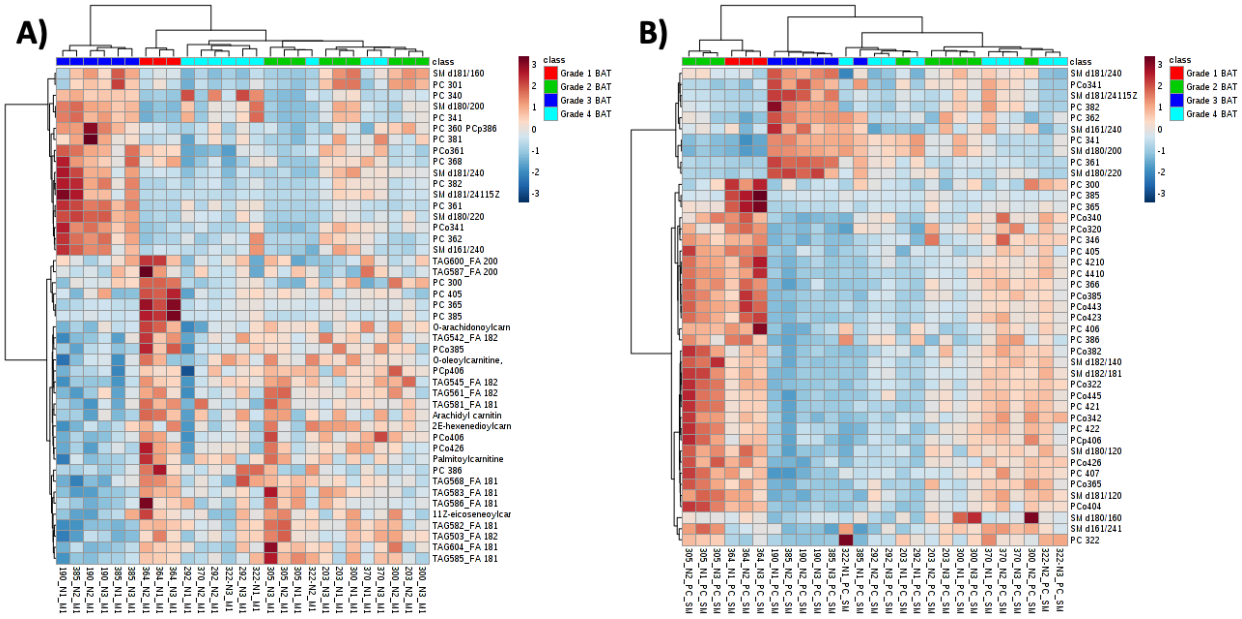

Figure 4.2 Cluster analysis demonstrated lipid composition distinctions in two MRM methods between BAT influenced by glioma grades I-IV. A) M1-top 45 lipids, B) PC-top 44 lipids.

4.3.2 Low grade v high grade brain around tumor

PCA

PCA plots for M1 and PC screening methods identified discrimination trends in clusters between low- and high-grade BAT groups (Figure 4.3). Lipids with VIP score ≥ 1.0 were considered in the PCA plot. Both plots shared localization of several points within the group cluster, indicating a certain level of overlap in lipid expression. However, distinctions between groups were noted, especially in the PC method plot (Figure 4.3B). PC method cluster separation was determined by differential expression of unsaturated PC lipid species between groups. M1 also exhibited discrimination in low- and high-grade BAT clusters (Figure 4.3A). Relative abundances differences in carnitine and TAG species were observed to distinctly cluster these two BAT groups. In summary, PCA plots demonstrate distinctions in low- and high-grade BAT lipid composition.

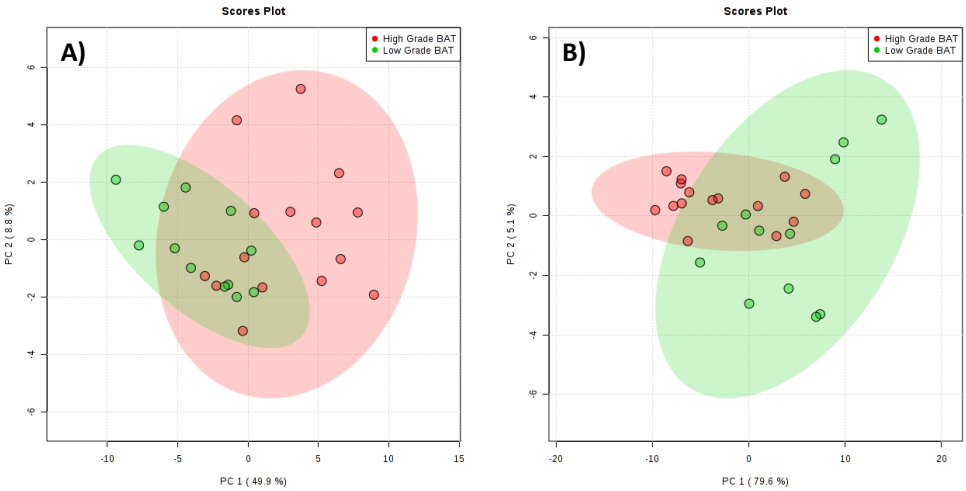

C)

Profiling Method	**PC1** (%)	**PC2** (%)
M1 Method	49.9	79.6
PC Method	8.8	5.1

Figure 4.3 PCA plots indicate distinct lipid profiles between low- and high-grade BAT points through discriminate group clustering. A) M1 method, B) PC method, C) PC1 and PC2 scores for both screening methods.

T-test

T-test analysis for significantly different relative abundances between groups identified a total of 75 distinct lipids across both methods. The M1 method had 23 differentially expressed lipids between low- and high-grade BAT samples, statistical analysis data are noted in Appendix Table B.3. Primarily carnitines and TAGs comprised lipids maintaining distinct expression, but also included several PC and SM species. The PC screening method observed 52 lipids with significantly different expression between BAT types and are described in Appendix Table B.4. Unsaturated PC species largely were differentially expressed between low- and high-grade BAT, most notably high unsaturated PC in low grade BAT. Taken together, t-tests demonstrate the markedly distinct lipid compositions maintained between BAT manipulated by low- and high-grade glioma. Significant lipids shared between M1 and PC methods are further described in Appendix C Figure C.6.

Cluster analysis (Heatmap)

Cluster analysis demonstrated distinct grouping between low- and high-grade BAT groups in both M1 and PC screening methods (Figure 4.4). The heatmap for M1, displaying the top 55 lipids profiled, indicated the separation of BAT types by differential expression of three lipid classes: PC, TAG, and carnitines (Figure 4.4A). Low-grade BAT expressed greater relative abundances of carnitine and TAG class lipids compared to the high-grade group. Conversely, SM and unsaturated PC species were observed at elevated relative abundances in high-grade BAT with lower levels of carnitines and TAGs. The M1 heatmap displayed a shift from carnitine and TAG dominant composition in low-grade BAT to PC and SM dominant in high-grade BAT highlighting a shift in lipid composition. Distinctions between BAT types were also visualized in the PC heatmap (Figure 4.4B). Low-grade BAT expressed higher relative abundance of high unsaturated PC than high-grade BAT. High-grade BAT displayed two noticeable lipid patterns; low relative abundances of high unsaturated PCs with elevated levels of low unsaturated PCs, or intermediate levels of high unsaturated PCs and low relative abundance of low unsaturated PCs. Taken together, cluster analysis identified carnitine, TAG, and high unsaturated PC relative abundances to be distinctly expressed in low-grade BAT, and short and low unsaturated PCs distinct in high-grade BAT, elucidating changes in lipid composition BAT undergoes during glioma malignant transition.

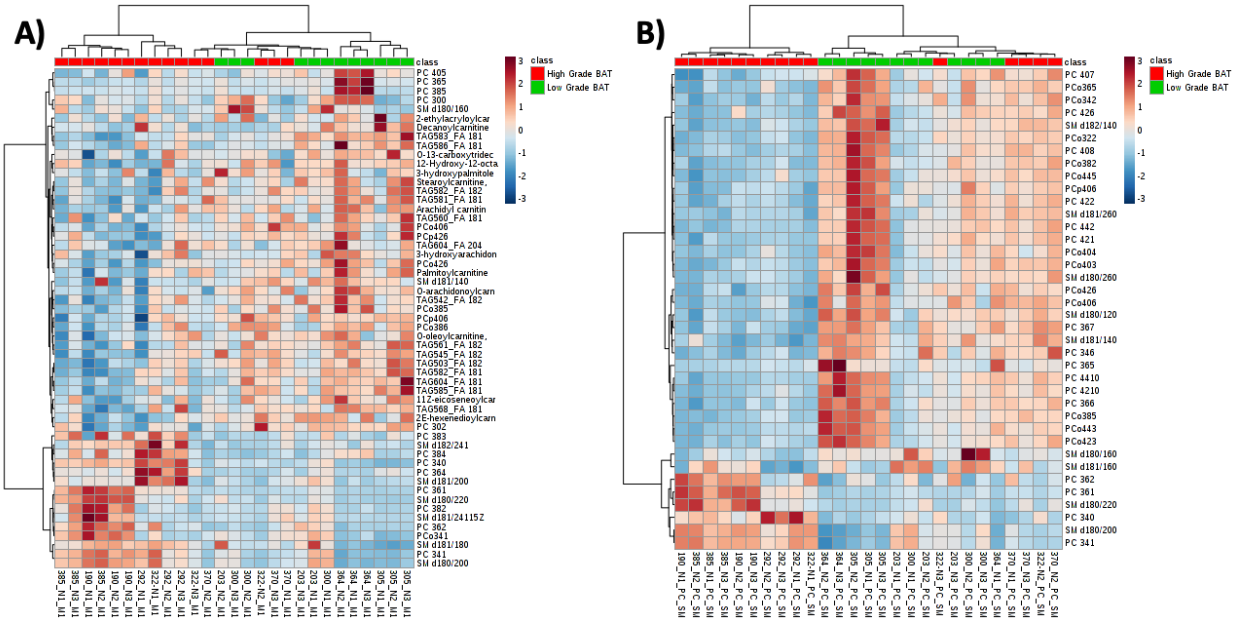

Figure 4.4 Heatmap analysis indicates distinct low- and high-grade BAT clustering based on distinctions in PC, carnitine, and TAG relative abundance in M1 and PC methods. A) M1- top 55 lipids, B) PC- top 38 lipids.

Lipid chain length and saturation analysis

Lipid chain length and saturation analysis identified distinctions in total lipid relative abundances between low- and high-grade BAT based on chemical characteristics (Figure 4.5). PC and SM were the only two lipid classes with significantly different expression between tissue types. Level of PC saturation was observed to shift between low- and high-grade BAT. Low-grade BAT maintained significantly greater average sum relative abundance of high unsaturated PC (Figure 4.5C, $p \leq 0.01$). Conversely, high-grade BAT expressed greater average sum relative abundance of low unsaturated PC than low-grade BAT (Figure 4.5A, $p \leq 0.01$). Short PC average sum relative abundance was also significantly elevated in high-grade BAT (Figure 4.5B, $p \leq 0.05$). A change in SM chain length was observed to change during BAT types exposed to glioma during malignant transition. Average sum relative abundance of short chain SM were significantly higher in low-grade BAT (Figure 4.5D, $p \leq 0.0001$). Lastly, as glioma transitioned to high-grade, medium chain SM were expressed at significantly higher average sum relative abundance (Figure 4.5E, $p \leq 0.01$). In conclusion, alteration to PC saturation status and SM chain length were trends observed in BAT influenced by glioma tissue, exposing a potential lipid composition change that may be relevant to malignant glioma progression.

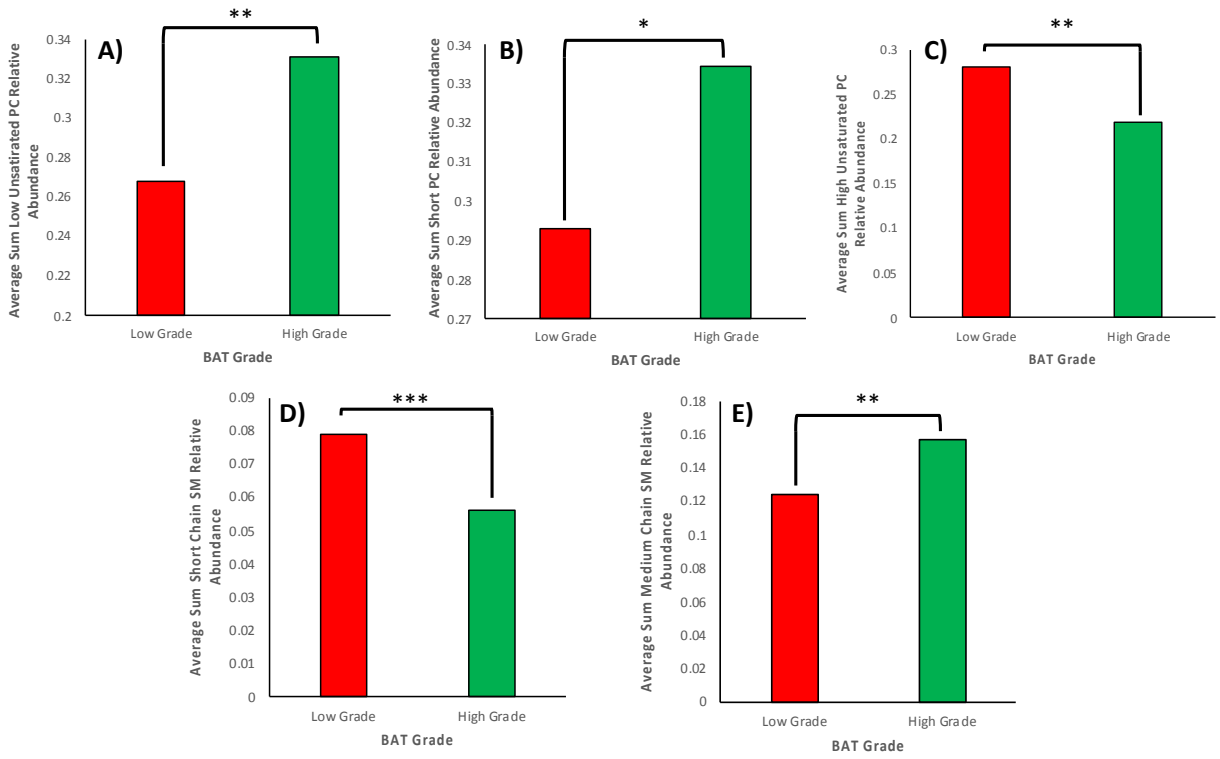

Figure 4.5 Chain length and saturation analysis indicated distinct alterations to PC saturation and SM chain low- and high-grade BAT undergo during malignant transition. A) Low unsaturated PC, B) short chain PC, C) high unsaturated PC, D) Short chain SM, and E) Medium chain SM. *p≤0.05, **p≤0.01, ***p≤0.0001

ROC Curve

ROC curve analysis was performed to determine discrimination power of detected lipids, in M1 and PC methods, to correctly label BAT type. 17 individual lipids captured in the M1 screening method maintained an AUC greater than 0.8 Appendix Table B.5. The top 5 AUC scores consisted of three TAG species and two PC species (Figure 4.6). Comparison of low- and high-grade BAT showed discriminant PC, TAG, and carnitine lipids for these groups. TAGs were predominantly expressed in low-grade BAT, supporting their discrimination capacity for this tissue type (Figure 4.6A-C). Additionally, several low and high unsaturated PCs possessed an AUC greater than 0.8; differential expression of these lipid types demonstrated their applicability to distinguish between high- and low-grade BAT respectively.

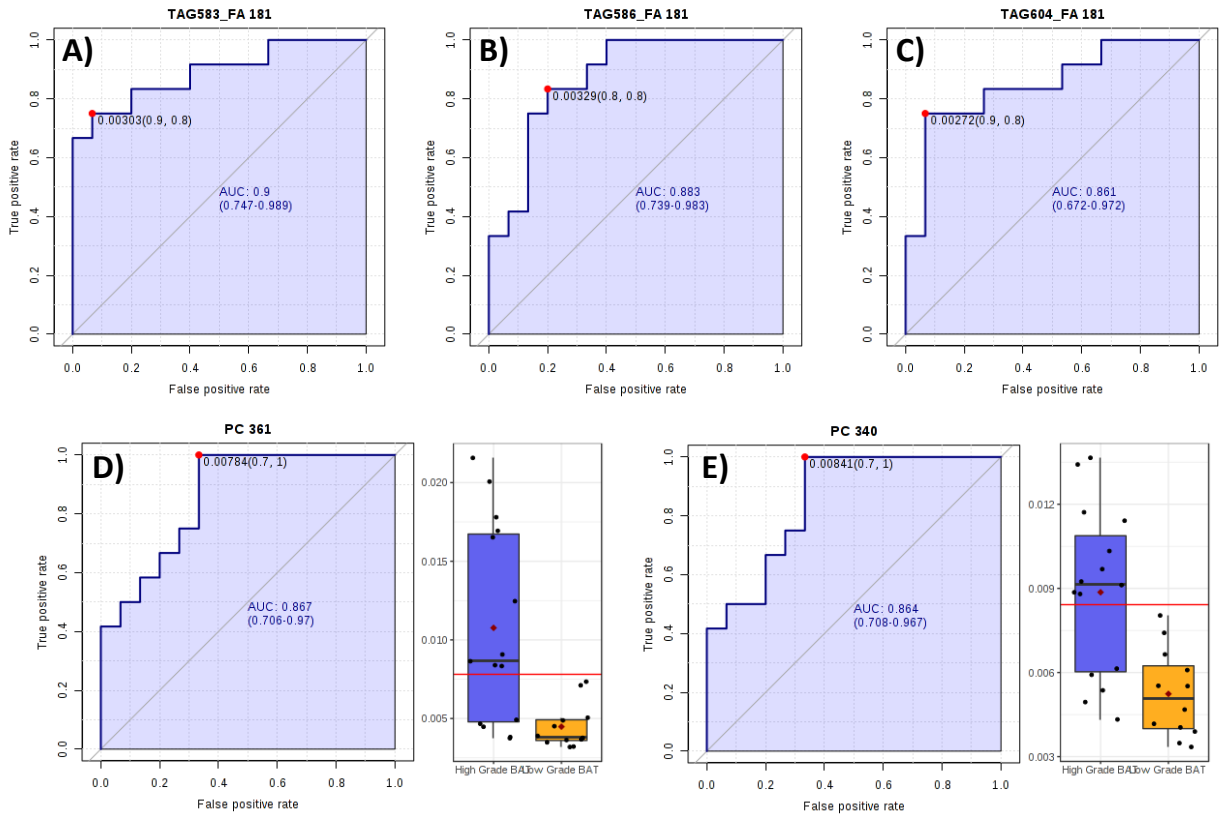

Figure 4.6 ROC curve analysis of top 5 lipids discriminant lipids detected by M1 method to distinguish between low- and high-grade BAT.

ROC analysis identified 24 lipids from the PC method containing an AUC >0.8 Appendix Table B.6. The top 5 most discriminant lipids consisted of saturated and low unsaturated PC, as well as, short and long chain SM. Short chain SMs, like SM d(18:0/12:0) and SM d(18:0/16:0), were observed to be most discriminant in low-grade BAT (Figure 4.7 A-B). In addition, low unsaturated PC, PC(36:1), and long chain SM, SM d(18:0/22:0), were showed differential expression in high-grade glioma (Figure 4.7 C, E). In summary, ROC curve analysis showed 41 lipids, across two MRM-profiling methods, to effectively discriminate between low- and high-grade BAT tissue.

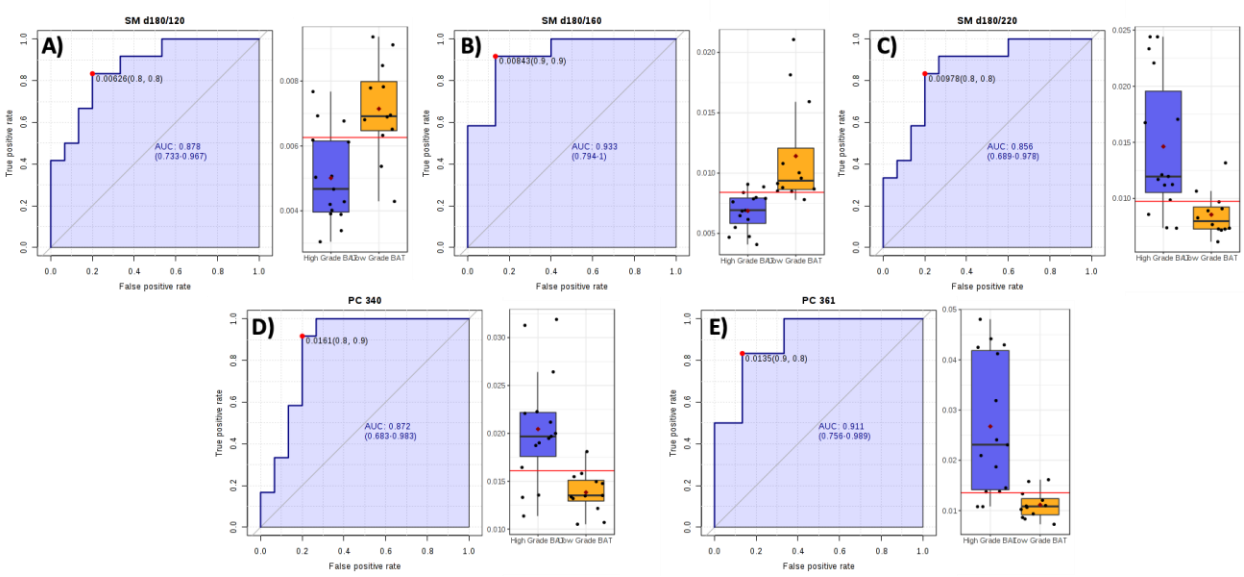

Figure 4.7 Individual ROC curves of top 5 most discriminant lipids from PC method to differentiate between low- and high-grade BAT.

Combined discrimination power of lipids with greater than 0.8 AUC from M1 and PC methods were evaluated, and sufficient attribution of tissue type was reached (Figure 4.8). Tester analysis identified merging data from the 17 discriminant M1 lipids resulted in an AUC of 0.846 (Figure 4.8A). Additionally, pooling the 24 individual PC lipids produced an AUC of 0.832 (Figure 4.8B). Both tests were greater than the 0.8 AUC threshold indicating their potential diagnostic capacity.

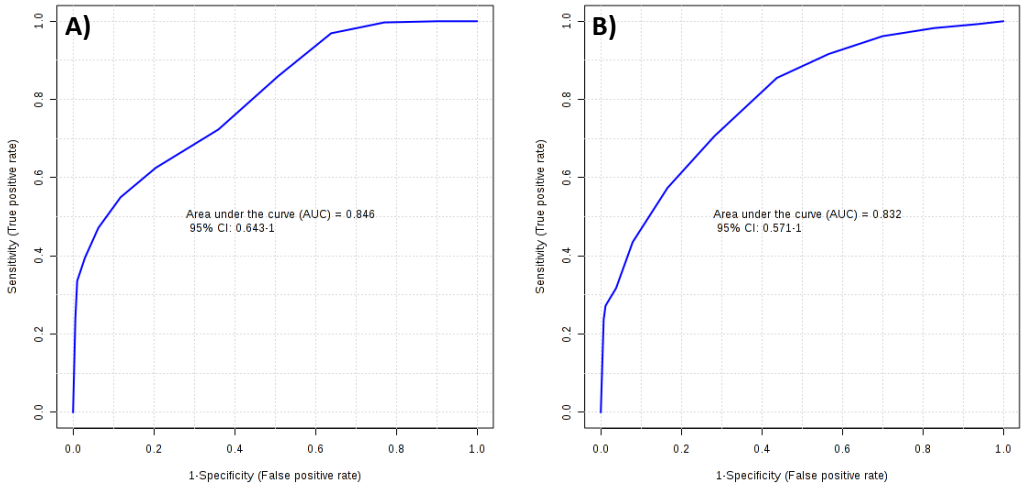

Figure 4.8 Discrimination capacity of combined differentially expressed lipids to distinguish between low- and high-grade BAT. A) M1 method, B) PC method.

4.3.3 Grade II v. grade III brain around tumor

PCA

Principal component analysis demonstrated distinct clusters between grade II and grade III BAT groups (Figure 4.9). Lipids with VIP score ≥ 1.0 were included in this multivariate analysis. Robust grade II and grade III BAT cluster separation was observed in both M1 and PC plots. Distinction of the grade II cluster in the M1 PCA plot was produced by predominantly by carnitine and TAG lipid differential expression (Figure 4.9A). Even further, the grade III cluster was distinguished by elevated relative abundances of unsaturated PC and long chain SM. Even greater cluster separation was noted in the PC PCA plot. Grade II BAT points were separate from grade III due to increased expression of high unsaturated PC species in their lipid profile (Figure 4.9B). Also, low unsaturated PC and long chain SM were discriminating lipid species in grade III BAT, localizing the cluster distinctly in the plot. Taken together, multivariate analysis indicated grade II and grade III BAT possess highly distinct lipid profiles from one another. Lipid composition changes suggest potential influence of glioma progression on expression of PC, SM, carnitine, and TAG lipid classes.

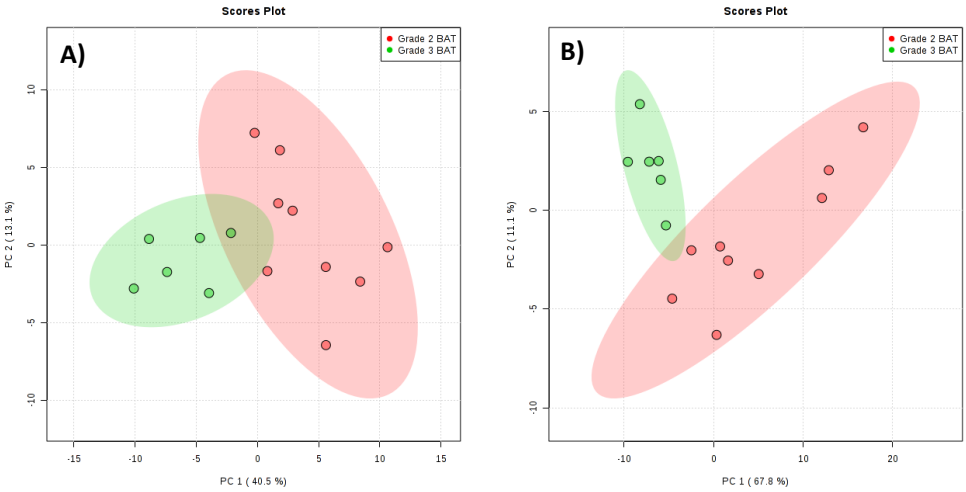

C)

Profiling Method	PC1 (%)	PC2 (%)
M1 Method	40.5	67.8
PC Method	13.1	11.1

Figure 4.9 PCA plots identified grade II and III BAT expressed distinct lipid profiles in two screening methods. A) M1 method, B) PC method, C) PC1 and PC2 scores for both screening methods.

T-test

Statistical testing to determine significantly different relative abundances between groups, t-test, identified a total of 114 lipids with distinct expression between screening methods. The M1 screening method detected 44 differentially expressed lipids between grade II and grade III BAT groups Appendix Table B.7. Significant M1 lipids primarily consisted of unsaturated PC and carnitine species. The PC method identified 70 lipid species with distinct expression between grade II and III BAT Appendix Table B.8. Unsaturated PC as well as short and long chain SM were significant discriminant lipids between BAT groups. Significance testing has indicated BAT expresses highly distinct lipid profiles when exposed to tumor undergoing low- to high-grade transition, based on PC, SM, TAG, and carnitine expression. Significant lipids shared between M1 and PC methods are further described in Appendix C Figure C.9.

Cluster analysis (Heatmap)

Cluster analysis identified distinct clustering of grade II and III BAT groups in both M1 and PC MRM methods (Figure 4.10). Top 50 lipids were visualized in the M1 heatmap, and separation of grade II and III BAT based on PC, TAG, and carnitines were observed (Figure 4.10A). Carnitines and TAG maintained greater relative abundance in grade II BAT vs grade III BAT. Additionally, grade III BAT expressed higher relative abundance of unsaturated PC and long chain SM. A marked decrease in TAG and carnitine relative abundance in grade III BAT indicating a decreased reliance on these lipid types. Grade II and grade III BAT groups were also discriminated using the top 50 lipids profiled in the PC method (Figure 4.10B). Saturation and chain length of PC and SM lipids were distinguishing factors in clustering BAT groups. Grade II BAT demonstrated elevated relative abundance of both high unsaturated PC and short chain SM species compared to grade III BAT. Greater relative abundance of low unsaturated PC and long chain SM were noted in grade III BAT with generally low expression of high unsaturated PC lipids. Overall, M1 and PC heatmaps showed two notable trends. First, a decrease in TAG and carnitine species in BAT tissue indicates a transition from low-grade tumor to high-grade tumor, represented in BAT lipid composition. Also, the shift from high unsaturated PC to low unsaturated PC is another indicator of glioma high grade transition.

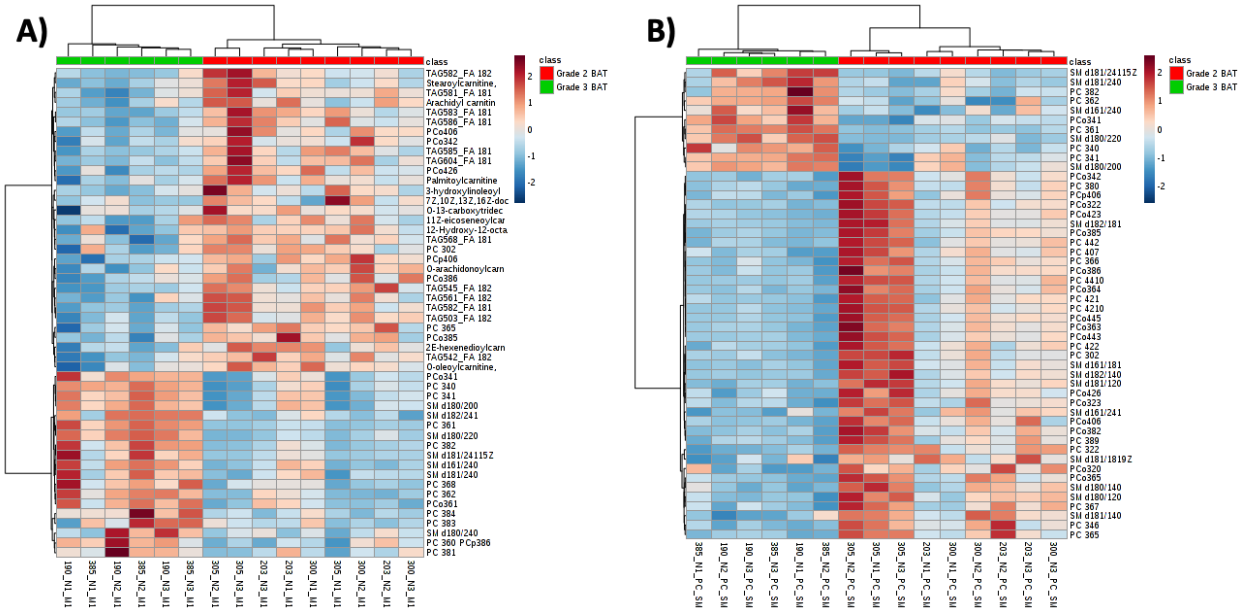

Figure 4.10 Cluster analysis of top 50 lipids from M1 and PC methods differentiating between grade II and grade III BAT. A) M1 method, B) PC method.

ROC Curve

ROC curve analysis was utilized to evaluate differentially expressed lipids profiled by M1 and PC methods to discriminate between grade II and III BAT. 49 lipid species were determined to possess an AUC greater than 0.8 from the M1 profiling method Appendix Table B.9. The 5 most discriminant lipids from the M1 method consisted of PC, SM, and TAG species, maintained a 1.0 AUC (Figure 4.11). Low unsaturated PC and long chain SM, like PC(36:1) and SM d(18:0/22:0) respectively, were distinctly expressed in grade III BAT and is noted in its high discriminating power (Figure 4.11 A, C). TAG species, like TAG50:3_FA18:2 and TAG58:2_FA18:1, were elevated in grade II BAT, thus improving diagnostic capability (Figure 4.11 D-E). Additionally, carnitine species were also found to possess great discriminating power, due to their differential expression in grade II BAT, as 12 species have an AUC ≥ 0.8.

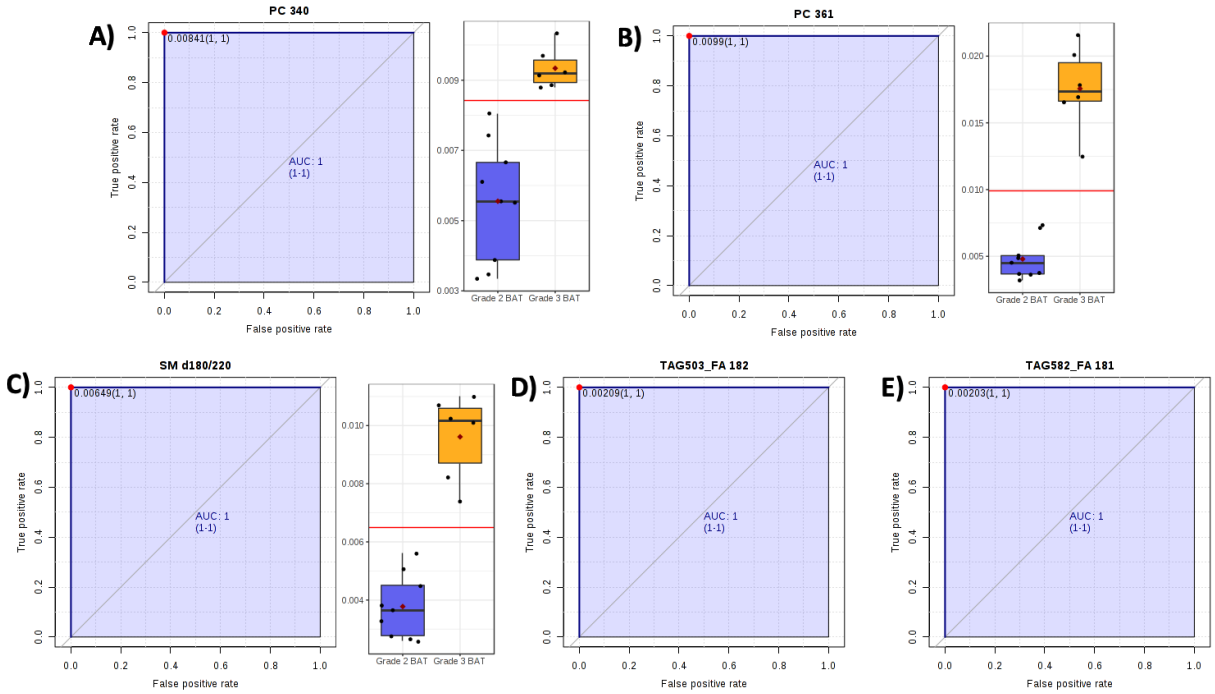

Figure 4.11 ROC curve analysis of top 5 discriminate lipids identified in the M1 profiling method.

ROC curve analysis also identified 76 lipids from the PC method to maintain an AUC ≥ 0.8 Appendix Table B.10. The analysis also determined the top 19 lipids had an AUC of 1.0. The top 5 most discriminant lipids consisted entirely of low unsaturated PC and long chain SM (Figure 4.12). Low unsaturated PC lipids, i.e. PC(36:1) and PCo(34:1) as well as long chain SMs, like SM d(18:0/22:0) were observed in grade III BAT to be maintained at significantly higher relative abundances than in grade II BAT (Figure 4.12 A-C). Additionally, high unsaturated PCs, like PC(36:5), were characteristic of grade II BAT, as it is expressed at significantly higher relative abundances than in grade III BAT. To conclude, ROC curve analysis revealed 114 individual lipids, from M1 and PC profiling methods, with strong discriminating capacity to differentiate between grade II and grade III.

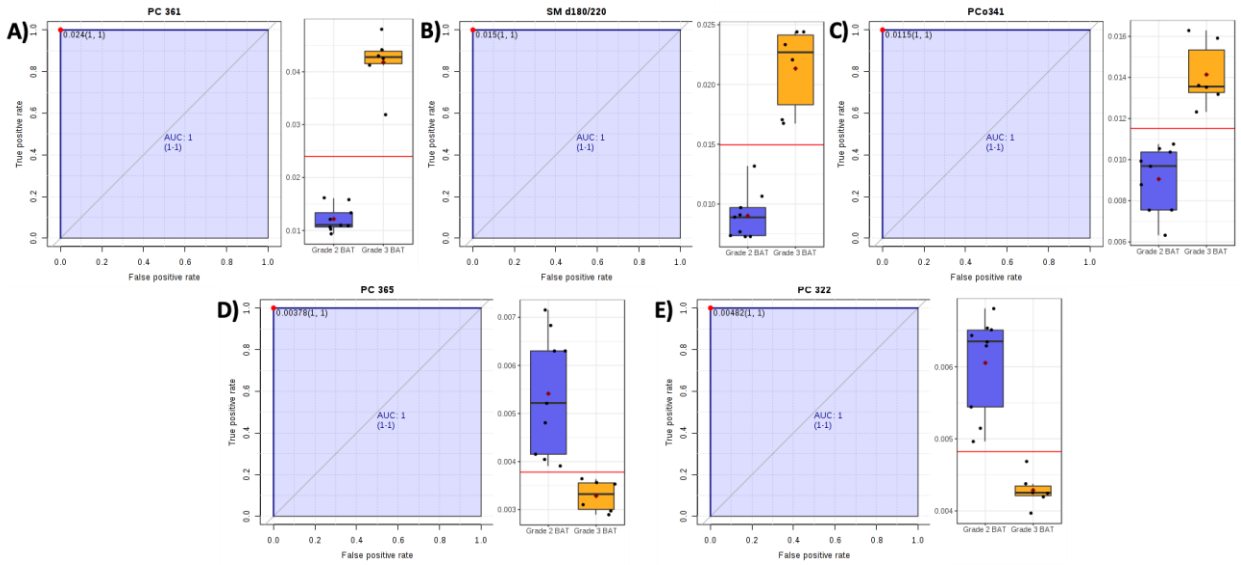

Figure 4.12 ROC curve analysis of top 5 lipids detected by the PC screening method with robust capacity to discriminate between grade II and grade III BAT.

Integration of information from individual lipids with AUC ≥ 0.8 were combined to determine discriminating power and ROC curve analysis identified strong distinguishing capacity (Figure 4.13). An AUC of 1.0 was observed when combining the 49 lipids with AUC ≥ 0.8 (Figure 4.13A). Similarly, an an AUC of 1.0 was also achieved when integrating all 70 lipid data pointes from the PC screening method (Figure 4.13B). Both tests indicated the strong discriminating capacity PC, SM, TAG and carnitine lipids have in distinguishing between grade II and grade III BAT.

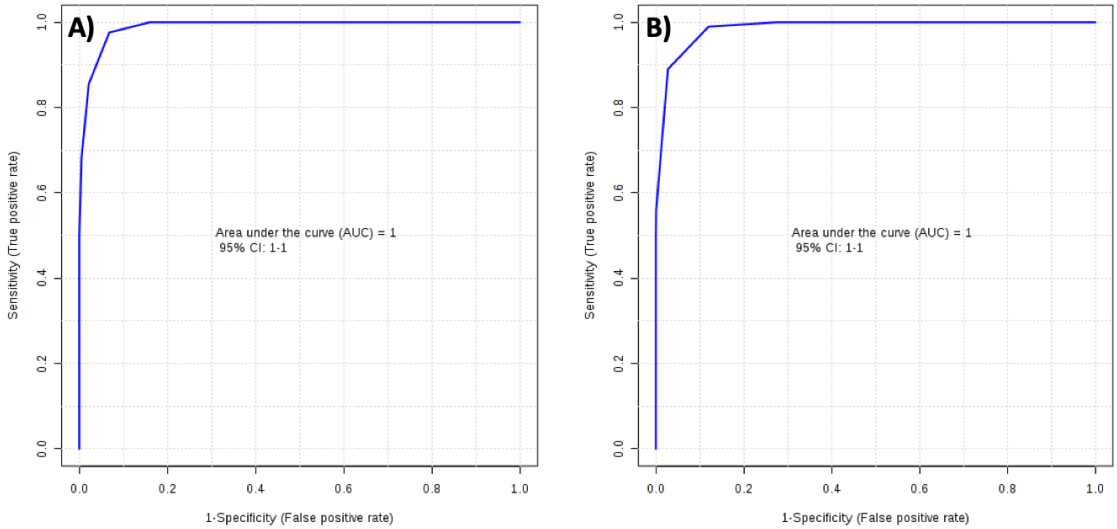

Figure 4.13 PCA plots integrating all discriminant lipids indicated robust distinguishing capacity of grade II and grade III BAT. A) M1 method, B) PC method.

4.4 Discussion

Given the evidence that glioma tumors compromise the surrounding brain tissue, there are concerns about the manipulation of brain around tumor lipid profiles by glioma throughout progression to support tumorigenesis. Lipidomics studies evaluating tumor-adjacent brain tissue lipid composition are currently limited in the literature. In this study, we report significant alterations to BAT lipid profiles as the neighboring glioma undergoes malignant transition. In two MRM-screening methods, M1 and PC, expression patterns of PC, SM, TAG, and carnitine lipid species were significantly different between low-grade and high-grade BAT groups.

Carnitine relative abundance was observed to decrease in high-grade BAT tissue from levels detected in low-grade glioma tissue. In healthy brain, carnitine is expressed at high levels, especially in neurons[124]. Physiologically, carnitines in the brain assist in facilitation of fatty acid transport across mitochondrial membranes for utilization in β-oxidation[125]. The brain has high energy demands, and 20% of the energy produced in the brain is generated through β-oxidation, demonstrating the importance of carnitine expression in healthy brain[126]. Carnitine deficiency has been connected to several neurodegenerative disorders, like Parkinson's and Alzheimer's disease, due to mitochondrial dysfunction[127]. Diminished carnitine relative abundance was detected in high-grade BAT samples, mimicking trends in carnitine expression characteristics of other neuropathologies. Studies have determined excess carnitine levels induces senescence in GBM cells[128]. Interestingly, the adverse effects of carnitine expression in glioma directly opposes the beneficial impact it has in healthy brain cells. The results indicate low-grade BAT expresses greater levels of carnitine lipids, more similar to that seen in healthy brain, and high-grade BAT maintains lower carnitine relative abundance, which is representative of a diseased brain. Carnitine expression patterns demonstrates not only that high-grade glioma could be manipulating BAT lipid composition, but also though histologically considered non-cancerous brain, molecularly high-grade BAT is presenting similar to diseased brain.

In addition to carnitines, TAGs were also observed to be differentially expressed between low- and high-grade BAT groups. Triglycerides function as common cell membrane structural components and for energy storage in the body[129]. However, unlike in the periphery, studies have found healthy brain to be devoid of TAG[29]. The same study also showed high-grade brain tumors possessed greater TAG than lower grade neoplasms. BAT showed the opposite trend in this study as low-grade BAT was identified to express greater levels of TAG than high-grade BAT. While

the role of TAG expressed in BAT has not been explored, TAG are understood to be a source of unsaturated fatty acids, containing three per molecule, that are characteristic of high-grade glioma[32]. Lipid transport occurs frequently in the brain to regulate neurological functioning[130]. TAG are commonly packaged in the lipoprotein-based vessel, due to their hydrophobic nature, and target cells can uptake these molecules for their fatty acid content[131]. As low-grade glioma has lower metabolic demands than high-grade gliomas, TAG shuttling from BAT to glioma is not necessary and could account for greater TAG abundance in low-grade BAT. The opposite could also be occurring, high-grade gliomas have great energy demands, while also maintaining greater composition of unsaturated fatty acids[31]. High-grade BAT may be transporting produced TAG to glioma to support growth, accounting for lower TAG levels in surrounding BAT tissue. To date, the role of TAGs in glioma, nor the surrounding brain, have not been explored[132]. This study demonstrated change in TAG expression between low- and high-grade BAT that have potential implications that BAT can support glioma progression.

Significant differences in phosphatidylcholine saturation state were also present in low- and high-grade BAT tissue. PC lipids are essential membrane structural components and influence the membrane fluidity based on the saturation level. Low-grade BAT expressed greater high unsaturated (≥ 3 double bonds) PC than high-grade BAT. Polyunsaturated fatty acids (PUFAs), docosahexaenoic acid (DHA) and arachidonic acid (ARA), are the most common fatty acids in the brain and are predominantly esterified to plasma membrane phospholipids[133]. PC lipids containing DHA or ARA, which have 6 and 4 double bonds respectively, produce high membrane fluidity within normal brain cells. PC lipid desaturation pattern in low-grade BAT suggested greater membrane fluidity, similar to healthy brain, than high-grade BAT. Conversely, low unsaturated PC (1-2 double bonds) were elevated in high-grade BAT. Studies observed membrane fluidity was a critical factor in determining resistances to treatment[134]. A decrease in membrane fluidity, due to lower PC saturation, in high-grade BAT parallels the PC expression patterns of high-grade glioma tissue (Section 3.3.2.3). High-grade gliomas are highly resistant to treatment, contributed to by the maintained level of membrane fluidity. Brain surrounding high-grade gliomas having a similar degree of membrane fluidity indicates a potential role in high drug resistance present in malignant gliomas. Osuka et al. demonstrated drug resistant glioma persist in the brain paraenchyma surrounding the tumor following treatment, and stated targeting cells proximal to the tumor lesion would be essential to prevent recurrence[135]. Lipid desaturation has been shown to be

a critical factor in cancer development and targeted approaches increasing the saturation of lipids has induced lipotoxicity within cancer cells[99,136]. Supported by this study, PC desaturation in BAT emerges as a potential influencing factor in glioma drug resistance and highlights a mechanism to further study to improve treatment efficacy.

Lastly, sphingomyelin species were differentially expressed between low- and high-grade BAT based on chain length. More specifically, short- and long-chain SM were maintained at significantly greater relative abundance in low-grade and high-grade BAT respectively. Similar to phosphatidylcholine, sphingomyelin lipids are integral membrane lipids as well as a major component of myelin sheaths coating neuronal axons. The SM chain length shift observed in this study between low- and high-grade BAT indicates not only a change in membrane fluidity, but also lipid raft expression. Diminished expression of short-chain SM in high-grade BAT indicates a more rigid cell membrane is present[137]. A similar trend toward membrane rigidity was also noted with greater low unsaturated PC expression. Literature has shown increased focus on targeting brain surrounding tumor to sensitize glioma toward therapeutic intervention, however the increase in membrane rigidity would diminish their efficacy[138]. Higher long-chain SM relative abundance also suggests increased levels of lipid rafts localized in the membrane. Lipid rafts in tumors are comprised largely of long-chain SM and induce a variety of aggressive tumor behaviors by reinforcing signal transduction[108]. Studies reported increased lipid rafts in BAT acts as an indicator of disease brain[139]. Elevated lipid rafts also provide a mechanism glioma can utilized to manipulate BAT. However significant research investigating this potential mechanism is required.

Based on these findings, there is decreased confidence describing BAT as non-cancerous as BAT possesses highly similar lipid composition of screened lipids with glioma tissue**.** On the micro level, the BAT lipidome, does not match the analysis on the macro level, BAT morphology. According to pathological parameters, BAT maintains a distinct morphology compared to glioma, thus it would be expected BAT lipid profiles would follow this pattern. However, molecular changes present within BAT cells, shifting their profiles toward a more cancer-like composition, are not recognized by current histological guidelines. These findings reduce our confidence in classifying BAT as non-cancerous and raises several important questions to further investigate. First and foremost, should molecular profiles be considered when performing pathology on resected tissue to improve patient diagnosis? Studies have shown the BAT is influenced by tumor, manipulating the surrounding brain to support tumor progression[140–142]. Taken together with these

findings, BAT appears to be more than simply an uninvolved party in the glioma paradigm. It is unclear if BAT cells manipulated by glioma eventually transform into brain cancer cells, thus further investigation is needed to confirm this outcome. However, recent findings suggest BAT acts as a supportive player in glioma development and survival to a greater degree than previously acknowledged[140–142]. Reevaluation of classification methods defining BAT as non-cancerous may be necessary. It is possible BAT may need to be considered pre-cancerous, though current guidelines mainly consider morphological characteristics observable under a microscope to determine this change. Pre-cancerous cells are considered abnormal cells that don't necessarily become cancer or invade tissue[143]. Under the influence of glioma, BAT has become abnormal in terms of lipid profile. This study indicates a change to one characteristic within BAT, lipid composition, but does not consider the multitude of other factors that could be altering glioma biology. It is critical to investigate if this continual influence by glioma eventually transforms BAT cells into cancer cells and also if the BAT cells can revert back to molecular profiles in non-cancerous brain. To conclude, BAT should be considered as an important factor in the glioma system and as a potentially target therapeutically to disrupt glioma growth.

4.5 Conclusions

The above study identified significant changes to lipid profiles of brain around tumor tissue proximal to glioma grades I-IV. TAG, carnitine, high unsaturated PC, and short-chain SM relative abundances were significantly higher in low-grade BAT, an indicator of greater membrane fluidity, and changed as surrounding glioma progressed. Low unsaturated PC and long-chain SM were distinctly expressed in high-grade BAT, similar to high-grade glioma, compared to low-grade BAT. ROC curve analysis demonstrated that low- and high-grade BAT can be discriminated based on the expression of these species in BAT lipid profiles. Taken together, focus should be given to brain around tumor as this study indicated manipulation of their molecular profile by tumor that may benefit glioma growth, worsening patient outcomes.

5 COMPARISION ANALYSIS OF GLIOMA AND BRAIN AROUND TUMOR LIPID PROFILES USING MULTIPLE REACTION MONITORING MASS SPECTROMETRY

5.1 Introduction

Glioma is the most common, deadliest form of brain cancer[1]. Due to the heterogeneous composition of glioma tumors, current clinically approved therapeutics available fail to improve patient quality of life and overall survival[144]. Treatment options for glioma patients have developed minimally over the last two decades since TMZ, the standard therapy, was approved in the early 2000's. Patient survival, at its highest tumor grade, remains a dismal average of 12-15 months following diagnosis, one of the lowest among all cancer types[2]. Knowing that most low-grade glioma eventually progress to high-grade tumor that are highly untreatable, it is important to identify novel therapeutic targets specific to glioma tumors that will expand current treatment options and improve patient outcomes.

Recently, lipids have received increased focus as metabolic reprogramming in glioma shifted toward lipid metabolism[145]. Instead of breaking down glucose fully through glycolysis, glycolytic intermediates are shuttled in biosynthesis pathways, generating most prominently lipids[36]. Studies have determined glioma maintain a higher concentration of lipids compared to surrounding brain tissue, which processes glucose through OXPHOS for ATP production[146]. Even further, imaging mass spectrometry studies have observed differential expression of membrane phospholipids, such as phosphatidylcholine, phosphoethanolamine, and ceramides, between grey and white brain matter and glioma tumors[9]. Taken together, gliomas still are largely untreatable, differences in total lipid concentration and lipid profiles have been observed, but the application of lipids clinically has been primarily geared toward diagnostics, and not on treatment. Lipids have potential as therapeutic targets, based on previous evidence in the literature detailing importance of lipids and lipid metabolism to glioma development, progression, and survival. Despite this understanding, limited evidence is available denoting effective lipid species and pathways to target in glioma.

Lipid diversity and complexity of lipid synthesis pathways poses a major challenge to the field; and must be characterized using a lipidomics, with a broad detection range, to capture the extensive lipid profiles contained in both glioma and BAT[78]. Additionally, lipids are essential to

healthy brain functioning, and therefore requires the precise targeting of glioma-specific lipids to avoid potentially severely toxic side effects in patients[147]. Brain pathologies have been connected to altered expression of lipids, therefore, it is critical to define glioma-specific lipids and their associated pathways to elucidate targets to further validate for potential clinical application[23,24,148]. In this study, multiple reaction monitoring-mass spectrometry was utilized to comprehensively characterize lipid profiles in glioma and BAT. Microdissected glioma and BAT tissue was analyzed by three screening methods, M1 and M2 (embryo) and PC (PC and SM lipids) to identify distinct lipids between tissue types. Lipid classes profiled in this work includes phosphatidylcholines, sphingomyelins, triglycerides, carnitines, and fatty acids. Lipid profiles between glioma and BAT were compared at low-grade, high-grade, and overall tumor vs BAT to observe notable distinctions in lipid expression throughout glioma progression. Results showed glioma and BAT maintained highly similar lipid profiles, with the exception of a few individual lipids, across lipids evaluated three screening methods indicating potential influence of glioma on neighboring brain's molecular profile.

5.2 Methods

Glioma and BAT lipid profiles were characterized in this study utilizing the methods of samples selection, histological analysis, LCM isolation, MRM-MS, and statistical analysis outlined in the Analytical Design section 2.2. A total of 59 samples, 32 glioma samples, grades I-IV, and 27 BAT surrounding each of the four tumor grades were profiled in this study. Sample size for each glioma grade included grade I (n=5), grade II (n =12), grade III (n = 9), and grade IV (n = 6). Additionally, BAT grade I (n = 3), BAT grade II (n = 9), BAT grade III (n = 6), and BAT grade IV (n = 9) comprised the BAT group. Sample processing for both groups in this experiment happened concurrently to maintain consistent experimental conditions. Lipid composition in glioma and BAT groups were defined by three MRM-MS screening methods: M1 and M2 (embryo) and PC (phosphatidylcholine and sphingomyelin). Detected lipids within each sample group were converted into relative abundances for statistical analysis. Lipid relative abundance data was processed using Metaboanalyst 4.0 (https://www.metaboanalyst.ca/) to determine significant differences in expression between glioma and BAT. Relative abundance data was also utilized for chain length and saturation analysis, significant differences in expression was performed using

JMP® Pro 14. Results in this chapter will focus on output from M1 and PC methods, M2 method results will be included in the Appendix D.

5.3 Results

5.3.1 Low-grade glioma v. low-grade BAT

Principal component analysis (PCA)

Multivariate analysis of low-grade glioma and BAT showed slight distinction in clusters by PCA plot (Figure 5.1). Lipids included in the PCA plot possessed VIP score ≥ 1.0. Similar localization of low-grade glioma and BAT clusters were noted in both plots for M1 and PC MRM-profiling methods. Proximal clustering in the M1 plot indicates comparable composition of PC, SM, TAG, and carnitine species within both groups (Figure 5.1A). Additionally, close clustering of points within the PC PCA plot indicates similar expression patterns of PC and SM species between tissue types (Figure 5.1B). Overall, plots for both M1 and PC plot demonstrate low-grade glioma and BAT share similarities in their lipid profiles.

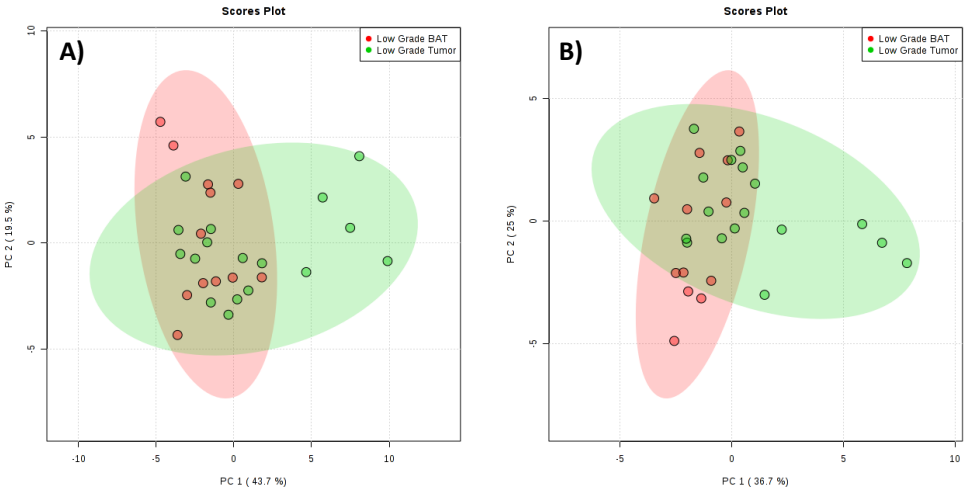

C)

Profiling Method	PC1 (%)	PC2 (%)
M1 Method	43.7	19.5
PC Method	36.7	25.0

Figure 5.1 PCA plots of M1 and PC screening method indicated similar lipid profiles between low-grade glioma and BAT. A) M1 method, B) PC method, and C) PC1 and PC2 scores for both screening methods.

T-test

Statistical analysis determined significantly different expression of the SM species SM d(18:1/24:0) between low-grade glioma and BAT (Figure 5.2). Low-grade BAT maintained elevated relative abundance of this long-chain SM species at a *p-value* < 0.001. The PC method was employed to identify this distinction.

A)

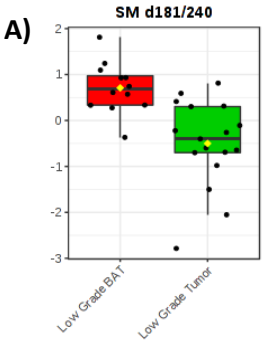

B)

Lipid	t.stat	p.value	-log10(p)	FDR
SM d18:1/24:0	3.9619	0.00048944	3.3103	0.049434

Figure 5.2 Differential expression of long-chain sphingomyelin species between low-grade glioma and BAT. A) SM d(18:1/24:0) concentration graph, B) statistical output.

Cluster analysis (heatmap)

Cluster analysis showed distinctions in lipid profiles between low-grade glioma and BAT across both MRM-screening methods (Figure 5.3). The heatmap for the M1 method displaying the top 14 lipids, displayed low-grade glioma and BAT were clustered based on differential expression of PC and SM species (Figure 5.3A). Low-grade BAT expressed greater relative abundance of low unsaturated PC, like PCo(32:1, 34:1, and 36:1), as well as short- and long-chain SM, i.e. SM d18:1/16:0 and SM d(18:1/24:0) respectively. Conversely, low-grade glioma were distinguished by higher relative abundance of saturated PC species, PC(30:0 and 32:0), and diminished expression of low unsaturated PC. The M1 cluster plot demonstrated a transition from low unsaturated PC to saturated PC between low-grade BAT and low-grade glioma. The PC heatmap of top 60 lipids demonstrated several distinct clusters within the plot (Figure 5.3B). More specifically, BAT and glioma samples clustered more closely with their neighboring tissue rather than clustering by tissue type. Grade I glioma and BAT (364) primarily grouped to the left in the plot based on elevated expression of high unsaturated PC. Grade II glioma samples (203, 237, 300, and 305) also clustered predominantly with their adjacent BAT tissue Grade II glioma and BAT

were distinguished from one another based on differential expression of low unsaturated PC species. Overall, cluster analysis indicates two patterns based on profiling method employed; the M1 method showed distinction between glioma and BAT groups driven by low unsaturated PC. The PC method displayed low-grade glioma and BAT clustered together, and distinctions were induced by heterogeneity between patients.

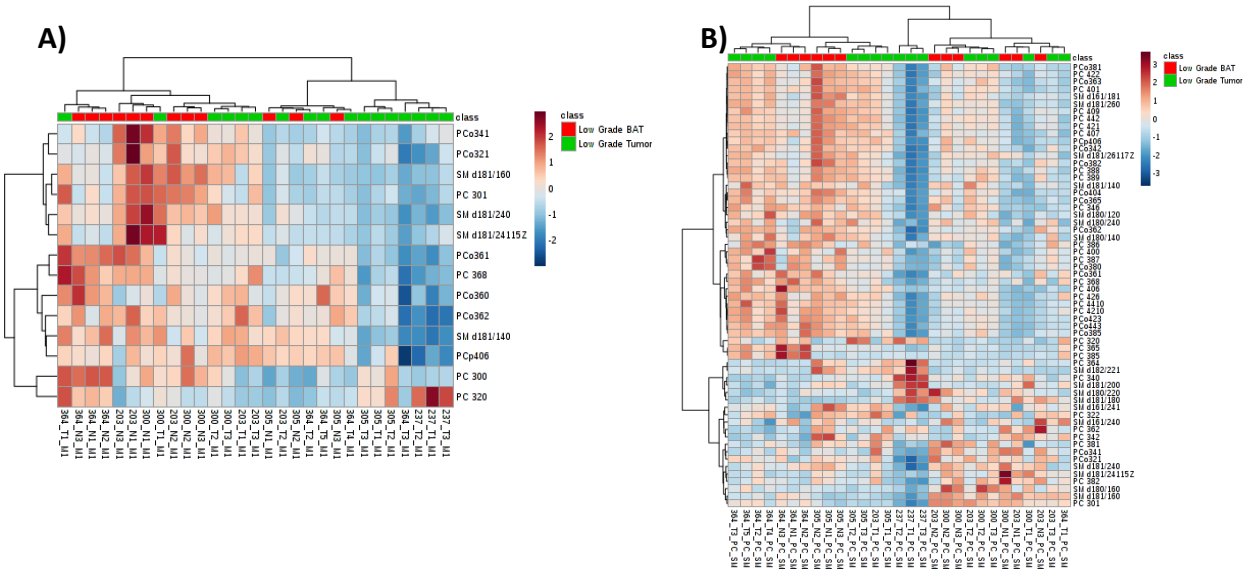

Figure 5.3 Cluster analysis identified lipid profile distinctions between low-grade glioma and BAT in M1 and PC MRM-profiling methods. A) M1 method, and B) PC method.

ROC curve

ROC Curve analysis identified one discriminant lipid species between low-grade glioma and BAT across M1 and PC profiling methods. SM d(18:1/24:0) was identified to be distinctly higher in low-grade BAT using the PC method (AUC= 0.897).

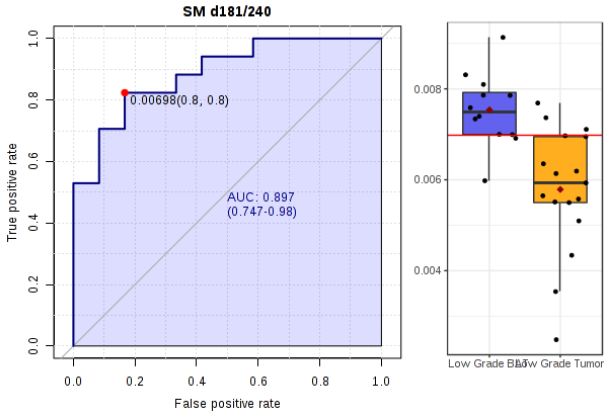

Figure 5.4 ROC Curve identified discriminant SM species between low-grade glioma and BAT.

5.3.2 High-grade glioma v. high-grade BAT

PCA

Principal component analysis demonstrated similar clustering of high-grade glioma and BAT points in plots for both M1 and PC screening methods (Figure 5.5). Lipids included in this multivariate analysis maintained a VIP score ≥ 1.0. Proximal localization of points was observed in M1 and PC plot, indicating similar lipid composition between tissue types. The M1 plot suggests comparable relative abundances of PC, SM, TAG, and carnitine species screened for in this method (Figure 5.5A). In addition, PC and SM relative abundances detected in the PC method were also maintained at similar levels in both high-grade glioma and BAT tissue (Figure 5.5B). The plots demonstrate high-grade glioma and BAT possess highly comparable lipid composition.

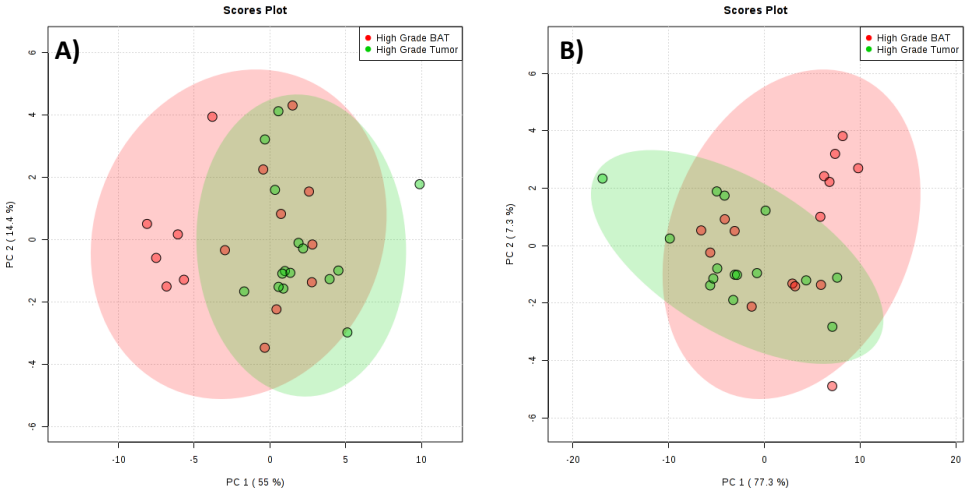

C)

Profiling Method	PC1 (%)	PC2 (%)
M1 Method	55	14.4
PC Method	77.3	7.3

Figure 5.5 PCA analysis of M1 and PC profiling methods indicate similar lipid profiles between high-grade glioma and BAT. A) M1 method, B) PC method, and C) PC1 and PC2 scores for both screening methods.

T-test

Statistical analysis identified the medium-chain, SM d(18:1/18:0) to be maintained at significantly different relative abundance between high-grade glioma and BAT (Figure 5.6). The PC screening method detected SM d(18:1/18:0) at greater relative abundance in high-grade BAT (Figure 5.6B, *p-value* < 0.001).

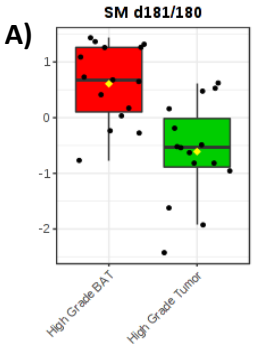

B)

Lipid	t.stat	p.value	-log10(p)	FDR
SM d18:1/18:0	4.1757	0.00026189	3.5819	0.026451

Figure 5.6 Differential expression of medium-chain SM species detected between high-grade glioma and BAT. A) SM d(18:1/18:0) concentration graph, B) statistical output.

Cluster analysis (heatmap)

Cluster analysis displayed distinctions in high-grade glioma and BAT groups in both M1 and PC screening methods (Figure 5.7). The M1 heatmap of the top 28 lipids identified glioma and BAT groups were distinguished based on differential expression of PC, SM, and carnitines (Figure 5.7A). High-grade BAT expressed greater relative abundance of low unsaturated PC species, such as PC(36:1 and 36:2) in addition to medium- and long-chain SM, like SM d(18:1/18:0) and SM d(18:1/24:0). Conversely, high-grade glioma comprised higher relative abundance of carnitine species concurrent with lower PC and SM expression. The PC method also denoted distinct clusters between high-grade glioma and BAT lipid profiles. The top 50 lipids in the PC heatmap displayed clustering due to PC saturation state (Figure 5.7B). High-grade glioma maintained elevated relative abundance for both saturated, i.e. PCo(38:0 and 40:00 and high-unsaturated PC, like PC(42:10 and 44:10), compared to high-grade BAT. Conversely, high-grade BAT expressed greater relative abundance of low unsaturated PC, PC(32:1 and 36:1), to distinguish from high-grade glioma. Taken together, cluster analysis demonstrated differences in PC saturation, SM, and carnitine relative abundance can discriminate between high-grade glioma and BAT.

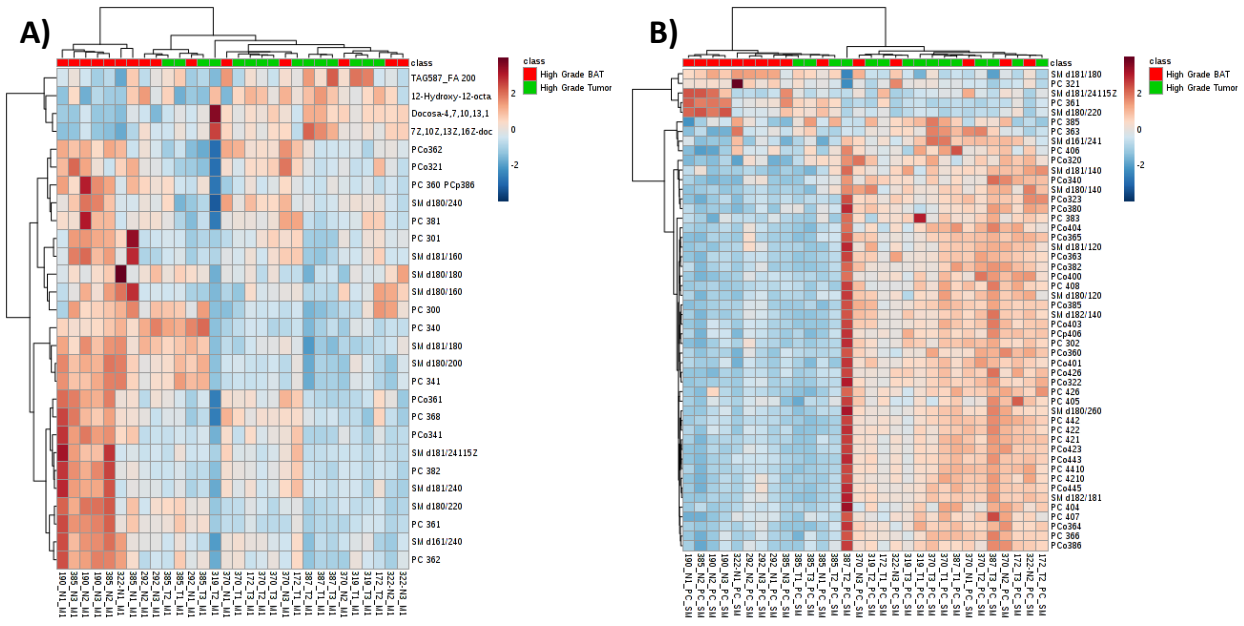

Figure 5.7 Cluster analysis indicates distinction between high-grade glioma and BAT lipid profiles through different PC, SM, and carnitine relative abundance. A) M1 method, B) PC method.

ROC curve

ROC curve analysis of lipids profiled by M1 and PC MRM-screening methods identified three lipids with discriminating power (Figure 5.8). From the M1 method, SM d(18:1/18:0) was determined to maintain an AUC of 0.849, and was expressed at higher relative abundance in high-grade BAT (Figure 5.8A). Two lipids were identified from the PC method to be distinct between tissue types, PC(32:1) and SM d(18:1/18:0), retaining AUC of 0.827 and 0.88 respectively (Figure 5.8B). Both PC(32:1) and SM d(18:1/18:0) were detected at higher relative abundance in high-grade BAT compared to high-grade glioma. In summary, ROC curve analysis suggests SM d(18:1/18:0), consistent across two screening methods, and PC(32:1) are discriminant lipid species between high-grade glioma and BAT.

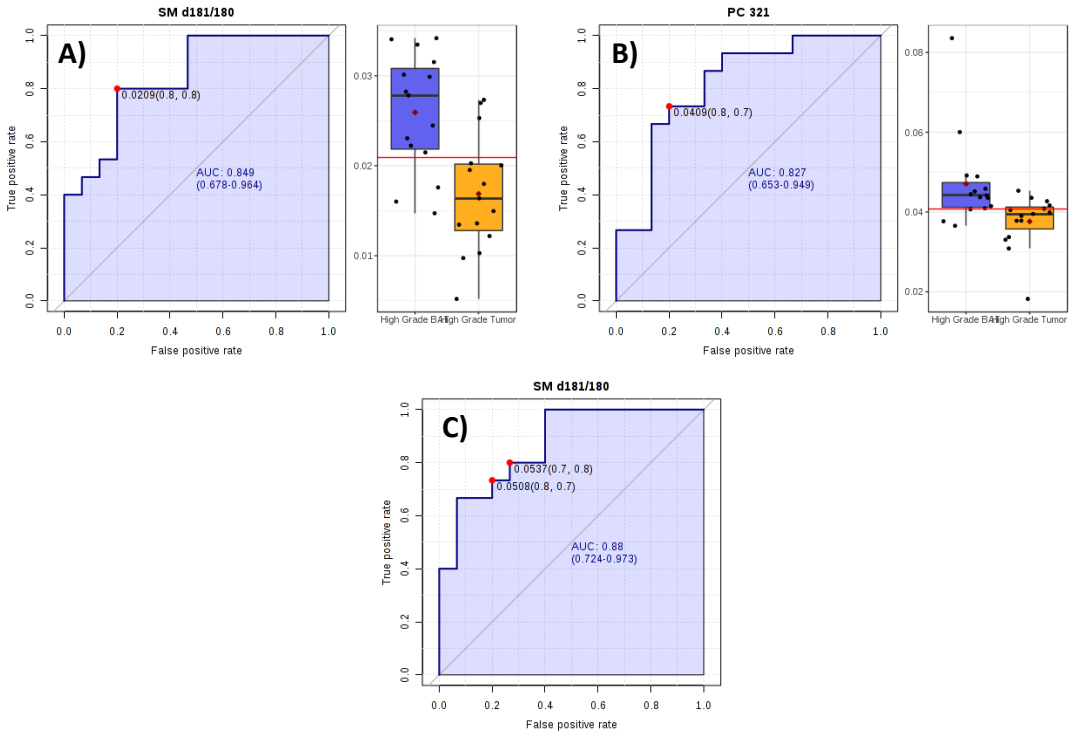

Figure 5.8 ROC curve analysis identified two discriminant PC and SM lipid species between high-grade glioma and BAT. A) M1 method, B-C) PC method.

5.3.3 Glioma v. BAT

PCA

PCA plots comparing lipid profiles of glioma and BAT profiled by M1 and PC screening methods demonstrated similar clustering within the plot (Figure 5.9). Multivariate plots include lipids from

each method with a VIP score ≥ 1.0. Glioma and BAT sample clusters in both M1 and PC plots located closely, indicating comparable lipid composition between tissue types. Sharing lipid profiles in the M1methods suggests similar relative abundances of PC, SM, TAG, and carnitine species between glioma and BAT (Figure 5.9A). Even further, PC and SM lipids profiled in the PC method were maintained at similar levels between tissue types (Figure 5.9B). Overall, both screening method plots indicate glioma and BAT share general lipid composition, with possible differences in individual lipid species.

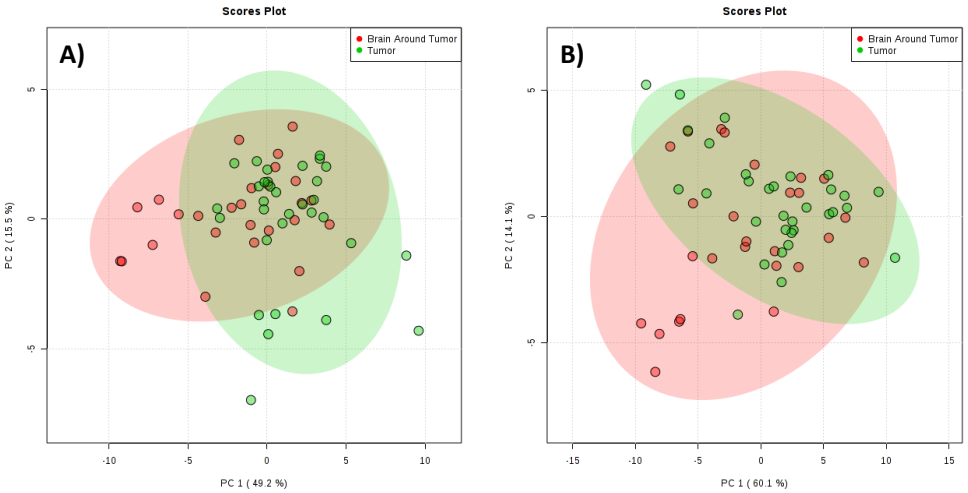

Profiling Method	**PC1** (%)	**PC2** (%)
M1 Method	49.2	15.5
PC Method	60.1	14.1

Figure 5.9 Multivariate analysis suggest similar lipid profiles between glioma and BAT in two screening methods. A) M1 method, B) PC method, and C) PC1 and PC2 scores for both screening methods.

T-test

Statistical analysis identified five individual lipids with significantly different relative abundances between glioma and BAT (Figure 5.10) All lipids determined to be differentially expressed in BAT were detected in the M1 profiling method. Three PC species were observed to maintain distinct expression between tissue types: PC(36:8) and PCo(34:1 and 36:1) (Figure 5.10A, *p-value*: $0.0001<p<0.01$). In addition, two SM were detected at greater relative abundances in BAT, SM d(16:1/24:0) and SM d(18:1/24:0) (*p-value*: $0.001<p<0.01$). To conclude, significance testing suggested low unsaturated PC and long-chain SM were critical lipid species to distinguish between glioma and BAT tissue.

A)

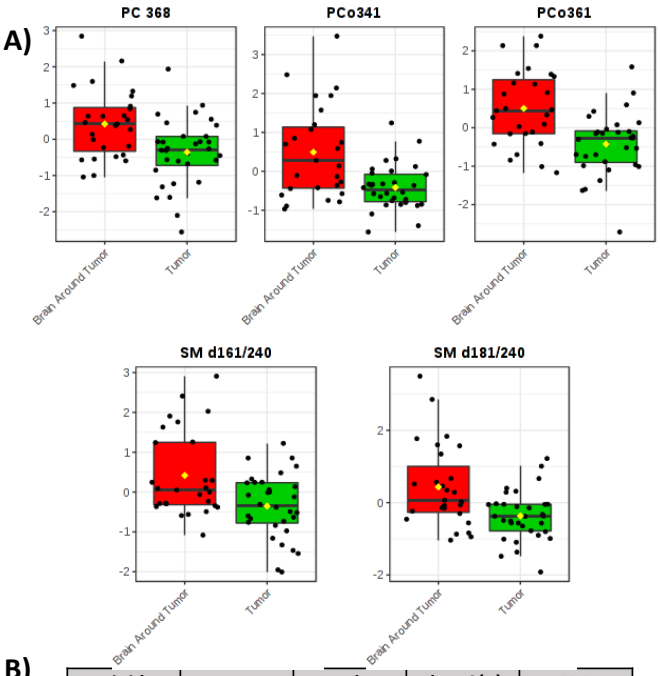

B)

Lipid	t.stat	p.value	-log10(p)	FDR
PCo36:1	3.9753	0.00020021	3.6985	0.013162
PCo34:1	3.8758	0.0002771	3.5574	0.013162
SM d18:1/24:0	3.3125	0.0016094	2.7933	0.047797
PC 36:8	3.2098	0.0021828	2.661	0.047797
SM d16:1/24:0	3.1613	0.0025156	2.5994	0.047797

Figure 5.10 Differential expression of PC and SM species between glioma and BAT detected using the M1 profiling method. A) Significant lipid concentration graphs, B) statistical output.

Lipid chain length and saturation analysis

Lipid chain length and saturation analysis identified significant differences in total lipid relative abundances between glioma and BAT based on these chemical characteristics (Figure 5.11). PC and SM were the two lipid classes that maintain discriminant expression due to chain length and saturation. A shift in PC saturation type between glioma and BAT was noted in the analysis. Glioma maintained significantly greater relative abundance of saturated PC than BAT (Figure 5.11A, $p<0.01$). Additionally, BAT comprised significantly greater low unsaturated PC compared to glioma (Figure 5.11B, $p<0.05$). Conversely to saturated PC, saturated SM had significantly higher relative abundance in BAT than glioma (Figure 5.11C, $p<0.05$). Lastly, BAT possessed significantly greater short- and long-chain SM vs glioma tissue (Figure 5.11D-E, $p<0.05$). Taken together, PC and SM chain length and saturation were differentiating factors between glioma and BAT groups.

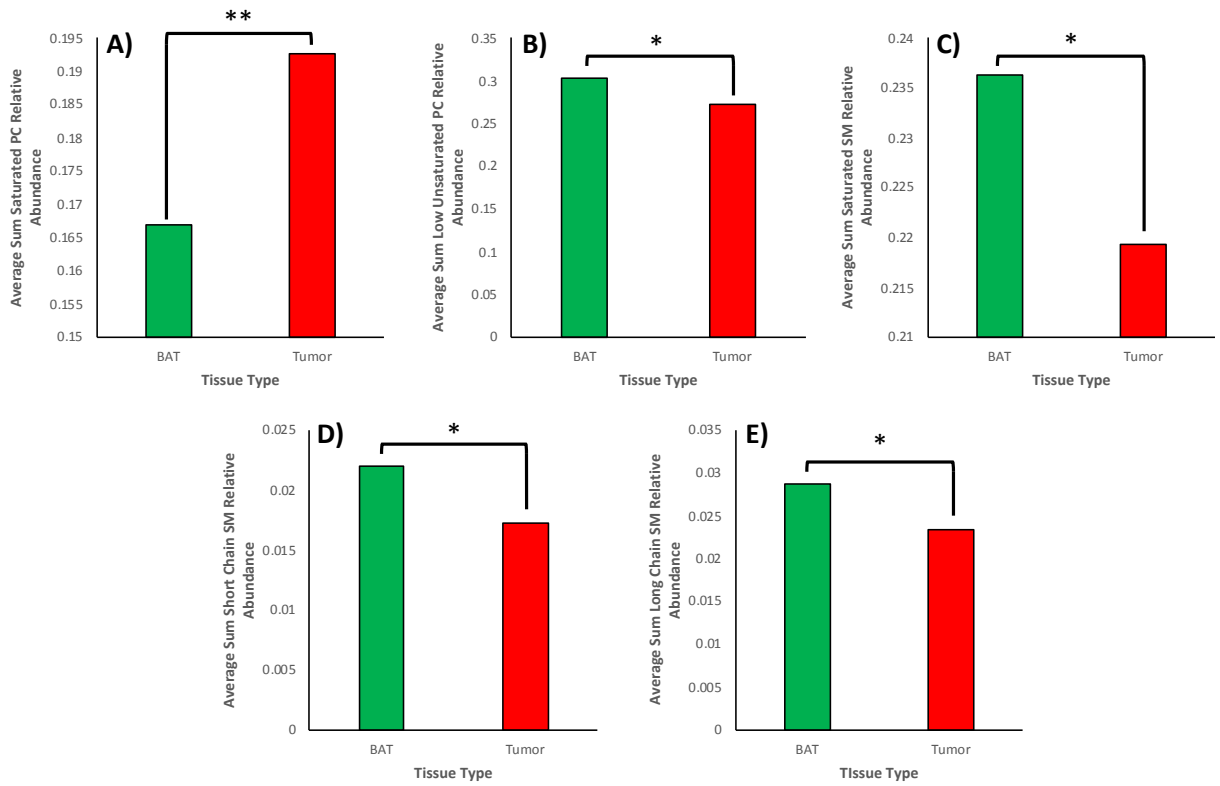

Figure 5.11 Significant differences in PC and SM chain length and saturation detected between glioma and BAT tissue. A-C) PC method, D-E) M1 method. * p≤0.05, ** p≤0.01.

Cluster analysis (heatmap)

Cluster analysis indicated a trend toward distinction between glioma and BAT groups (Figure 5.12). The M1 heatmap visualizing the top 10 lipids displayed a mild clustering trend based on low unsaturated PC lipids (Figure 5.12A). BAT expressed greater relative abundance of low unsaturated PC, supporting two distinct clusters within the plot. Low to intermediate expression levels of low unsaturated PC was observed in glioma samples, grouping them into two main clusters. Overall, the M1 plot demonstrated fairly comparable levels of both PC and SM relative abundances between groups with the exception of species like PCo(34:1) and PC(30:1 and 38:2). The PC heatmap of the top 35 lipids demonstrated clearly clustering of BAT and glioma groups due to differential expression of low and high unsaturated PC respectively (Figure 5.12B). Elevated expression of low unsaturated PC lipids, such as PC(36:1, 36:2, and 38:2) distinguished the BAT cluster from glioma. Additionally, glioma maintained greater relative abundance of high unsaturated PC, like PC(36:6 and 38:7), to differentiate from the BAT sample cluster. In summary,

cluster analysis suggests differences in membrane lipids, predominantly phosphatidylcholines, saturation state is a discriminating factor between glioma and BAT tissue.

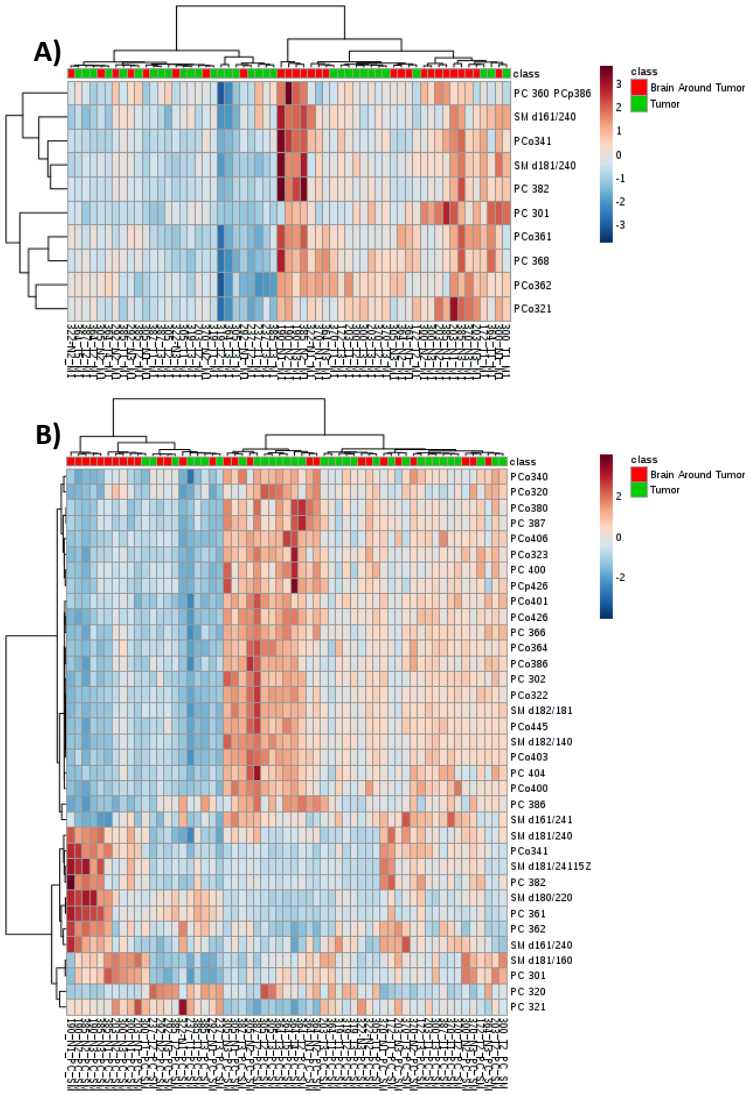

Figure 5.12 Cluster analysis identified PC saturation state as important distinguishing factor in differentiating between glioma and BAT. A) M1 method, B) PC method.

5.4 Discussion

With the minimal efficacy of currently approved therapeutics available to treat glioma patients, there continues to be an urgency to identify a novel therapeutic target to improve patient outcomes and overall survival. Recent lipidomics studies have detected distinctions in several lipid classes between glioma and brain that are currently being validated for diagnostic applications. However,

comprehensive molecular profile changes, specifically involving lipids, between glioma and the surrounding brain remains limited in the literature. To address this gap, in this study, we profiled glioma and BAT tissue across grades I-IV using MRM-MS to better define distinction in lipid composition between tissue types. Here, we observed similar lipid profiles, based on lipids evaluated within three screening methods, in each comparison group investigated: low-grade glioma vs low-grade BAT, high-grade glioma vs high-grade BAT, and glioma vs BAT. In addition, distinctions between tissue types were noted in several individual PC and SM species as well as changes in saturation type.

Glioma are characteristically highly aggressive tumors that undergo metabolic reprogramming to meet the energetic demands to sustain growth and survival[36]. Recent evidence supports increased reliance on biosynthetic pathways, especially lipid metabolism, to drive tumorigenesis[149]. Elevated lipid metabolism in glioma is distinct from healthy brain and was observed to generate distinct lipid concentration between tissue types[7,31]. Even further, IMS studies noted emphasis on lipid metabolism in glioma produced differential expression of lipid species from brain matter[6,9]. However, the findings in this study contrast this evidence as we report similar lipid compositions, based on interrogated lipids in each method, between glioma and BAT. Morphologically, glioma and BAT in this study were distinct, as WHO histological criteria differentiated between the tissue types in the sections, but clear molecular profile distinction was not detected. Studies investigating molecular profiles in breast cancer and its surrounding tissue observed a similar trend, molecular changes in tissue surrounding tumor occurred prior to morphological alterations[14,122]. Identifying this trend suggests paracrine- and autocrine-based lipid profile modulation in cells surrounding glioma, though possible mechanisms are not well understood.

One potential mechanism altering lipid composition involves glioma's manipulation of neuronal activity. Glioma's relationship with neurons has long been understood[150]. Neurons were identified to stimulate glioma growth through the release of neuroligin-3, a post-synaptic adhesion molecule found primarily in excitatory synapses, inducing the PI3K-mTOR signaling pathway[151]. Additionally, glioma can also stimulate neurons through the release of glutamate, an excitatory neurotransmitter[152,153]. Glioma glutamate release has been linked to epileptic seizures commonly occurring in glioma patients, but also to engaging in similar synaptic behaviors seen between neurons, oligodendroglial cells, and astrocytes[142]. The neuron-glioma relationship is both

bidirectional and cyclical; neurons are consistently stimulated by glioma glutamate release and produce neuroligin-3 that induces glioma growth, proliferation, and glutamate production to continue this cycle[141]. Inhibition of neuroligin-3 cleavage and NMDA glutamate binding individually abrogated the benefits of this glioma-neuron interaction, effectively reducing tumor growth and progression[153,154]. Despite these studies not directly studying lipids, it is conceivable that lipid composition is altered, during neuronal-glioma bidirectional stimulation, as lipids provide critical metabolic intermediates to meet high energetic demands of both tumor growth and neuron activity. However, further study characterizing lipid profile changes through this mechanism is needed.

Lipid profile similarities between glioma and BAT may also been explained through mechanisms glioma regulates in glial cells proximal to the tumor microenvironment (TME). Studies have recognized crosstalk between glioma, astrocytes, and microglia play an important role in progression[155,156]. Anti-inflammatory cytokine release from glioma induced phenotypic changes in both astrocytes and microglia[157,158]. Microglia possessing this anti-inflammatory phenotype were identified to release factors, like TGF-β, which support glioma growth and invasion[159]. Others demonstrated transcriptional profiles of microglia exposed to glioma had distinct gene expression compared to non-TME microglia[158]. The same study identified tumor-manipulated microglia also induced differential gene expression in astrocytes compared to astrocytes in epilepsy patients[158]. A recent study found anti-inflammatory astrocytes stimulate glioma migration and invasion through IL-6-mediated membrane type 1 matrix metalloproteinase release[160]. Henrik Heiland et al[158] determined glioma manipulate microglia and astrocytes through the JAK/STAT pathway. Inhibiting this pathway stimulated upregulation of pro-inflammatory cytokines in the TME, effectively reversing the anti-inflammatory phenotype in microglia and astrocytes. Like the neuronal mechanisms discussed above, these studies did not specifically measure lipid composition of cells regulated by glioma. Although, these mechanisms highlight the strong influence glioma has to alter genetic profiles and secreted protein factors in surrounding cells. Taken together, it is reasonable to hypothesize glioma utilizes mechanisms like those discussed to change lipid profiles in surrounding tissue comparable to that detected in this study.

Advantages of lipid composition changes in glioma are multifaceted. Glioma, like other cancers, possess high energetic demands to drive tumorigenic processes[146]. Metabolic reprogramming shifts glycolysis toward biosynthetic processes, such as lipid synthesis, to generate

alternative sources of energy[37]. Elevated lipid synthesis and metabolism supports increased glioma proliferation[105]. Synthesized lipids, like phospholipids, are consolidated for plasma membrane formation in current and newly divided glioma cells[132]. Lipids also protect glioma cells from oxidative stress stimulated by reactive oxygen species generated from aberrant metabolic processes[100]. Taken together, lipid composition changes provide aid to several key tumorigenic processes that initiate cancer development and maintain cancer progression. The extensive capacity for adaptation cancer possesses also supports the perspective lipid composition changes could be a result of cancerous changes. Abnormal cell signaling, characteristic of cancer, has been identified to modulate lipid synthesis[161]. In conclusion, lipid composition is an important factor to core processes within various forms of cancer, but compositional changes could be influenced based on other cancerous changes. This perspective is similar to the "chicken or the egg" scenario; signaling processes support lipid synthesis while the inverse is also true, as lipids provide energy to power cell signaling in cancer. The mutualistic relationship between lipids and cell signaling makes identifying whether lipid compositional changes being core to cancer or a result of cancerous changes difficult to discern.

This study demonstrated that tumor manipulation of BAT lipid composition occurs as early as low-grade glioma. Most studies investigating glioma-brain crosstalk utilized high-grade glioma, thus elucidating an interaction potentially critical to glioma progression. General similarity in lipid profile between glioma and BAT, across the three comparison groups, was also detected in studies investigating medulloblastoma (MB) and breast cancer. Paine et al found healthy grey matter around maintained a comparable lipid profile to MB with the exception of several individual phospholipid species[162]. Azordegan et al[14] demonstrated the marginal tissue surrounding breast cancer represented a transitional state between normal tissue and tumor, possessing similar phospholipid composition to tumor. In line with these studies, the reported results suggest BAT may be part of the problem, as the altered molecular profiles appear to support tumorigenic behaviors in glioma. Understanding this puts increased emphasis on better understanding the mechanisms glioma employs to regulate lipid composition in surrounding brain to support growth and how to potentially target BAT to hinder glioma progression. Evidence in both of these aspects remains limited, however, and requires additional study.

5.5 Conclusions

The above study identified that glioma and the neighbor brain tissue share highly comparable lipid composition to one another. MRM-profiling demonstrated that the alterations to BAT lipid profiles is influenced by glioma as early as grades I and II. High-grade glioma and BAT showed similar trends as low-grade samples, with subtle distinctions between tissue types based on PC lipid relative abundance. Cluster analysis, in low- and high-grade samples, showed differentiation between tissue types due to PC lipid saturation state. Low-grade BAT maintained higher relative abundances of low unsaturated PCs vs low-grade glioma tissues. Additionally, high-grade glioma was found to possess greater levels of high unsaturated PC compared to high-grade BAT that had more relative abundance of low unsaturated PC. Significant differences in average sum PC and SM, based on chain length and saturation, was also determined in glioma vs BAT. Brain around tumor maintained significantly higher low unsaturated PC as well as saturated, short- and long-chain SM compared to glioma. Also, glioma was comprised of significantly greater average sum saturated PC relative abundance than BAT. In conclusion, this study emphasizes the potential relevance of BAT to glioma growth and progression indicated by high similarity in lipid profiles. Future studies should focus on the mechanisms glioma employs to manipulate cells, proximal to the TME that could lead to poor patient outcomes as these pathways influencing lipid composition are currently unknown.

6 CONCLUSIONS AND FUTURE WORK

In the presented work, we highlighted the efficacy of our workflow, integrating pathology, laser capture microdissection, and multiple reaction monitoring-mass spectrometry, to analyze lipid composition in human glioma and brain around tumor samples. Utilizing this approach, we investigated lipid profile changes in glioma grades I-IV, the surround brain, and distinctions between tissue types to better define lipid expression throughout glioma progression. The overall goal of this project was to comprehensively define lipid profiles in glioma and BAT to identify novel lipid targets, that were glioma-specific, to be validated further for clinical translation. Below is an overview of each study, corresponding future work and limitations.

6.1 Glioma grade lipid profiling

Current clinically approved treatments for glioma, especially high-grade, are generally ineffective in prolonging patient survival, remains an average of 12-15 months[2]. Even further, therapeutic approaches targeting low-grade gliomas are limited in their ability to prevent tumor progression as 80% eventually progress to grade IV within a decade[13]. Knowing this merits investigation into alterations lipid profiles undergo at each glioma grade to elucidate key lipid species driving tumor progression. Exploring these molecular changes, through comprehensive MRM-profiling, will define lipids that can serve as potential targets to hinder glioma malignant transition. Glioma was identified to maintain an embryonic phenotype, due to expression of cancer stem cells, as well as elevated levels of membrane phospholipids; thus, two embryonic methods (M1 and M2) and a phosphatidylcholine method was used to screen samples[32,163]. This approach identified distinctions between glioma grades, predominantly in the PC method. PC and SM lipids were discriminant species based on their chain length and saturation state. ANOVA and cluster analysis indicated high unsaturated PC, PC(36:5 and 38:5), were differentially expressed in grade I glioma. Additionally, low unsaturated PC and long-chain SM maintained greater relative abundance in high grade glioma. Grade-based significant differences was also identified as PC(36:1) and PC(34:2 and 36:3) were distinct in grade III and IV respectively. ROC curve analysis demonstrated individual, as well as combined, low unsaturated PC and long-chain SM possessed strong discriminating power between low- and high-grade glioma suggesting alterations in chain length

and saturation during glioma progression. Several limitations were noted in this study. First, low sample size for each glioma grade group were tested in this study; grade I (n=1) and grades II-IV (n=12, 4 per grade). Human brain tumor samples are invaluable, but to increase the power and validity of reported results, additional tumor samples must be investigated to compare and support our findings. Second, blind and random selection limited bias in samples chosen for analysis but introduced variability in glioma subtypes in each tumor grade. Glioma maintains multiple subtypes that are comprised of difference concentrations of cell types. Diverse oligodendrocyte and astrocyte levels could vary the lipid composition detected in isolated samples, due to their distinct functioning, and glioma subtypes were not considered in this study[164,165]. To address this limitation, future studies can specifically select samples, based on subtype, for analysis to determine glioma subtype-related differences in lipid profile. Lastly, this study did not consider all lipid classes during analysis. Ceramides and phosphatidylserines were found to be distinct in glioma tissue, therefore, future studies profiling these and other lipid classes in glioma would better define lipid profiles and pathways to identify novel lipid targets to improve patient outcomes.

6.2 Brain around tumor lipid profiling

Brain around glioma is understood to be highly compromised compared to healthy brain[115]. Compromised brain can be attributed, partly, to factors released by glioma into the tumor microenvironment, altering the genetic and protein expression of surrounding tissue. Despite this understanding however, limited evidence is available defining the influence of glioma-related factors on BAT lipid profiles. Even further, it is unclear how lipid alteration in BAT could promote glioma growth. Noting this gap, it was critical to investigate BAT lipid profiles at each grade of glioma to better understand alterations in composition throughout disease progression. Comprehensively profiling lipids in BAT by grade will identify distinct lipid species at each stage of glioma progression that could contribute to malignant transition. 13 BAT patient samples from grades I-IV were analyzed using the three profiling methods applied to screen glioma samples, M1, M2, and PC. Significant changes to lipid composition were identified between BAT exposed to different glioma grades. Multivariate analysis in both M1 and PC screening methods displayed distinct clusters between BAT groups indicated overall lipid profile changes as glioma progresses. Discrimination between BAT groups was driven by differential expression of PC, SM, carnitine, and TAG species. Low-grade BAT was distinguished based on elevated relative abundance of

carnitine and TAG in the M1 method and high unsaturated PC in the PC method. Distinction of high-grade BAT was determined by elevated relative abundance of low unsaturated PC in both M1 and PC methods. Significance testing, by t-test and ANOVA, identified TAG, carnitine, high-unsaturated PC, and short-chain SM were significantly higher in low-grade glioma, supporting cluster analysis findings. In addition, low unsaturated PC relative abundance were significantly greater in high-grade glioma. ROC curve analysis indicated significant lipid composition changes between grade II and grade III BAT, also considered the low- to high-grade transition. Discrimination of grade II from grade III was determined by distinct TAG, carnitine, and high unsaturated PC expression. Transition to grade III comprised increased low unsaturated PC and long-chain SM. This transition could indicate a significant alteration in BAT that supports glioma growth. Taken together, significant lipid profile changes were detected between BAT grades. Composition changes could potentially be due to glioma manipulating BAT lipids through autocrine and paracrine factors released into the TME. There were several limitations of note in this study. Similar to the glioma profiling study, there was a small sample size. 13 patient samples, BAT grade I (n=1) and BAT grades II to IV (n=12, 4 per grade). Further validation of our results will be needed to confirm findings by testing additional BAT samples under the same experimental parameters. H&E staining utilized in this study also did not distinguish between grey and white matter in brain. White matter contains myelin, comprised highly of sphingolipids and cholesterol, making its lipid composition distinct from grey matter. To further evaluate distinctions in BAT groups or in comparisons against glioma, additional staining differentiating grey and white matter will need to be conducted to guide LCM isolation to evaluate as separate tissue types. Future work should focus on investigating non-tumor compromised together with glioma and BAT to fully characterize the alterations in lipid profiles that occur in this disease. Studies have identified tissue around tumor as a transition state between healthy and tumor tissue and including healthy brain into the analysis would highlight the impact glioma has on neighboring brain tissue.

6.3 Glioma vs brain around tumor lipid profiling

Metabolic reprograming in glioma has increased importance lipid metabolism to meet energetic demands and sustain development, growth, and survival[104]. Imaging mass spectrometry studies have detected distinctions between glioma and surrounding brain tissue, possibly due to metabolic alterations in tumor[9]. Observed lipid differences have benefitted diagnostics but has not been

translated towards improving therapeutics. Lipids, and their associated synthesis pathways, are highly diverse and limited characterization of each is currently available. This study addressed this gap by comprehensively profiling both glioma and BAT lipid composition to better understand distinct glioma lipids and pathways to potentially utilize as therapeutic targets. A total of 59 samples, 32 glioma and 27 BAT, were analyzed from 13 human glioma tumors using M1, M2, and PC MRM-methods. Comparison testing of low-grade, high-grade, and overall glioma and BAT groups indicated that glioma and the surrounding brain have highly similar lipid profiles, based on lipids detected in the M1, M2, and PC screening methods. These findings were supported by minimal cluster separation in PCA, few significantly different lipids determined by t-test, and minimal discriminant lipids through ROC curve analysis. Comparable molecular profiles observed in this experiment preceded morphological changes in BAT as histological analysis distinguished these cells from glioma by H&E staining. These findings suggest BAT is subject to TME factors released by glioma to influence molecular profile alterations. Studies have shown glioma manipulates neighboring cell types through release of cytokines, neurotransmitters, and growth factors to promote tumor growth, migration, and proliferation[151,155,156,166]. Though not specifically investigated in this study, we postulate that lipid composition profiled in BAT were influenced by secreted glioma factors in the TME. The reported findings support future investigation of mechanisms glioma exploits to alter BAT lipid profiles and the implications of inhibiting these interactions on glioma growth and survival. Additionally, it would be important to establish a new screening method specifically tailored for evaluating glioma and BAT lipid composition. Due to small sample volume, generating a novel method was not feasible. In addition, it would be important to increase the sample size of both glioma and BAT groups to increase the power of these findings. Lastly, these findings suggest a shift in focus, expanding the perspective when investigating therapeutic options to include BAT into the equation, as recent evidence indicates cells proximal to the tumor could be part of the problem.

6.4 Concluding Remarks

In closing, the integrated workflow applied in this project can be used to profile distinct lipids in glioma and BAT at small sample volumes. The work demonstrated distinctions in PC and SM species as glioma progressed from low- and high-grade. Analysis of BAT indicated lipid profiles differences between grades most likely due to glioma grade-related factors. Lastly, we identified

glioma and BAT have similar lipid profiles based on screened lipids. Future work should focus on furthering goals of each study to identify a novel lipid target to improve glioma patient survival.

REFERENCES

1. Weller M, Wick W, Aldape K, et al. Glioma. *Nat Rev Dis Prim*. 2015;1:15017. doi:10.1038/nrdp.2015.17
2. Stupp R, Mason WP, van den Bent MJ, et al. Radiotherapy plus concomitant and adjuvant temozolomide for glioblastoma. *N Engl J Med*. 2005;352(10):987-996. doi:10.1056/NEJMoa043330
3. Sharma S, Salehi F, Scheithauer BW, Rotondo F, Syro L V., Kovacs K. Role of MGMT in tumor development, progression, diagnosis, treatment and prognosis. *Anticancer Res*. 2009;29(10):3759-3768. http://www.ncbi.nlm.nih.gov/pubmed/19846906.
4. Claus EB, Walsh KM, Wiencke JK, et al. Survival and low-grade glioma: The emergence of genetic information. *Neurosurg Focus*. 2015;38(1):E6. doi:10.3171/2014.10.FOCUS12367
5. Nørøxe DS, Poulsen HS, Lassen U. Hallmarks of glioblastoma: A systematic review. *ESMO Open*. 2016;1(6):e000144. doi:10.1136/esmoopen-2016-000144
6. Pirro V, Alfaro CM, Jarmusch AK, Hattab EM, Cohen-Gadol AA, Cooks RG. Intraoperative assessment of tumor margins during glioma resection by desorption electrospray ionization-mass spectrometry. *Proc Natl Acad Sci U S A*. 2017;114(26):6700-6705. doi:10.1073/pnas.1706459114
7. Guo D, Bell EH, Chakravarti A. Lipid metabolism emerges as a promising target for malignant glioma therapy. *CNS Oncol*. 2013;2(3):289-299. doi:10.2217/cns.13.20
8. Venneti S, Thompson CB. Metabolic Reprogramming in Brain Tumors. *Annu Rev Pathol Mech Dis*. 2017;12(1):515-545. doi:10.1146/annurev-pathol-012615-044329
9. Jarmusch AK, Alfaro CM, Pirro V, Hattab EM, Cohen-Gadol AA, Cooks RG. Differential Lipid profiles of normal human brain matter and gliomas by positive and negative mode desorption electrospray ionization - Mass spectrometry imaging. Zhou S, ed. *PLoS One*. 2016;11(9):e0163180. doi:10.1371/journal.pone.0163180
10. Cordeiro FB, Ferreira CR, Sobreira TJP, et al. Multiple reaction monitoring (MRM)-profiling for biomarker discovery applied to human polycystic ovarian syndrome. *Rapid Commun Mass Spectrom*. 2017;31(17):1462-1470. doi:10.1002/rcm.7927

11. Maher EA, Furnari FB, Bachoo RM, et al. Malignant glioma: Genetics and biology of a grave matter. *Genes Dev*. 2001;15(11):1311-1333. doi:10.1101/gad.891601
12. Hervey-Jumper SL, Berger MS. Role of surgical resection in low- and high-grade gliomas. *Curr Treat Options Neurol*. 2014;16(4):284. doi:10.1007/s11940-014-0284-7
13. Ostrom QT, Gittleman H, Fulop J, et al. CBTRUS statistical Report: primary brain and central nervous system tumors diagnosed in the United States in 2008-2012. *Neuro Oncol*. 2015;17(suppl 4):iv1-iv62. doi:10.1093/neuonc/nov189
14. Azordegan N, Fraser V, Le K, et al. Carcinogenesis alters fatty acid profile in breast tissue. *Mol Cell Biochem*. 2013;374(1-2):223-232. doi:10.1007/s11010-012-1523-4
15. Brennan CW, Verhaak RGW, McKenna A, et al. The somatic genomic landscape of glioblastoma. *Cell*. 2013;155(2):462. doi:10.1016/j.cell.2013.09.034
16. Niclou SP, Fack F, Rajcevic U. Glioma proteomics: Status and perspectives. *J Proteomics*. 2010;73(10):1823-1838. doi:10.1016/j.jprot.2010.03.007
17. Eberlin LS, Norton I, Dill AL, et al. Classifying human brain tumors by lipid imaging with mass spectrometry. *Cancer Res*. 2012;72(3):645-654. doi:10.1158/0008-5472.CAN-11-2465
18. Haag M. *Essential Fatty Acids and the Brain*. Vol 48.; 2003. http://journals.sagepub.com/doi/pdf/10.1177/070674370304800308. Accessed October 21, 2018.
19. Köhler M, MacHill S, Salzer R, Krafft C. Characterization of lipid extracts from brain tissue and tumors using Raman spectroscopy and mass spectrometry. *Anal Bioanal Chem*. 2009;393(5):1513-1520. doi:10.1007/s00216-008-2592-9
20. Viswanath P, Radoul M, Izquierdo-Garcia JL, et al. Mutant IDH1 gliomas downregulate phosphocholine and phosphoethanolamine synthesis in a 2-hydroxyglutarate-dependent manner. *Cancer Metab*. 2018;6(1):3. doi:10.1186/s40170-018-0178-3
21. Krafft C, Neudert L, Simat T, Salzer R. Near infrared Raman spectra of human brain lipids. *Spectrochim Acta - Part A Mol Biomol Spectrosc*. 2005;61(7):1529-1535. doi:10.1016/j.saa.2004.11.017
22. Nygren C, Von Holst H, Månsson JE, Fredman P. Increased levels of cholesterol esters in glioma tissue and surrounding areas of human brain. *Br J Neurosurg*. 1997;11(3):216-220. doi:10.1080/02688699746276

23. Karasinska JM, Hayden MR. Cholesterol metabolism in Huntington disease. *Nat Rev Neurol*. 2011;7(10):561-572. doi:10.1038/nrneurol.2011.132
24. Di Paolo G, Kim T-W. Linking lipids to Alzheimer's disease: cholesterol and beyond. *Nat Rev Neurosci*. 2011;12(5):284-296. doi:10.1038/nrn3012
25. Dawson G. Measuring brain lipids. *Biochim Biophys Acta - Mol Cell Biol Lipids*. 2015;1851(8):1026-1039. doi:10.1016/j.bbalip.2015.02.007
26. Röhrig F, Schulze A. The multifaceted roles of fatty acid synthesis in cancer. *Nat Rev Cancer*. 2016;16(11):732-749. doi:10.1038/nrc.2016.89
27. Srivastava NK, Pradhan S, Gowda GAN, Kumar R. In vitro, high-resolution 1H and31P NMR based analysis of the lipid components in the tissue, serum, and CSF of the patients with primary brain tumors: One possible diagnostic view. *NMR Biomed*. 2010;23(2):113-122. doi:10.1002/nbm.1427
28. Gonçalves VM, Baltazar F, Reis RM. Brain Tumor Metabolism — Unraveling Its Role in Finding New Therapeutic Targets. In: *Molecular Considerations and Evolving Surgical Management Issues in the Treatment of Patients with a Brain Tumor*. InTech; 2015. doi:10.5772/59606
29. Tugnoli V, Tosi MR, Tinti A, Trinchero A, Bottura G, Fini G. Characterization of lipids from human brain tissues by multinuclear magnetic resonance spectroscopy. *Biopolym - Biospectroscopy Sect*. 2001;62(6):297-306. doi:10.1002/bip.10005
30. Lin H, Patel S, Affeck VS, et al. Fatty acid oxidation is required for the respiration and proliferation of malignant glioma cells. *Neuro Oncol*. 2017;19(1):43-54. doi:10.1093/neuonc/now128
31. Gopal K, Grossi E, Paoletti P, Usardi M. Lipid composition of human intracranial tumors: A biochemical study. *Acta Neurochir (Wien)*. 1963;11(2):333-347. doi:10.1007/BF01402012
32. Guo D, Bell E, Chakravarti A. Lipid metabolism emerges as a promising target for malignant glioma therapy. *CNS Oncol*. 2013;2(3):289-299. doi:10.2217/cns.13.20.Lipid
33. Offer S, Menard JA, Pérez JE, et al. Extracellular lipid loading augments hypoxic paracrine signaling and promotes glioma angiogenesis and macrophage infiltration. *J Exp Clin Cancer Res*. 2019;38(1):241. doi:10.1186/s13046-019-1228-6

34. Guo D. Lipid droplets, potential biomarker and metabolic target in glioblastoma. *Intern Med Rev*. 2017;3(5). doi:10.18103/imr.v3i5.443
35. Poteet E, Choudhury GR, Winters A, et al. Reversing the Warburg effect as a treatment for glioblastoma. *J Biol Chem*. 2013;288(13):9153-9164. doi:10.1074/jbc.M112.440354
36. Ru P, Williams T, Chakravarti A, Guo D. Tumor Metabolism of Malignant Gliomas. *Cancers (Basel)*. 2013;5(4):1469-1484. doi:10.3390/cancers5041469
37. Strickland M, Stoll EA. Metabolic Reprogramming in Glioma. *Front Cell Dev Biol*. 2017;5:43. doi:10.3389/fcell.2017.00043
38. Dong G, Mao Q, Xia W, et al. PKM2 and cancer: The function of PKM2 beyond glycolysis (Review). *Oncol Lett*. 2016;11(3):1980-1986. doi:10.3892/ol.2016.4168
39. Stephenson DJ, Hoeferlin LA, Chalfant CE. Lipidomics in translational research and the clinical significance of lipid-based biomarkers. *Transl Res*. 2017;189:13-29. doi:10.1016/j.trsl.2017.06.006
40. Ferreira CR, Yannell KE, Mollenhauer B, et al. Chemical profiling of cerebrospinal fluid by multiple reaction monitoring mass spectrometry. *Analyst*. 2016;141(18):5252-5255. doi:10.1039/c6an01618a
41. de Lima CB, Ferreira CR, Milazzotto MP, Sobreira TJP, Vireque AA, Cooks RG. Comprehensive lipid profiling of early stage oocytes and embryos by MRM profiling. *J Mass Spectrom*. 2018;53(12):1247-1252. doi:10.1002/jms.4301
42. Bou Khalil M, Hou W, Zhou H, et al. Lipidomics era: Accomplishments and challenges. *Mass Spectrom Rev*. 2010;29(6):877-929. doi:10.1002/mas.20294
43. Chang RYK, Etheridge N, Dodd P, Nouwens A. Quantitative multiple reaction monitoring analysis of synaptic proteins from human brain. *J Neurosci Methods*. 2014;227:189-210. doi:10.1016/j.jneumeth.2014.02.016
44. Lehnert S, Jesse S, Rist W, et al. ITRAQ and multiple reaction monitoring as proteomic tools for biomarker search in cerebrospinal fluid of patients with Parkinson's disease dementia. *Exp Neurol*. 2012;234(2):499-505. doi:10.1016/j.expneurol.2012.01.024
45. XIAO Y, CHEN Y, KENNEDY AW, BELINSON J, XU Y. Evaluation of Plasma Lysophospholipids for Diagnostic Significance Using Electrospray Ionization Mass Spectrometry (ESI-MS) Analyses. *Ann N Y Acad Sci*. 2006;905(1):242-259. doi:10.1111/j.1749-6632.2000.tb06554.x

46. Fillet M, Van Heugen JC, Servais AC, De Graeve J, Crommen J. Separation, identification and quantitation of ceramides in human cancer cells by liquid chromatography-electrospray ionization tandem mass spectrometry. *J Chromatogr A*. 2002;949(1-2):225-233. doi:10.1016/S0021-9673(01)01422-4
47. Yoon HR, Kim H, Cho SH. Quantitative analysis of acyl-lysophosphatidic acid in plasma using negative ionization tandem mass spectrometry. *J Chromatogr B Anal Technol Biomed Life Sci*. 2003;788(1):85-92. doi:10.1016/S1570-0232(02)01031-0
48. Zhou Q, Gallo JM. Quantification of sunitinib in mouse plasma, brain tumor and normal brain using liquid chromatography-electrospray ionization-tandem mass spectrometry and pharmacokinetic application. *J Pharm Biomed Anal*. 2010;51(4):958-964. doi:10.1016/j.jpba.2009.10.006
49. Ha SJ. Lipid and Metabolite Profiling Mass Spectrometry of Human Glioblastoma Using Mouse Xenograft Model. *ProQuest Diss Theses*. 2018. https://search.proquest.com/docview/2112857128?accountid=49007%0Ahttp://www.yidu.edu.cn/educhina/educhina.do?artifact=&svalue=Lipid+and+Metabolite+Profiling+Mass+Spectrometry+of+Human+Glioblastoma+Using+Mouse+Xenograft+Model&stype=2&s=on%0Ahttp://sfx.cceu.
50. Eberlin LS, Ferreira CR, Dill AL, Ifa DR, Cheng L, Cooks RG. Nondestructive, histologically compatible tissue imaging by desorption electrospray ionization mass spectrometry. *ChemBioChem*. 2011;12(14):2129-2132. doi:10.1002/cbic.201100411
51. Eberlin LS, Norton I, Orringer D, et al. Ambient mass spectrometry for the intraoperative molecular diagnosis of human brain tumors. *Proc Natl Acad Sci U S A*. 2013;110(5):1611-1616. doi:10.1073/pnas.1215687110
52. Gopal K, Grossi E, Paoletti P, Usardi M. Lipid composition of human intracranial tumors: A biochemical study. *Acta Neurochir (Wien)*. 1963;11(2):333-347. doi:10.1007/BF01402012
53. Eberlin LS, Ferreira CR, Dill AL, Ifa DR, Cooks GR. Desorption Electrospray Ionization Mass Spectrometry for Lipid Characterization and Biological Tissue Imaging. *Biochem Biophys Acta*. 2011;1811(11):946-960. doi:10.1016/j.bbalip.2011.05.006.Desorption

54. Eberlin LS, Liu X, Ferreira CR, Santagata S, Agar NYR, Cooks RG. DESI then MALDI mass spectrometry imaging of lipid and protein distributions in single tissue sections. *Anal Chem*. 2011;83(22):8366-8371. doi:10.1021/ac202016x
55. Jarmusch AK, Alfaro CM, Pirro V, Hattab EM, Cohen-Gadol AA, Cooks RG. Differential Lipid profiles of normal human brain matter and gliomas by positive and negative mode desorption electrospray ionization - Mass spectrometry imaging. Zhou S, ed. *PLoS One*. 2016;11(9):e0163180. doi:10.1371/journal.pone.0163180
56. Pandey R, Caflisch L, Lodi A, Brenner AJ, Tiziani S. Metabolomic signature of brain cancer. *Mol Carcinog*. 2017;56(11):2355-2371. doi:10.1002/mc.22694
57. Sandrone SS, Repossi G, Candolfi M, Eynard AR. Polyunsaturated fatty acids and gliomas: A critical review of experimental, clinical, and epidemiologic data. *Nutrition*. 2014;30(10):1104-1109. doi:10.1016/j.nut.2014.01.009
58. Lewis CA, Brault C, Peck B, et al. SREBP maintains lipid biosynthesis and viability of cancer cells under lipid- and oxygen-deprived conditions and defines a gene signature associated with poor survival in glioblastoma multiforme. *Oncogene*. 2015;34(40):5128-5140. doi:10.1038/onc.2014.439
59. Grösch S, Schiffmann S, Geisslinger G. Chain length-specific properties of ceramides. *Prog Lipid Res*. 2012;51(1):50-62. doi:10.1016/j.plipres.2011.11.001
60. Piyarathna DWB, Rajendiran TM, Putluri V, et al. Distinct Lipidomic Landscapes Associated with Clinical Stages of Urothelial Cancer of the Bladder. *Eur Urol Focus*. 2018;4(6):907-915. doi:10.1016/j.euf.2017.04.005
61. Kros JM. Grading of gliomas: The road from eminence to evidence. *J Neuropathol Exp Neurol*. 2011;70(2):101-109. doi:10.1097/NEN.0b013e31820681aa
62. Ferreira CR, Cooks RG. Overview and Latest Developments in Desorption Electrospray Ionization (DESI) Mass Spectrometry Imaging. *Microsc Microanal*. 2016;19(S2):650-651. doi:10.1017/S1431927613005242
63. Bonner RF, Emmert-Buck M, Cole K, et al. Laser capture microdissection: Molecular analysis of tissue. *Science (80-).* 1997;278(5342):1481-1491. doi:10.1126/science.278.5342.1481
64. Bevilacqua C, Ducos B. Laser microdissection: A powerful tool for genomics at cell level. *Mol Aspects Med*. 2018;59:5-27. doi:10.1016/j.mam.2017.09.003

65. Datta S, Malhotra L, Dickerson R, Chaffee S, Sen CK, Roy S. Laser capture microdissection: Big data from small samples. *Histol Histopathol*. 2015;30(11):1255-1269. doi:10.14670/HH-11-622

66. Xu BJ, Caprioli RM, Sanders ME, Jensen RA. Direct analysis of laser capture microdissected cells by MALDI mass spectrometry. *J Am Soc Mass Spectrom*. 2002;13(11):1292-1297. doi:10.1016/S1044-0305(02)00644-X

67. Hebbar S, Schulz WD, Sauer U, Schwudke D. Laser capture microdissection coupled with on-column extraction LC-MS n Enables lipidomics of fluorescently labeled drosophila neurons. *Anal Chem*. 2014;86(11):5345-5352. doi:10.1021/ac500276r

68. Dilillo M, Ait-Belkacem R, Esteve C, et al. Ultra-High Mass Resolution MALDI Imaging Mass Spectrometry of Proteins and Metabolites in a Mouse Model of Glioblastoma. *Sci Rep*. 2017;7(1):603. doi:10.1038/s41598-017-00703-w

69. Nyalwidhe JO, Grzesik WJ, Burch TC, et al. Comparative quantitative proteomic analysis of disease stratified laser captured microdissected human islets identifies proteins and pathways potentially related to type 1 diabetes. Pietropaolo M, ed. *PLoS One*. 2017;12(9):e0183908. doi:10.1371/journal.pone.0183908

70. Knittelfelder O, Traikov S, Vvedenskaya O, et al. Shotgun Lipidomics Combined with Laser Capture Microdissection: A Tool to Analyze Histological Zones in Cryosections of Tissues. *Anal Chem*. 2018;90(16):9868-9878. doi:10.1021/acs.analchem.8b02004

71. Molina ES, Pillat MM, Moura-Neto V, Lah TT, Ulrich H. Glioblastoma stem-like cells: approaches for isolation and characterization. *J Cancer Stem Cell Res*. 2014;821(15):e1007. doi:10.14343/JCSCR.2014.2e1007

72. Ahmed AU, Auffinger B, Lesniak MS. Understanding glioma stem cells: rationale, clinical relevance and therapeutic strategies. *Expert Rev Neurother*. 2013;13(5):545-555. doi:10.1586/ern.13.42

73. Bligh EG, Dyer WJ. A RAPID METHOD OF TOTAL LIPID EXTRACTION AND PURIFICATION1. *Can J Biochem Physiol*. 1959;37(8):911-917. doi:10.1145/3163918

74. Kyle JE, Zhang X, Weitz KK, et al. Uncovering biologically significant lipid isomers with liquid chromatography, ion mobility spectrometry and mass spectrometry. *Analyst*. 2016;141(5):1649-1659. doi:10.1039/c5an02062j

75. Chong J, Soufan O, Li C, et al. MetaboAnalyst 4.0: Towards more transparent and integrative metabolomics analysis. *Nucleic Acids Res*. 2018;46(W1):W486-W494. doi:10.1093/nar/gky310
76. Abdi H, Williams L. Principal component analysis. *Anal Methods*. 2014;6(4):1-16. doi:10.1002/wics.101
77. Jarmusch AK, Pirro V, Baird Z, Hattab EM, Cohen-Gadol AA, Cooks RG. Lipid and metabolite profiles of human brain tumors by desorption electrospray ionization-MS. *Proc Natl Acad Sci*. 2016;113(6):1486-1491. doi:10.1073/pnas.1523306113
78. Shevchenko A, Simons K. Lipidomics: coming to grips with lipid diversity. *Nat Rev Mol Cell Biol*. 2010;11(8):593-598. doi:10.1038/nrm2934
79. May-Zhang AA, Deal KK, Southard-Smith EM. Optimization of laser-capture microdissection for the isolation of enteric ganglia from fresh-frozen human tissue. *J Vis Exp*. 2018;2018(136). doi:10.3791/57762
80. Sharma B, Kanwar SS. Phosphatidylserine: A cancer cell targeting biomarker. *Semin Cancer Biol*. 2018;52:17-25. doi:10.1016/j.semcancer.2017.08.012
81. Wang L, Habib AA, Mintz A, Li KC, Zhao D. Phosphatidylserine-targeted nanotheranostics for brain tumor imaging and therapeutic potential. *Mol Imaging*. 2017;16:153601211770872. doi:10.1177/1536012117708722
82. Vallabhapurapu SD, Blanco VM, Sulaiman MK, et al. Variation in human cancer cell external phosphatidylserine is regulated by flippase activity and intracellular calcium. *Oncotarget*. 2015;6(33):34375-34388. doi:10.18632/oncotarget.6045
83. Zhao D, Stafford JH, Zhou H, Thorpe PE. Near-infrared Optical Imaging of Exposed Phosphatidylserine in a Mouse Glioma Model. *Transl Oncol*. 2011;4(6):355-364. doi:10.1593/tlo.11178
84. Claes A, Idema AJ, Wesseling P. Diffuse glioma growth: A guerilla war. *Acta Neuropathol*. 2007;114(5):443-458. doi:10.1007/s00401-007-0293-7
85. Guan X, Vengoechea J, Zheng S, et al. Molecular subtypes of glioblastoma are relevant to lower grade glioma. Jiang T, ed. *PLoS One*. 2014;9(3):e91216. doi:10.1371/journal.pone.0091216

86. Baenke F, Peck B, Miess H, Schulze A. Hooked on fat: the role of lipid synthesis in cancer metabolism and tumour development. *Dis Model Mech*. 2013;6(6):1353-1363. doi:10.1242/dmm.011338

87. Ramli N, Khairy AM, Seow P, et al. Novel application of chemical shift gradient echo in- and opposed-phase sequences in 3 T MRI for the detection of H-MRS visible lipids and grading of glioma. *Eur Radiol*. 2016;26(7):2019-2029. doi:10.1007/s00330-015-4045-0

88. Eberlin LS, Dill AL, Golby AJ, et al. Discrimination of human astrocytoma subtypes by lipid analysis using desorption electrospray ionization imaging mass spectrometry. *Angew Chemie - Int Ed*. 2010;49(34):5953-5956. doi:10.1002/anie.201001452

89. Stensjøen AL, Solheim O, Kvistad KA, Håberg AK, Salvesen Ø, Berntsen EM. Growth dynamics of untreated glioblastomas in vivo. *Neuro Oncol*. 2015;17(10):1402-1411. doi:10.1093/neuonc/nov029

90. Bakovic M, Fullerton MD, Michel V. Metabolic and molecular aspects of ethanolamine phospholipid biosynthesis: The role of CTP:phosphoethanolamine cytidylyltransferase (Pcyt2). *Biochem Cell Biol*. 2007;85(3):283-300. doi:10.1139/O07-006

91. Hattingen E, Bähr O, Rieger J, Blasel S, Steinbach J, Pilatus U. Phospholipid Metabolites in Recurrent Glioblastoma: In Vivo Markers Detect Different Tumor Phenotypes before and under Antiangiogenic Therapy. Platten M, ed. *PLoS One*. 2013;8(3):e56439. doi:10.1371/journal.pone.0056439

92. Yeagle PL. Biogenesis of Membrane Lipids. In: *The Membranes of Cells*. Elsevier; 2016:57-71. doi:10.1016/b978-0-12-800047-2.00003-6

93. Constantin A, Elkhaled A, Jalbert L, et al. Identifying malignant transformations in recurrent low grade gliomas using high resolution magic angle spinning spectroscopy. *Artif Intell Med*. 2012;55(1):61-70. doi:10.1016/j.artmed.2012.01.002

94. Podo F. Tumour phospholipid metabolism. *NMR Biomed*. 2011;12(7):413-439. doi:10.1002/(SICI)1099-1492(199911)12:7<413::AID-NBM587>3.0.CO;2-U

95. Cheng M, Bhujwalla ZM, Glunde K. Targeting phospholipid metabolism in cancer. *Front Oncol*. 2016;6(DEC):266. doi:10.3389/fonc.2016.00266

96. Zalba S, ten Hagen TLM. Cell membrane modulation as adjuvant in cancer therapy. *Cancer Treat Rev*. 2017;52:48-57. doi:10.1016/j.ctrv.2016.10.008

97. Kim HJ, Miyazaki M, Ntambi JM. Dietary cholesterol opposes PUFA-mediated repression of the stearoyl-CoA desaturase-1 gene by SREBP-1 independent mechanism. *J Lipid Res*. 2002;43(10):1750-1757. doi:10.1194/jlr.M100433-JLR200
98. Guo D, Prins RM, Dang J, et al. EGFR signaling through an Akt-SREBP-1-dependent, rapamycin-resistant pathway sensitizes glioblastomas to antilipogenic therapy. *Sci Signal*. 2009;2(101):ra82-ra82. doi:10.1126/scisignal.2000446
99. Williams KJ, Argus JP, Zhu Y, et al. An essential requirement for the SCAP/SREBP signaling axis to protect cancer cells from lipotoxicity. *Cancer Res*. 2013;73(9):2850-2862. doi:10.1158/0008-5472.CAN-13-0382-T
100. Munir R, Lisec J, Swinnen J V., Zaidi N. Lipid metabolism in cancer cells under metabolic stress. *Br J Cancer*. 2019;120(12):1090-1098. doi:10.1038/s41416-019-0451-4
101. Rysman E, Brusselmans K, Scheys K, et al. De novo lipogenesis protects cancer cells from free radicals and chemotherapeutics by promoting membrane lipid saturation. *Cancer Res*. 2010;70(20):8117-8126. doi:10.1158/0008-5472.CAN-09-3871
102. Rabinovich AL, Ripatti PO. On the conformational, physical properties and functions of polyunsaturated acyl chains. *Biochim Biophys Acta (BBA)/Lipids Lipid Metab*. 1991;1085(1):53-62. doi:10.1016/0005-2760(91)90231-6
103. Madwar C, Gopalakrishnan G, Lennox RB. Lipid Microdomains in Synapse Formation. *ACS Chem Neurosci*. 2016;7(6):833-841. doi:10.1021/acschemneuro.6b00058
104. Beloribi-Djefaflia S, Vasseur S, Guillaumond F. Lipid metabolic reprogramming in cancer cells. *Oncogenesis*. 2016;5(1):e189. doi:10.1038/oncsis.2015.49
105. Santos CR, Schulze A. Lipid metabolism in cancer. *FEBS J*. 2012;279(15):2610-2623. doi:10.1111/j.1742-4658.2012.08644.x
106. Alberts B, Lewis J. The Lipid Bilayer. In: *Molecular Biology of the Cell*. Garland Science; 2013:6-11. https://www.ncbi.nlm.nih.gov/books/NBK26871/. Accessed October 26, 2019.
107. Nakada M, Kita D, Watanabe T, et al. Aberrant signaling pathways in Glioma. *Cancers (Basel)*. 2011;3(3):3242-3278. doi:10.3390/cancers3033242
108. Beloribi-Djefaflia S, Vasseur S, Guillaumond F. Lipid metabolic reprogramming in cancer cells. *Oncogenesis*. 2016;5(1):e189. doi:10.1038/oncsis.2015.49

109. Murai T, Maruyama Y, Mio K, Nishiyama H, Suga M, Sato C. Low cholesterol triggers membrane microdomain-dependent CD44 shedding and suppresses tumor cell migration. *J Biol Chem*. 2011;286(3):1999-2007. doi:10.1074/jbc.M110.184010
110. Hryniewicz-Jankowska A, Augoff K, Biernatowska A, Podkalicka J, Sikorski AF. Membrane rafts as a novel target in cancer therapy. *Biochim Biophys Acta - Rev Cancer*. 2014;1845(2):155-165. doi:10.1016/j.bbcan.2014.01.006
111. Ahmad F, Sun Q, Patel D, Stommel JM. Cholesterol metabolism: A potential therapeutic target in glioblastoma. *Cancers (Basel)*. 2019;11(2). doi:10.3390/cancers11020146
112. Wu H, Jiang H, Lu D, et al. Effect of simvastatin on glioma cell proliferation, migration, and apoptosis. *Neurosurgery*. 2009;65(6):1087-1097. doi:10.1227/01.NEU.0000360130.52812.1D
113. An Z, Weiss WA. Cholesterol: An Achilles' Heel for Glioblastoma? *Cancer Cell*. 2016;30(5):653-654. doi:10.1016/j.ccell.2016.10.011
114. Villa GR, Hulce JJ, Zanca C, et al. An LXR-Cholesterol Axis Creates a Metabolic Co-Dependency for Brain Cancers. *Cancer Cell*. 2016;30(5):683-693. doi:10.1016/j.ccell.2016.09.008
115. Lee J, Chaloner Winton Hall R. The Impact of Gliomas on Cognition and Capacity. *J Am Acad Psychiatry Law*. 2019;47(3):350-359. doi:10.29158/JAAPL.003841-19
116. Dwan TM, Ownsworth T, Chambers S, Walker DG, Shum DHK. Neuropsychological assessment of individuals with brain tumor: Comparison of approaches used in the classification of impairment. *Front Oncol*. 2015;5(FEB):56. doi:10.3389/fonc.2015.00056
117. Montano N, D'Alessandris QG, Bianchi F, et al. Communicating hydrocephalus following surgery and adjuvant radiochemotherapy for glioblastoma: Clinical article. *J Neurosurg*. 2011;115(6):1126-1130. doi:10.3171/2011.8.JNS11738
118. Bruce KD, Zsombok A, Eckel RH. Lipid processing in the brain: A key regulator of systemic metabolism. *Front Endocrinol (Lausanne)*. 2017;8(APR):60. doi:10.3389/fendo.2017.00060
119. Hamilton JA, Hillard CJ, Spector AA, Watkins PA. Brain uptake and utilization of fatty acids, lipids and lipoproteins: Application to neurological disorders. In: *Journal of Molecular Neuroscience*. Vol 33. Humana Press Inc; 2007:2-11. doi:10.1007/s12031-007-0060-1

120. Adibhatla RM, Hatcher JF. Role of lipids in brain injury and diseases. *Future Lipidol*. 2007;2(4):403-422. doi:10.2217/17460875.2.4.403
121. Hoelzinger DB, Demuth T, Berens ME. Autocrine factors that sustain glioma invasion and paracrine biology in the brain microenvironment. *J Natl Cancer Inst*. 2007;99(21):1583-1593. doi:10.1093/jnci/djm187
122. Hu M, Polyak K. Molecular characterisation of the tumour microenvironment in breast cancer. *Eur J Cancer*. 2008;44(18):2760-2765. doi:10.1016/j.ejca.2008.09.038
123. Le DM, Besson A, Fogg DK, et al. Exploitation of astrocytes by glioma cells to facilitate invasiveness: A mechanism involving matrix metalloproteinase-2 and the urokinase-type plasminogen activator-plasmin cascade. *J Neurosci*. 2003;23(10):4034-4043. doi:10.1523/jneurosci.23-10-04034.2003
124. Shug AL, Schmidt MJ, Golden GT, Fariello RG. The distribution and role of carnitine in the mammalian brain. *Life Sci*. 1982;31(25):2869-2874. doi:10.1016/0024-3205(82)90677-4
125. Nałęcz KA, Miecz D, Berezowski V, Cecchelli R. Carnitine: Transport and physiological functions in the brain. *Mol Aspects Med*. 2004;25(5-6):551-567. doi:10.1016/j.mam.2004.06.001
126. Ebert D, Haller RG, Walton ME. Energy contribution of octanoate to intact rat brain metabolism measured by 13C nuclear magnetic resonance spectroscopy. *J Neurosci*. 2003;23(13):5928-5935. doi:10.1523/jneurosci.23-13-05928.2003
127. Virmani A, Binienda Z. Role of carnitine esters in brain neuropathology. *Mol Aspects Med*. 2004;25(5-6):533-549. doi:10.1016/j.mam.2004.06.003
128. Yamada S, Matsuda R, Nishimura F, et al. Carnitine-induced senescence in glioblastoma cells. *Exp Ther Med*. 2012;4(1):21-25. doi:10.3892/etm.2012.556
129. Fahy E, Subramaniam S, Murphy RC, et al. Update of the LIPID MAPS comprehensive classification system for lipids. *J Lipid Res*. 2009;50 Suppl(Suppl):S9-14. doi:10.1194/jlr.R800095-JLR200
130. Wang H, Eckel RH. What are lipoproteins doing in the brainα. *Trends Endocrinol Metab*. 2014;25(1):8-14. doi:10.1016/j.tem.2013.10.003
131. Goldberg IJ. Lipoprotein lipase and lipolysis: Central roles in lipoprotein metabolism and atherogenesis. *J Lipid Res*. 1996;37(4):693-707. www.jlr.org.

132. Cheng C, Geng F, Cheng X, Guo D. Lipid metabolism reprogramming and its potential targets in cancer. *Cancer Commun*. 2018;38(1):27. doi:10.1186/s40880-018-0301-4
133. Bazinet RP, Layé S. Polyunsaturated fatty acids and their metabolites in brain function and disease. *Nat Rev Neurosci*. 2014;15(12):771-785. doi:10.1038/nrn3820
134. Peetla C, Vijayaraghavalu S, Labhasetwar V. Biophysics of cell membrane lipids in cancer drug resistance: Implications for drug transport and drug delivery with nanoparticles. *Adv Drug Deliv Rev*. 2013;65(13-14):1686-1698. doi:10.1016/j.addr.2013.09.004
135. Osuka S, Van Meir EG. Overcoming therapeutic resistance in glioblastoma: The way forward. *J Clin Invest*. 2017;127(2):415-426. doi:10.1172/JCI89587
136. Li J, Condello S, Thomes-Pepin J, et al. Lipid Desaturation Is a Metabolic Marker and Therapeutic Target of Ovarian Cancer Stem Cells. *Cell Stem Cell*. 2017;20(3):303-314.e5. doi:10.1016/j.stem.2016.11.004
137. Zalba S, ten Hagen TLM. Cell membrane modulation as adjuvant in cancer therapy. *Cancer Treat Rev*. 2017;52:48-57. doi:10.1016/j.ctrv.2016.10.008
138. Hoelzinger DB, Demuth T, Berens ME. Autocrine factors that sustain glioma invasion and paracrine biology in the brain microenvironment. *J Natl Cancer Inst*. 2007;99(21):1583-1593. doi:10.1093/jnci/djm187
139. Korade Z, Kenworthy AK. Lipid rafts, cholesterol, and the brain. *Neuropharmacology*. 2008;55(8):1265-1273. doi:10.1016/j.neuropharm.2008.02.019
140. Zeng Q, Michael IP, Zhang P, et al. Synaptic proximity enables NMDAR signalling to promote brain metastasis. *Nature*. September 2019:1-6. doi:10.1038/s41586-019-1576-6
141. Venkataramani V, Tanev DI, Strahle C, et al. Glutamatergic synaptic input to glioma cells drives brain tumour progression. *Nature*. September 2019:1-8. doi:10.1038/s41586-019-1564-x
142. Venkatesh HS, Morishita W, Geraghty AC, et al. Electrical and synaptic integration of glioma into neural circuits. *Nature*. 2019;in press:1-7. doi:10.1038/s41586-019-1563-y
143. Zheng Y-W, Tsuchida T, Taniguchi H. A novel concept of identifying precancerous cells to enhance anti-cancer therapies. *J Hepatobiliary Pancreat Sci*. 2012;19(6):621-625. doi:10.1007/s00534-012-0546-2
144. Soeda A, Hara A, Kunisada T, Yoshimura S, Iwama T, Park DM. The evidence of glioblastoma heterogeneity. *Sci Rep*. 2015;5:7979. doi:10.1038/srep07979

145. Zhou L, Wang Z, Hu C, et al. Integrated Metabolomics and Lipidomics Analyses Reveal Metabolic Reprogramming in Human Glioma with IDH1 Mutation. *J Proteome Res*. 2019;18(3):960-969. doi:10.1021/acs.jproteome.8b00663
146. Marie SKN, Shinjo SMO. Metabolism and brain cancer. *Clinics (Sao Paulo)*. 2011;66 Suppl 1(Suppl 1):33-43. doi:10.1590/S1807-59322011001300005
147. Müller CP, Reichel M, Mühle C, Rhein C, Gulbins E, Kornhuber J. Brain membrane lipids in major depression and anxiety disorders. *Biochim Biophys Acta - Mol Cell Biol Lipids*. 2015;1851(8):1052-1065. doi:10.1016/j.bbalip.2014.12.014
148. Block RC, Dorsey ER, Beck CA, Brenna JT, Shoulson I. Altered cholesterol and fatty acid metabolism in Huntington disease. *J Clin Lipidol*. 2010;4(1):17-23. doi:10.1016/j.jacl.2009.11.003
149. Agnihotri S, Zadeh G. Metabolic reprogramming in glioblastoma: The influence of cancer metabolism on epigenetics and unanswered questions. *Neuro Oncol*. 2016;18(2):160-172. doi:10.1093/neuonc/nov125
150. Scherer HJ. A CRITICAL REVIEW: THE PATHOLOGY OF CEREBRAL GLIOMAS. *J Neurol Neurosurg Psychiatry*. 1940;3(2):147-177. doi:10.1136/jnnp.3.2.147
151. Venkatesh HS, Johung TB, Caretti V, et al. Neuronal activity promotes glioma growth through neuroligin-3 secretion. *Cell*. 2015;161(4):803-816. doi:10.1016/j.cell.2015.04.012
152. Buckingham SC, Campbell SL, Haas BR, et al. Glutamate release by primary brain tumors induces epileptic activity. *Nat Med*. 2011;17(10):1269-1274. doi:10.1038/nm.2453
153. Takano T, Lin JH-C, Arcuino G, Gao Q, Yang J, Nedergaard M. Glutamate release promotes growth of malignant gliomas. *Nat Med*. 2001;7(9):1010-1015. doi:10.1038/nm0901-1010
154. Venkatesh HS, Tam LT, Woo PJ, Monje M. TARGETING NEURONAL ACTIVITY-REGULATED NEUROLIGIN-3 DEPENDENCY FOR HIGH-GRADE GLIOMA THERAPY. *Neuro Oncol*. 2017;19(suppl_4):iv27-iv27. doi:10.1093/neuonc/nox083.111
155. Pyonteck SM, Akkari L, Schuhmacher AJ, et al. CSF-1R inhibition alters macrophage polarization and blocks glioma progression. *Nat Med*. 2013;19(10):1264-1272. doi:10.1038/nm.3337
156. Lorger M. Tumor Microenvironment in the Brain. *Cancers (Basel)*. 2012;4(1):218-243. doi:10.3390/cancers4010218

157. Hambardzumyan D, Gutmann DH, Kettenmann H. The role of microglia and macrophages in glioma maintenance and progression. *Nat Neurosci*. 2015;19(1):20-27. doi:10.1038/nn.4185

158. Henrik Heiland D, Ravi VM, Behringer SP, et al. Tumor-associated reactive astrocytes aid the evolution of immunosuppressive environment in glioblastoma. *Nat Commun*. 2019;10(1):2541. doi:10.1038/s41467-019-10493-6

159. Wesolowska A, Kwiatkowska A, Slomnicki L, et al. Microglia-derived TGF-β as an important regulator of glioblastoma invasion - An inhibition of TGF-β-dependent effects by shRNA against human TGF-β type II receptor. *Oncogene*. 2008;27(7):918-930. doi:10.1038/sj.onc.1210683

160. Chen W, Xia T, Wang D, et al. Human astrocytes secrete IL-6 to promote glioma migration and invasion through upregulation of cytomembrane MMP14. *Oncotarget*. 2016;7(38):62425-62438. doi:10.18632/oncotarget.11515

161. Guri Y, Colombi M, Dazert E, et al. mTORC2 Promotes Tumorigenesis via Lipid Synthesis. *Cancer Cell*. 2017;32(6):807-823.e12. doi:10.1016/j.ccell.2017.11.011

162. Paine MRL, Liu J, Huang D, et al. Three-Dimensional Mass Spectrometry Imaging Identifies Lipid Markers of Medulloblastoma Metastasis. *Sci Rep*. 2019;9(1):2205. doi:10.1038/s41598-018-38257-0

163. Heddleston JM, Li Z, McLendon RE, Hjelmeland AB, Rich JN. The hypoxic microenvironment maintains glioblastoma stem cells and promotes reprogramming towards a cancer stem cell phenotype. *Cell Cycle*. 2009;8(20):3274-3284. doi:10.4161/cc.8.20.9701

164. Westphal M, Lamszus K. The neurobiology of gliomas: From cell biology to the development of therapeutic approaches. *Nat Rev Neurosci*. 2011;12(9):495-508. doi:10.1038/nrn3060

165. Hochberg FH, Atai NA, Gonda D, et al. Glioma diagnostics and biomarkers: an ongoing challenge in the field of medicine and science. *Expert Rev Mol Diagn*. 2014;14(4):439-452. doi:10.1586/14737159.2014.905202

166. Silver DJ, Siebzehnrubl FA, Schildts MJ, et al. Chondroitin sulfate proteoglycans potently inhibit invasion and serve as a central organizer of the brain tumor microenvironment. *J Neurosci*. 2013;33(39):15603-15617. doi:10.1523/JNEUROSCI.3004-12.2013

APPENDIX A. CHAPTER 2 SUPPLEMENTAL FIGURES

Table A.1 Lipid classes and species information screened in the M1 MRM-profiling method.

Lipid Class	Chain Length (# of Carbons)	Saturation (# of Double Bonds)
PC	30 - 40	0 - 8
PCo	32 - 40	0 - 6
PCp	36 - 42	5 - 6
SM	16 - 24	0 - 1
TAG	48 - 60	0 - 9
Carnitine	n = 26	

Table A.2 Lipid classes and species information screened in the M2 MRM-profiling method.

Lipid Class	Chain Length (# of Carbons)	Saturation (# of Double Bonds)
C	12 - 34	0 - 6
PE	18 - 40	0 - 9
PEo	34 - 40	1 - 6
PEp	36, 40	6 - 7
PG	16 - 40	0 - 8
PGo	20	0
PGp	38	6
PI	14 - 40	1 - 7
Pio	38	1 - 2
PIp	42	6
PS	14 - 40	1-7
PSo	16 - 20	0
PSp	16, 40, 42	0, 6
Steryl Ester	12 - 24	0 - 6

Table A.3 Lipid classes and species information screened in the PC MRM-profiling method.

Lipid Class	Chain Length (# of Carbons)	Saturation (# of Double Bonds)
PC	30 - 52	0 - 12
PCo	32 - 44	0 - 6
PCp	32 - 42	4 - 6
SM	12 - 26	0 - 1

Table A.4 Clinical and demographic information of patient samples screened by MRM-profiling across the three studies.

Patient ID	Case Comments	Body Site	Specific Site	Pathology Status	Histologic Type	Grade (final path)	Grade System (final path)	Ethnicity	Race	Gender	Subject Age	Specify other past Hx	Treatment	Resection Date	Survival Status
M-HBT 364	MH consent; tentative dx = low grade glioma	HN-BRAIN	BRAIN, NOS	cancer-primary	GLIOMA, NOS	I	WHO	N/A	N/A	N/A	N/A	final path this sx (Dysembbryoplastic neuroepitheliat tumour (DNET), WHO grade I, the glial componet is markedly hypercellular in some areas, occasional atypical glial cells and rare mitoses are also present. In DNETs, such changes do not suggest a worse biological behavior for these tumors).	N/A	N/A	N/A
M-HBT203	MH consent; final dx = mixed oligoastrocytoma, WHO II	HN-BRAIN	BRAIN, NOS	benign	OLIGOASTROCYTOMA	II	WHO	Non-Hispanic	White	M	29	N/A	Chemo	4/24/17	Alive as of 5/15/2019
M-HBT237	MH consent; final dx = oligoastrocytoma, WHO II	HN-BRAIN	BRAIN, NOS	benign	OLIGOASTROCYTOMA	II	WHO	Non-Hispanic	White	F	36	2009 - oligodendroglioma, crani + chemo	Radiation, Temodar	N/A	Alive as of 5/16/2019
M-HBT300	MH consent; final path dx = oligoastrocytoma, IDH-1 mutated, WHO grade II	HN-BRAIN	BRAIN, NOS	benign	OLIGOASTROCYTOMA	II	WHO	Non-Hispanic	White	F	N/A	N/A	N/A	N/A	Alive as of 12/12/14
M-HBT305	MH consent; final path dx = oligoastrocytoma, WHO grade II	HN-BRAIN	BRAIN, NOS	benign	OLIGOASTROCYTOMA	II	WHO	Non-Hispanic	White	F	N/A	N/A	Temodar, temozolomide, radiation	N/A	Alive as of 5/16/2019
M-HBT172	MH consent; final dx = anaplastic oligodendroglioma, WHO III	HN-BRAIN	BRAIN, NOS	cancer-primary	OLIGODENDROGLIOMA, NOS	III	WHO	Non-Hispanic	White	M	N/A	N/A	N/A	N/A	Deceased 2013
M-HBT190	MH consent; final dx = Crani - mixed oligoastrocytoma, WHO III	HN-BRAIN	BRAIN, NOS	cancer-primary	OLIGOASTROCYTOMA	III	WHO	Non-Hispanic	White	F	28	N/A	N/A	N/A	Alive as of 5/17/2019
M-HBT 385	MH consent; tentative dx = low grade glioma	HN-BRAIN	BRAIN, NOS	cancer-primary	GLIOMA, NOS	III	WHO	N/A	N/A	N/A	N/A	final path this sx (anaplastic astrocytoma, WHO Grade III)	N/A	8/4/17	Alive as of 5/20/19
M-HBT387	MH consent tentative dx = low grade glioma	HN-BRAIN	BRAIN, NOS	cancer-primary	GLIOMA, NOS	III	WHO	N/A	N/A	N/A	N/A	final path this sx (complex anaplastic astrocytoma, IDH-mutant, WHO Grade III)	Radiation, temozolomide	N/A	Alive as of 5/13/19
M-HBT 292	final dx=brain-oligoastrocytoma, IDH-1 mutated, WHO II (per path), malignant glioblastoma (per QC)	HN-BRAIN	BRAIN, NOS	cancer-primary	GLIOBLASTOMA, NOS	IV	WHO	Non-Hispanic	White	M	N/A	N/A	N/A	N/A	Alive as of 4/19/19
M-HBT319	MH consent; final path dx = glioblastoma w/oligodendroglial component	HN-BRAIN	BRAIN, NOS	cancer-primary	GLIOBLASTOMA, NOS	IV	WHO	Non-Hispanic	White	M	N/A	N/A	seizure, radiation, temozolomide, multiple resections since 2003	multiple resections since 2003	Deceased 2017
M-HBT322	MH consent; final path dx = glioblastoma w/large PNET-like components	HN-BRAIN	BRAIN, NOS	cancer-primary	GLIOBLASTOMA, NOS	IV	WHO	Non-Hispanic	White	N/A	N/A	N/A	radiation, temozolomide	N/A	Alive as of 11/15/16
M-HBT370	MH consent, tentative dx = oligodendroglioma	HN-BRAIN	BRAIN, NOS	cancer-primary	OLIGODENDROGLIOMA, NOS	IV	WHO	N/A		N/A	N/A	final path this sx (Glioblastoma, IDH-wildtype, WHO grade IV)	N/A	N/A	Alive as of 7/7/16

APPENDIX B. CHAPTER 3 SUPPLEMENTAL FIGURES

Lipid profiles by glioma grade

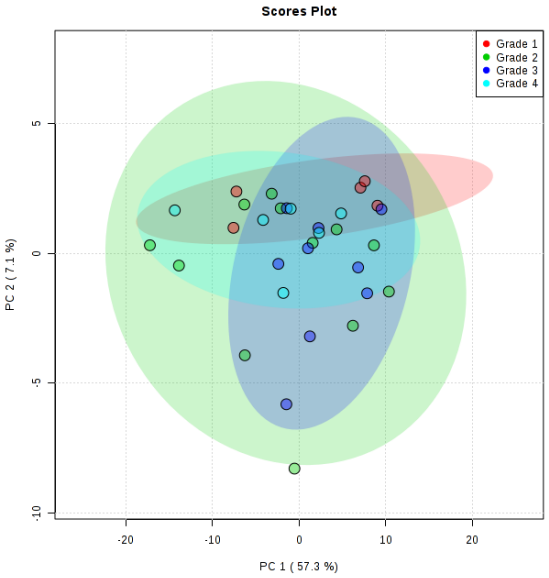

Figure B.1 M2 method PCA plot indicated similar lipid composition between glioma grades.

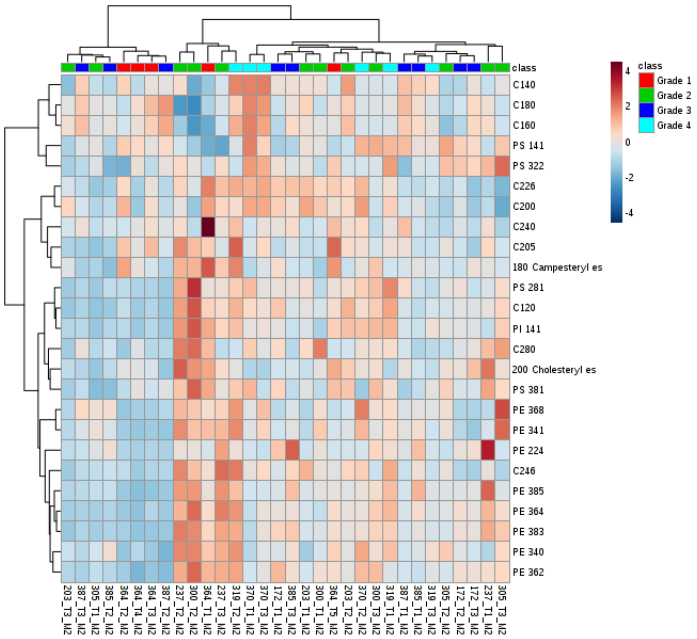

Figure B.2 M2 method cluster analysis of top 25 lipids demonstrated indiscriminate differences between glioma grades.

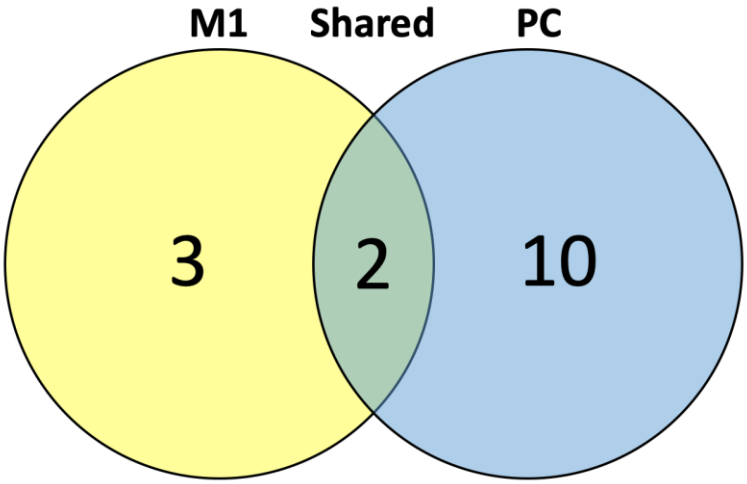

Figure B.3 Lipids with significantly different relative abundance by method between glioma by grade.

Low grade v. high grade lipid profiles

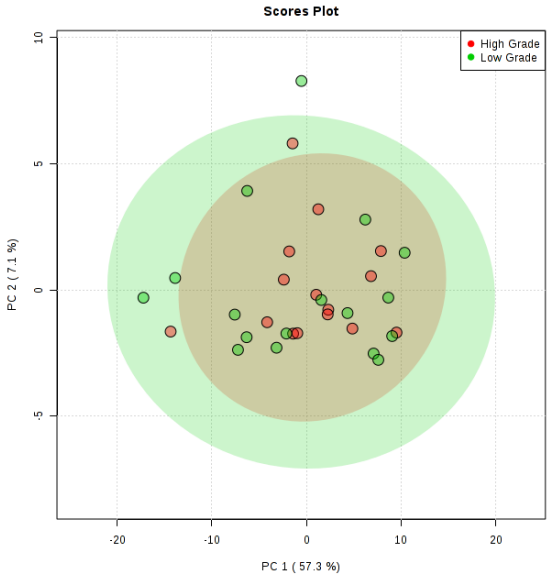

Figure B.4 Multivariate analysis identified comparable lipid profiles between low- and high-grade glioma using the M2 screening method.

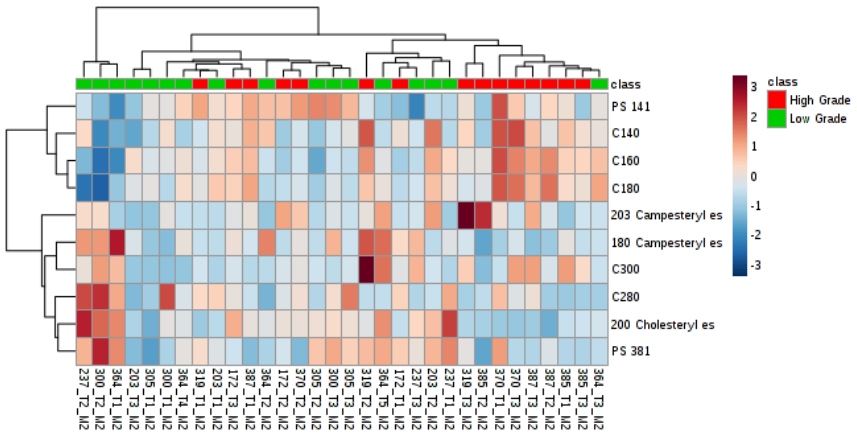

Figure B.5 Heatmap analysis visualization of top 10 lipids showed slight clustering trend between low- and high-grade glioma based on distinct C(14:0, 16:0, and C18:0) relative abundance in M2 method.

Glioma grade 2 v grade 3

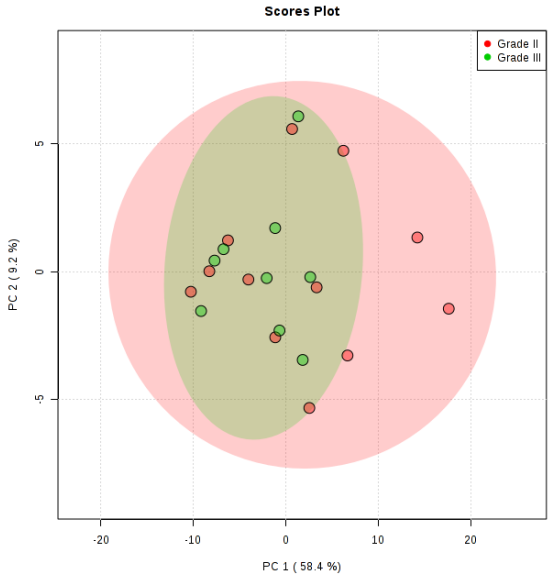

Figure B.6 PCA plot indicated similar lipid profiles between grade II and grade III glioma through the M2 profiling method.

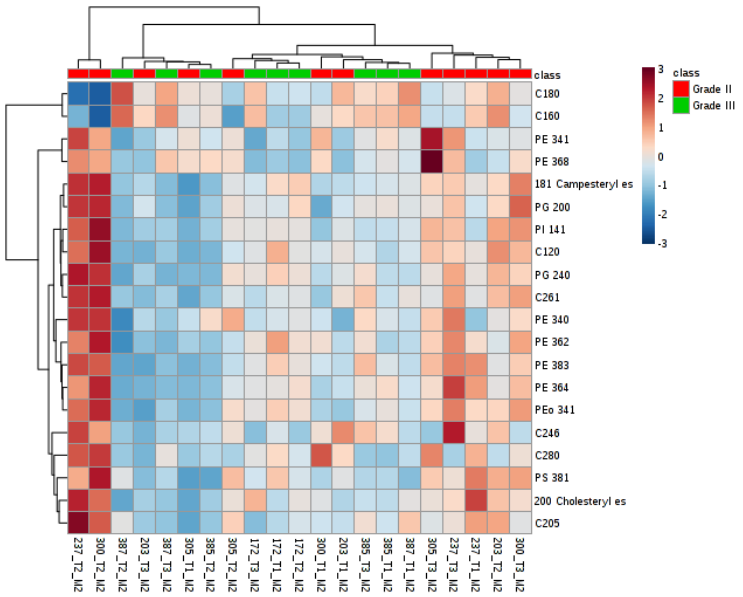

Figure B.7 Top 20 lipids in cluster analysis demonstrated subtle clustering trend due to differential expression of PE lipids in M2 method.

APPENDIX C. CHAPTER 4 SUPPLEMENTAL FIGURES

Brain around tumor by grade

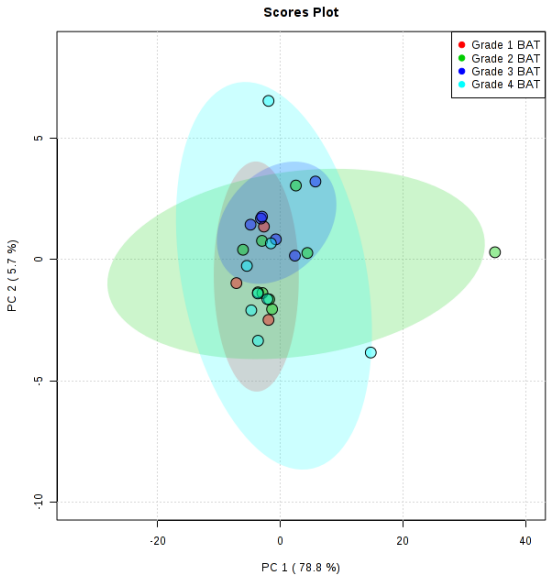

Figure C.1 PCA plot indicated similar lipid profiles between BAT grades according to the M2 screening method.

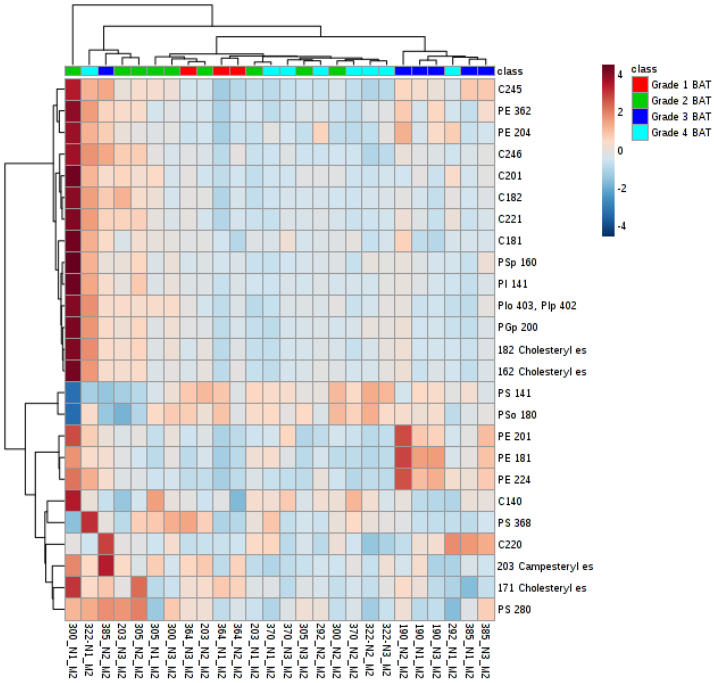

Figure C.2 Cluster analysis of top 25 M2 profiled lipids demonstrated limited distinction between BAT grade clusters.

Table C.1 Significant lipid species identified between BAT grades by ANOVA (M1 method)

Lipid	f.value	p.value	-log10(p)	FDR	Fisher's LSD
PC 36:5	137.5	7.89E-15	14.103	7.50E-13	Grade 1 BAT - Grade 2 BAT; Grade 1 BAT - Grade 3 BAT; Grade 1 BAT - Grade 4 BAT; Grade 2 BAT - Grade 3 BAT; Grade 4 BAT - Grade 3 BAT
PC 38:5	128.21	1.69E-14	13.773	8.01E-13	Grade 1 BAT - Grade 2 BAT; Grade 1 BAT - Grade 3 BAT; Grade 1 BAT - Grade 4 BAT
PC 36:1	50.514	2.80E-10	9.5535	8.85E-09	Grade 3 BAT - Grade 1 BAT; Grade 3 BAT - Grade 2 BAT; Grade 3 BAT - Grade 4 BAT
SM d18:0/22:0	43.055	1.34E-09	8.8727	3.18E-08	Grade 3 BAT - Grade 1 BAT; Grade 3 BAT - Grade 2 BAT; Grade 3 BAT - Grade 4 BAT
PC 38:2	18.882	2.12E-06	5.674	4.02E-05	Grade 3 BAT - Grade 1 BAT; Grade 3 BAT - Grade 2 BAT; Grade 3 BAT - Grade 4 BAT
PCo34:1	14.843	1.37E-05	4.8644	0.00021634	Grade 3 BAT - Grade 1 BAT; Grade 3 BAT - Grade 2 BAT; Grade 3 BAT - Grade 4 BAT
TAG58:2_FA 18:1	13.525	2.70E-05	4.5694	0.00036577	Grade 1 BAT - Grade 3 BAT; Grade 2 BAT - Grade 3 BAT; Grade 4 BAT - Grade 3 BAT
PC 36:2	13.02	3.54E-05	4.4516	0.00041978	Grade 3 BAT - Grade 1 BAT; Grade 3 BAT - Grade 2 BAT; Grade 3 BAT - Grade 4 BAT
TAG58:3_FA 18:1	12.463	4.80E-05	4.3185	0.00050702	Grade 1 BAT - Grade 3 BAT; Grade 1 BAT - Grade 4 BAT; Grade 2 BAT - Grade 3 BAT; Grade 2 BAT - Grade 4 BAT; Grade 4 BAT - Grade 3 BAT
PC 40:5	12.232	5.47E-05	4.262	0.00051972	Grade 1 BAT - Grade 2 BAT; Grade 1 BAT - Grade 3 BAT; Grade 1 BAT - Grade 4 BAT
SM d18:1/24:1 15Z	10.594	0.00014324	3.8439	0.001237	Grade 3 BAT - Grade 1 BAT; Grade 3 BAT - Grade 2 BAT; Grade 3 BAT - Grade 4 BAT
TAG50:3_FA 18:2	9.7631	0.00024094	3.6181	0.0019075	Grade 1 BAT - Grade 3 BAT; Grade 2 BAT - Grade 3 BAT; Grade 4 BAT - Grade 3 BAT

PC 36:0 PCp38:6	9.3149	0.0003221 7	3.4919	0.002215 3	Grade 3 BAT - Grade 1 BAT; Grade 3 BAT - Grade 2 BAT; Grade 3 BAT - Grade 4 BAT
TAG54:2_ FA 18:2	9.2947	0.0003264 7	3.4862	0.002215 3	Grade 1 BAT - Grade 2 BAT; Grade 1 BAT - Grade 3 BAT; Grade 1 BAT - Grade 4 BAT; Grade 2 BAT - Grade 3 BAT; Grade 4 BAT - Grade 3 BAT
PCo38:5	8.9547	0.0004090 3	3.3882	0.002547	Grade 1 BAT - Grade 2 BAT; Grade 1 BAT - Grade 3 BAT; Grade 1 BAT - Grade 4 BAT; Grade 2 BAT - Grade 3 BAT
PCo36:1	8.8095	0.0004509 9	3.3458	0.002547	Grade 1 BAT - Grade 4 BAT; Grade 3 BAT - Grade 2 BAT; Grade 3 BAT - Grade 4 BAT
SM d18:1/24:0	8.7939	0.0004557 8	3.3412	0.002547	Grade 3 BAT - Grade 1 BAT; Grade 3 BAT - Grade 2 BAT; Grade 3 BAT - Grade 4 BAT
SM d18:0/20:0	8.1504	0.0007098 3	3.1488	0.003746 3	Grade 3 BAT - Grade 1 BAT; Grade 4 BAT - Grade 1 BAT; Grade 3 BAT - Grade 2 BAT; Grade 3 BAT - Grade 4 BAT
PC 38:6	8.0118	0.0007826 3	3.1064	0.003787 8	Grade 1 BAT - Grade 2 BAT; Grade 1 BAT - Grade 3 BAT; Grade 1 BAT - Grade 4 BAT; Grade 4 BAT - Grade 2 BAT; Grade 4 BAT - Grade 3 BAT
PC 34:1	7.9853	0.0007974 3	3.0983	0.003787 8	Grade 3 BAT - Grade 1 BAT; Grade 4 BAT - Grade 1 BAT; Grade 3 BAT - Grade 2 BAT; Grade 3 BAT - Grade 4 BAT
TAG54:5_ FA 18:2	7.8813	0.0008586 2	3.0662	0.003884 2	Grade 1 BAT - Grade 3 BAT; Grade 2 BAT - Grade 3 BAT; Grade 4 BAT - Grade 3 BAT
SM d16:1/24:0	7.7815	0.0009221 5	3.0352	0.003982	Grade 3 BAT - Grade 1 BAT; Grade 3 BAT - Grade 2 BAT; Grade 3 BAT - Grade 4 BAT
PCo42:6	7.5717	0.0010728	2.9695	0.004431 3	Grade 1 BAT - Grade 2 BAT; Grade 1 BAT - Grade 3 BAT; Grade 1 BAT - Grade 4 BAT; Grade 2 BAT - Grade 3 BAT
PC 36:8	7.4341	0.0011861	2.9259	0.004695 1	Grade 1 BAT - Grade 4 BAT; Grade 3 BAT - Grade 2 BAT; Grade 3 BAT - Grade 4 BAT
TAG56:8_ FA 18:1	7.3121	0.0012974	2.8869	0.004930 2	Grade 1 BAT - Grade 2 BAT; Grade 1 BAT - Grade 3 BAT;

					Grade 2 BAT - Grade 3 BAT; Grade 4 BAT - Grade 3 BAT
O-arachidonoylcarnitine	7.1266	0.0014889	2.8271	0.0054403	Grade 1 BAT - Grade 2 BAT; Grade 1 BAT - Grade 3 BAT; Grade 1 BAT - Grade 4 BAT; Grade 2 BAT - Grade 3 BAT
TAG58:6_FA 18:1	6.8896	0.0017793	2.7497	0.0062605	Grade 1 BAT - Grade 3 BAT; Grade 1 BAT - Grade 4 BAT; Grade 2 BAT - Grade 3 BAT
TAG58:1_FA 18:1	6.8414	0.0018457	2.7338	0.0062622	Grade 1 BAT - Grade 3 BAT; Grade 1 BAT - Grade 4 BAT; Grade 2 BAT - Grade 3 BAT
PC 30:0	6.5901	0.0022374	2.6503	0.0073294	Grade 1 BAT - Grade 2 BAT; Grade 1 BAT - Grade 3 BAT; Grade 1 BAT - Grade 4 BAT
Palmitoylcarnitine, 5Z-13-carboxytridec-5-enoylcarnitine	6.32	0.0027613	2.5589	0.0087441	Grade 1 BAT - Grade 3 BAT; Grade 1 BAT - Grade 4 BAT; Grade 2 BAT - Grade 3 BAT; Grade 4 BAT - Grade 3 BAT
TAG60:4_FA 18:1	5.9357	0.0037486	2.4261	0.011488	Grade 1 BAT - Grade 3 BAT; Grade 2 BAT - Grade 3 BAT; Grade 2 BAT - Grade 4 BAT
Arachidylcarnitine, O-9Z-17-carboxyheptadec-9-enoylcarnitine	5.8467	0.0040281	2.3949	0.011958	Grade 1 BAT - Grade 2 BAT; Grade 1 BAT - Grade 3 BAT; Grade 1 BAT - Grade 4 BAT; Grade 2 BAT - Grade 3 BAT; Grade 4 BAT - Grade 3 BAT
SM d18:1/16:0	5.611	0.0048834	2.3113	0.014058	Grade 2 BAT - Grade 4 BAT; Grade 3 BAT - Grade 4 BAT
TAG60:0_FA 20:0	5.5708	0.0050479	2.2969	0.014104	Grade 1 BAT - Grade 2 BAT; Grade 1 BAT - Grade 3 BAT; Grade 1 BAT - Grade 4 BAT
TAG58:5_FA 18:1	5.2766	0.0064506	2.1904	0.017509	Grade 1 BAT - Grade 3 BAT; Grade 2 BAT - Grade 3 BAT; Grade 4 BAT - Grade 3 BAT
TAG56:1_FA 18:2	5.0412	0.0078767	2.1037	0.020786	Grade 1 BAT - Grade 3 BAT; Grade 2 BAT - Grade 3 BAT
PC 34:0	4.8758	0.0090819	2.0418	0.023318	Grade 3 BAT - Grade 1 BAT; Grade 4 BAT - Grade 1 BAT; Grade 3 BAT - Grade 2 BAT; Grade 4 BAT - Grade 2 BAT

PC 30:1	4.5666	0.011901	1.9244	0.029752	Grade 2 BAT - Grade 4 BAT; Grade 3 BAT - Grade 4 BAT
PCp40:6	4.0028	0.019783	1.7037	0.048123	Grade 1 BAT - Grade 3 BAT; Grade 2 BAT - Grade 3 BAT
O-oleoylcarnitine, Elaidic carnitine	3.9768	0.020262	1.6933	0.048123	Grade 1 BAT - Grade 3 BAT; Grade 2 BAT - Grade 3 BAT; Grade 4 BAT - Grade 3 BAT

Table C.2 Significant lipid species identified between BAT grades by ANOVA (PC method)

Lipid	**f.value**	**p.value**	**-log10(p)**	**FDR**	**Fisher's LSD**
PC 38:5	153.55	2.37E-15	14.625	2.39E-13	Grade 1 BAT - Grade 2 BAT; Grade 1 BAT - Grade 3 BAT; Grade 1 BAT - Grade 4 BAT
PC 36:5	84.84	1.38E-12	11.859	6.99E-11	Grade 1 BAT - Grade 2 BAT; Grade 1 BAT - Grade 3 BAT; Grade 1 BAT - Grade 4 BAT; Grade 2 BAT - Grade 3 BAT; Grade 4 BAT - Grade 3 BAT
PC 36:1	74.695	5.24E-12	11.281	1.76E-10	Grade 3 BAT - Grade 1 BAT; Grade 4 BAT - Grade 1 BAT; Grade 3 BAT - Grade 2 BAT; Grade 4 BAT - Grade 2 BAT; Grade 3 BAT - Grade 4 BAT
SM d18:0/22:0	42.856	1.40E-09	8.8532	3.54E-08	Grade 3 BAT - Grade 1 BAT; Grade 3 BAT - Grade 2 BAT; Grade 3 BAT - Grade 4 BAT
PCo34:1	13.645	2.53E-05	4.597	0.00051093	Grade 3 BAT - Grade 1 BAT; Grade 3 BAT - Grade 2 BAT; Grade 3 BAT - Grade 4 BAT
PC 40:6	12.914	3.75E-05	4.4264	0.00052714	Grade 1 BAT - Grade 2 BAT; Grade 1 BAT - Grade 3 BAT; Grade 1 BAT - Grade 4 BAT; Grade 2 BAT - Grade 3 BAT; Grade 4 BAT - Grade 3 BAT
PC 36:2	12.729	4.15E-05	4.3823	0.00052714	Grade 3 BAT - Grade 1 BAT; Grade 4 BAT - Grade 1 BAT; Grade 3 BAT - Grade 2 BAT; Grade 3 BAT - Grade 4 BAT
PCo44:3	12.636	4.36E-05	4.3601	0.00052714	Grade 1 BAT - Grade 2 BAT; Grade 1 BAT - Grade 3 BAT; Grade 1 BAT - Grade 4 BAT;

					Grade 2 BAT - Grade 3 BAT; Grade 4 BAT - Grade 3 BAT
SM d18:1/24:1 15Z	12.504	4.70E-05	4.3282	0.0005271 4	Grade 3 BAT - Grade 1 BAT; Grade 3 BAT - Grade 2 BAT; Grade 3 BAT - Grade 4 BAT
SM d18:1/24:0	12.123	5.82E-05	4.2354	0.0005873 8	Grade 3 BAT - Grade 1 BAT; Grade 3 BAT - Grade 2 BAT; Grade 2 BAT - Grade 4 BAT; Grade 3 BAT - Grade 4 BAT
PC 34:1	11.89	6.64E-05	4.1776	0.0006100 2	Grade 2 BAT - Grade 1 BAT; Grade 3 BAT - Grade 1 BAT; Grade 4 BAT - Grade 1 BAT; Grade 3 BAT - Grade 2 BAT; Grade 3 BAT - Grade 4 BAT
SM d18:0/20:0	11.629	7.72E-05	4.1122	0.0006102 5	Grade 2 BAT - Grade 1 BAT; Grade 3 BAT - Grade 1 BAT; Grade 4 BAT - Grade 1 BAT; Grade 3 BAT - Grade 2 BAT; Grade 3 BAT - Grade 4 BAT
PC 38:6	11.558	8.05E-05	4.0942	0.0006102 5	Grade 1 BAT - Grade 2 BAT; Grade 1 BAT - Grade 3 BAT; Grade 2 BAT - Grade 3 BAT; Grade 4 BAT - Grade 2 BAT; Grade 4 BAT - Grade 3 BAT
PC 42:10	11.473	8.46E-05	4.0727	0.0006102 5	Grade 1 BAT - Grade 2 BAT; Grade 1 BAT - Grade 3 BAT; Grade 1 BAT - Grade 4 BAT; Grade 2 BAT - Grade 3 BAT; Grade 4 BAT - Grade 3 BAT
PC 30:0	9.438	0.0002972 5	3.5269	0.0018884	Grade 1 BAT - Grade 2 BAT; Grade 1 BAT - Grade 3 BAT; Grade 1 BAT - Grade 4 BAT
PCo38:5	9.4282	0.0002991 5	3.5241	0.0018884	Grade 1 BAT - Grade 2 BAT; Grade 1 BAT - Grade 3 BAT; Grade 1 BAT - Grade 4 BAT; Grade 2 BAT - Grade 3 BAT; Grade 4 BAT - Grade 3 BAT
PC 44:10	9.071	0.0003785	3.4219	0.0022487	Grade 1 BAT - Grade 2 BAT; Grade 1 BAT - Grade 3 BAT; Grade 1 BAT - Grade 4 BAT; Grade 2 BAT - Grade 3 BAT; Grade 4 BAT - Grade 3 BAT
PCo42:3	8.8639	0.0004347 6	3.3617	0.0023734	Grade 1 BAT - Grade 2 BAT; Grade 1 BAT - Grade 3 BAT; Grade 1 BAT - Grade 4 BAT;

					Grade 2 BAT - Grade 3 BAT; Grade 4 BAT - Grade 3 BAT
PC 36:6	8.8244	0.0004464 9	3.3502	0.0023734	Grade 1 BAT - Grade 3 BAT; Grade 1 BAT - Grade 4 BAT; Grade 2 BAT - Grade 3 BAT; Grade 4 BAT - Grade 3 BAT
PC 40:7	8.123	0.0007236 4	3.1405	0.0036544	Grade 1 BAT - Grade 3 BAT; Grade 2 BAT - Grade 3 BAT; Grade 4 BAT - Grade 3 BAT
SM d18:1/12:0	8.0461	0.0007639 2	3.117	0.0036741	Grade 1 BAT - Grade 3 BAT; Grade 2 BAT - Grade 3 BAT; Grade 4 BAT - Grade 3 BAT
SM d18:0/12:0	7.7939	0.0009139 4	3.0391	0.0041958	Grade 1 BAT - Grade 3 BAT; Grade 1 BAT - Grade 4 BAT; Grade 2 BAT - Grade 3 BAT; Grade 4 BAT - Grade 3 BAT
SM d16:1/24:1	7.3586	0.0012537	2.9018	0.0054642	Grade 2 BAT - Grade 3 BAT; Grade 4 BAT - Grade 3 BAT
PCo32:0	7.2669	0.0013415	2.8724	0.0054642	Grade 1 BAT - Grade 2 BAT; Grade 1 BAT - Grade 3 BAT; Grade 1 BAT - Grade 4 BAT; Grade 2 BAT - Grade 3 BAT; Grade 4 BAT - Grade 3 BAT
PC 38:2	7.2558	0.0013525	2.8689	0.0054642	Grade 3 BAT - Grade 1 BAT; Grade 3 BAT - Grade 2 BAT; Grade 3 BAT - Grade 4 BAT
PC 32:2	7.1989	0.0014109	2.8505	0.0054808	Grade 4 BAT - Grade 1 BAT; Grade 2 BAT - Grade 3 BAT; Grade 4 BAT - Grade 3 BAT
PCo34:0	6.9133	0.0017477	2.7575	0.0063653	Grade 1 BAT - Grade 2 BAT; Grade 1 BAT - Grade 3 BAT; Grade 1 BAT - Grade 4 BAT; Grade 2 BAT - Grade 3 BAT; Grade 4 BAT - Grade 3 BAT
PC 34:6	6.9006	0.0017646	2.7533	0.0063653	Grade 1 BAT - Grade 3 BAT; Grade 2 BAT - Grade 3 BAT; Grade 4 BAT - Grade 3 BAT
PC 40:5	6.7788	0.0019357	2.7132	0.0067415	Grade 1 BAT - Grade 2 BAT; Grade 1 BAT - Grade 3 BAT; Grade 1 BAT - Grade 4 BAT; Grade 2 BAT - Grade 3 BAT
PCo44:5	6.5896	0.0022383	2.6501	0.0075356	Grade 1 BAT - Grade 3 BAT; Grade 2 BAT - Grade 3 BAT; Grade 4 BAT - Grade 3 BAT
PCo42:6	6.4994	0.0024002	2.6198	0.00782	Grade 1 BAT - Grade 3 BAT; Grade 1 BAT - Grade 4 BAT;

					Grade 2 BAT - Grade 3 BAT; Grade 4 BAT - Grade 3 BAT
SM d18:2/14:0	6.2166	0.0029956	2.5235	0.0094548	Grade 1 BAT - Grade 3 BAT; Grade 2 BAT - Grade 3 BAT; Grade 4 BAT - Grade 3 BAT
SM d16:1/24:0	6.0023	0.0035533	2.4494	0.010875	Grade 3 BAT - Grade 1 BAT; Grade 3 BAT - Grade 2 BAT; Grade 3 BAT - Grade 4 BAT
PCo36:5	5.9029	0.0038493	2.4146	0.011435	Grade 1 BAT - Grade 3 BAT; Grade 2 BAT - Grade 3 BAT; Grade 4 BAT - Grade 3 BAT
SM d18:2/18:1	5.7872	0.0042276	2.3739	0.012034	Grade 1 BAT - Grade 3 BAT; Grade 2 BAT - Grade 3 BAT; Grade 4 BAT - Grade 3 BAT
PCo38:2	5.7694	0.0042893	2.3676	0.012034	Grade 1 BAT - Grade 3 BAT; Grade 2 BAT - Grade 3 BAT; Grade 4 BAT - Grade 3 BAT
PCo34:2	5.6547	0.004711	2.3269	0.012608	Grade 1 BAT - Grade 3 BAT; Grade 2 BAT - Grade 3 BAT; Grade 4 BAT - Grade 3 BAT
PC 42:1	5.6304	0.0048059	2.3182	0.012608	Grade 1 BAT - Grade 3 BAT; Grade 2 BAT - Grade 3 BAT; Grade 4 BAT - Grade 3 BAT
SM d18:0/16:0	5.6147	0.0048683	2.3126	0.012608	Grade 2 BAT - Grade 3 BAT; Grade 2 BAT - Grade 4 BAT
PCo40:4	5.5395	0.00518	2.2857	0.013079	Grade 1 BAT - Grade 3 BAT; Grade 2 BAT - Grade 3 BAT
PC 42:2	5.4264	0.00569	2.2449	0.013339	Grade 1 BAT - Grade 3 BAT; Grade 2 BAT - Grade 3 BAT; Grade 2 BAT - Grade 4 BAT
PCp40:6	5.4196	0.0057224	2.2424	0.013339	Grade 1 BAT - Grade 3 BAT; Grade 2 BAT - Grade 3 BAT; Grade 2 BAT - Grade 4 BAT
PCo32:2	5.4097	0.0057696	2.2389	0.013339	Grade 1 BAT - Grade 3 BAT; Grade 2 BAT - Grade 3 BAT; Grade 4 BAT - Grade 3 BAT
PCo40:6	5.3799	0.0059152	2.228	0.013339	Grade 1 BAT - Grade 3 BAT; Grade 2 BAT - Grade 3 BAT; Grade 4 BAT - Grade 3 BAT
PC 44:2	5.3742	0.0059433	2.226	0.013339	Grade 1 BAT - Grade 3 BAT; Grade 2 BAT - Grade 3 BAT; Grade 4 BAT - Grade 3 BAT
PC 42:5	5.225	0.0067372	2.1715	0.014793	Grade 1 BAT - Grade 3 BAT; Grade 2 BAT - Grade 3 BAT; Grade 4 BAT - Grade 3 BAT

PCo36:3	5.1716	0.0070491	2.1519	0.015056	Grade 1 BAT - Grade 3 BAT; Grade 2 BAT - Grade 3 BAT; Grade 4 BAT - Grade 3 BAT
PCo40:5	5.154	0.0071553	2.1454	0.015056	Grade 1 BAT - Grade 3 BAT; Grade 2 BAT - Grade 3 BAT; Grade 4 BAT - Grade 3 BAT
PCo36:4	5.0966	0.0075133	2.1242	0.015163	Grade 1 BAT - Grade 3 BAT; Grade 2 BAT - Grade 3 BAT; Grade 4 BAT - Grade 3 BAT
PC 38:9	5.0595	0.0077549	2.1104	0.015163	Grade 1 BAT - Grade 3 BAT; Grade 2 BAT - Grade 3 BAT; Grade 4 BAT - Grade 3 BAT
PC 30:2	5.0514	0.0078088	2.1074	0.015163	Grade 1 BAT - Grade 3 BAT; Grade 2 BAT - Grade 3 BAT; Grade 4 BAT - Grade 3 BAT
PC 32:0	5.0408	0.00788	2.1035	0.015163	Grade 1 BAT - Grade 2 BAT; Grade 1 BAT - Grade 3 BAT; Grade 1 BAT - Grade 4 BAT; Grade 4 BAT - Grade 3 BAT
PCo36:0	5.0135	0.008066	2.0933	0.015163	Grade 1 BAT - Grade 3 BAT; Grade 1 BAT - Grade 4 BAT; Grade 2 BAT - Grade 3 BAT
PCo38:6	5.0076	0.0081068	2.0912	0.015163	Grade 1 BAT - Grade 3 BAT; Grade 2 BAT - Grade 3 BAT; Grade 4 BAT - Grade 3 BAT
PC 36:3	4.9375	0.0086105	2.065	0.015812	Grade 2 BAT - Grade 1 BAT; Grade 4 BAT - Grade 1 BAT; Grade 2 BAT - Grade 3 BAT; Grade 4 BAT - Grade 3 BAT
SM d18:1/14:0	4.8965	0.0089206	2.0496	0.016089	Grade 1 BAT - Grade 3 BAT; Grade 1 BAT - Grade 4 BAT; Grade 2 BAT - Grade 3 BAT
PC 36:7	4.8032	0.0096719	2.0145	0.017138	Grade 1 BAT - Grade 3 BAT; Grade 1 BAT - Grade 4 BAT; Grade 2 BAT - Grade 3 BAT
PC 36:0 PCp38:6	4.7013	0.010571	1.9759	0.018102	Grade 3 BAT - Grade 1 BAT; Grade 3 BAT - Grade 2 BAT; Grade 3 BAT - Grade 4 BAT
PC 38:0	4.701	0.010574	1.9757	0.018102	Grade 1 BAT - Grade 3 BAT; Grade 2 BAT - Grade 3 BAT; Grade 4 BAT - Grade 3 BAT
PC 34:0	4.6681	0.010883	1.9632	0.01832	Grade 3 BAT - Grade 1 BAT; Grade 4 BAT - Grade 1 BAT; Grade 4 BAT - Grade 2 BAT

PCo40:3	4.6061	0.011493	1.9396	0.01903	Grade 1 BAT - Grade 3 BAT; Grade 2 BAT - Grade 3 BAT; Grade 4 BAT - Grade 3 BAT
SM d18:1/16:0	4.5773	0.011789	1.9285	0.019204	Grade 1 BAT - Grade 4 BAT; Grade 2 BAT - Grade 4 BAT; Grade 3 BAT - Grade 4 BAT
SM d16:1/18:1	4.5235	0.012365	1.9078	0.019823	Grade 2 BAT - Grade 3 BAT; Grade 4 BAT - Grade 3 BAT
PCo32:3	4.3382	0.014587	1.836	0.022987	Grade 1 BAT - Grade 3 BAT; Grade 2 BAT - Grade 3 BAT; Grade 4 BAT - Grade 3 BAT
PCo40:0	4.3225	0.014794	1.8299	0.022987	Grade 1 BAT - Grade 3 BAT; Grade 2 BAT - Grade 3 BAT; Grade 4 BAT - Grade 3 BAT
PC 42:6	4.2702	0.015508	1.8094	0.023732	Grade 1 BAT - Grade 3 BAT; Grade 2 BAT - Grade 3 BAT
SM d18:1/26:0	4.1129	0.017886	1.7475	0.026963	Grade 1 BAT - Grade 3 BAT; Grade 2 BAT - Grade 3 BAT
PC 40:8	4.0965	0.018157	1.741	0.026968	Grade 1 BAT - Grade 3 BAT; Grade 2 BAT - Grade 3 BAT
PC 40:4	3.6858	0.026563	1.5757	0.038882	Grade 1 BAT - Grade 3 BAT; Grade 2 BAT - Grade 3 BAT; Grade 4 BAT - Grade 3 BAT
SM d18:0/26:0	3.6676	0.027021	1.5683	0.038988	Grade 1 BAT - Grade 3 BAT; Grade 2 BAT - Grade 3 BAT
PCo38:0	3.6251	0.028126	1.5509	0.04001	Grade 1 BAT - Grade 3 BAT; Grade 1 BAT - Grade 4 BAT
SM d18:1/18:1 9Z	3.5273	0.030855	1.5107	0.043283	Grade 4 BAT - Grade 1 BAT; Grade 4 BAT - Grade 3 BAT
SM d18:0/14:0	3.437	0.033629	1.4733	0.045931	Grade 1 BAT - Grade 3 BAT; Grade 2 BAT - Grade 3 BAT; Grade 4 BAT - Grade 3 BAT
SM d18:1/20:0	3.4363	0.033652	1.473	0.045931	Grade 4 BAT - Grade 1 BAT; Grade 4 BAT - Grade 2 BAT; Grade 4 BAT - Grade 3 BAT
PC 30:1	3.4205	0.034163	1.4664	0.046006	Grade 2 BAT - Grade 4 BAT; Grade 3 BAT - Grade 4 BAT

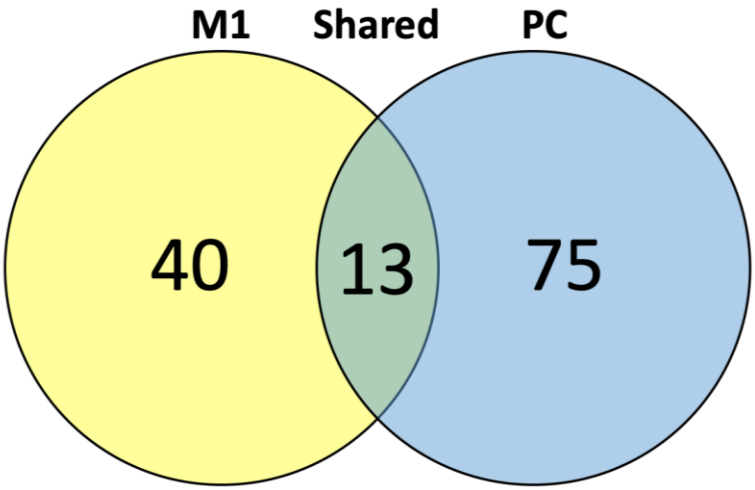

Figure C.3 Lipids with significantly different relative abundance by method between BAT by grade.

Low grade v. high grade brain around tumor

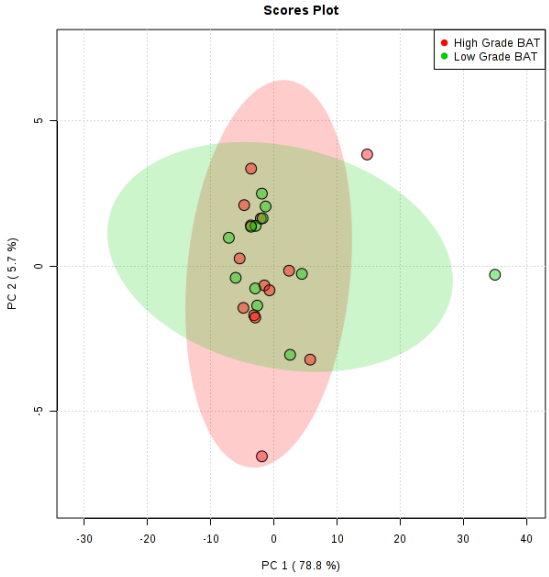

Figure C.4 Multivariate analysis of M2 method lipids demonstrated comparable lipid profiles between low- and high-grade BAT.

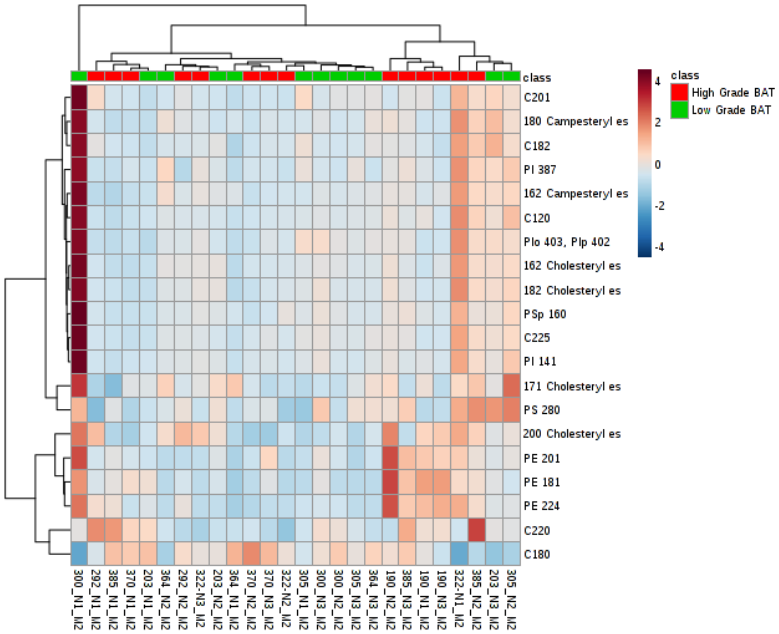

Figure C.5 Heatmap of top 20 lipids displayed indiscriminate separate of low- and high-grade BAT clusters based on M2 method screened lipids.

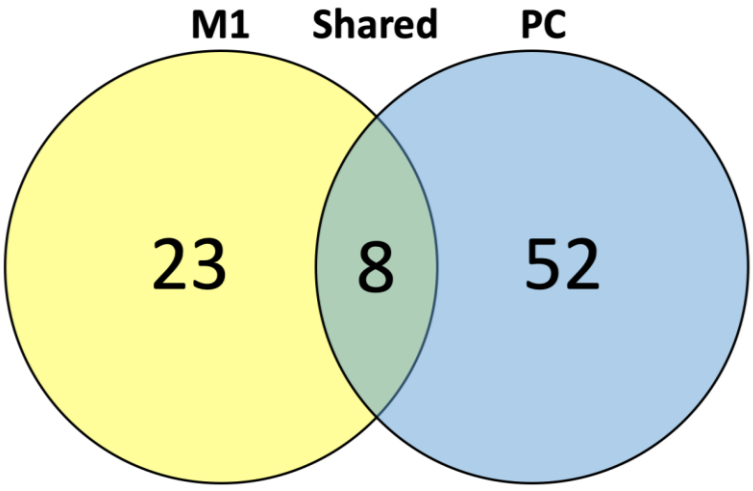

Figure C.6 Lipids with significantly different relative abundance by method between low- and high-grade BAT.

Table C.3 Significant lipid species identified between BAT low-grade v high-grade by t-test (M1 method)

Lipid	t.stat	p.value	-log10(p)	FDR
TAG58:3_FA 18:1	-4.4775	0.00014437	3.8405	0.013715
PC 34:0	3.7857	0.0008573	3.0669	0.030746
TAG60:4_FA 18:1	-3.6111	0.0013349	2.8746	0.030746
TAG58:6_FA 18:1	-3.5697	0.001482	2.8292	0.030746
TAG56:1_FA 18:2	-3.39	0.0023243	2.6337	0.030746
PC 36:1	3.3774	0.0023981	2.6201	0.030746
TAG58:1_FA 18:1	-3.3732	0.002423	2.6156	0.030746
TAG54:2_FA 18:2	-3.3465	0.0025892	2.5868	0.030746
TAG50:3_FA 18:2	-3.2682	0.0031422	2.5028	0.031049
PCo42:6	-3.2512	0.0032765	2.4846	0.031049
TAG58:2_FA 18:1	-3.196	0.0037529	2.4256	0.031049
O-arachidonoylcarnitine	-3.178	0.003922	2.4065	0.031049
2-ethylacryloylcarnitine, Tiglylcarnitine	-3.0851	0.0049176	2.3082	0.035936
TAG58:5_FA 18:1	-3.047	0.0053923	2.2682	0.036591
SM d18:0/22:0	2.9953	0.0061069	2.2142	0.038036
PCo38:5	-2.9753	0.0064061	2.1934	0.038036
TAG54:5_FA 18:2	-2.9398	0.0069742	2.1565	0.038973
PC 34:1	2.8939	0.0077799	2.109	0.041061
2E-hexenedioylcarnitine, O-octanoylcarnitine	-2.843	0.008776	2.0567	0.043801
O-13-carboxytridecanoylcarnitine	-2.822	0.0092212	2.0352	0.043801
11Z-eicoseneoylcarnitine	-2.7827	0.010112	1.9952	0.044054
PCp40:6	-2.7789	0.010202	1.9913	0.044054
SM d18:0/20:0	2.7187	0.01174	1.9303	0.04849

Table C.4 Significant lipid species identified between BAT low-grade v high-grade by t-test (PC method)

Lipid	t.stat	p.value	-log10(p)	FDR
PC 36:1	3.873	0.00068597	3.1637	0.01824
SM d18:0/12:0	-3.828	0.00076968	3.1137	0.01824
SM d18:0/16:0	-3.7158	0.0010239	2.9897	0.01824
PC 36:6	-3.6857	0.0011052	2.9566	0.01824
PC 34:0	3.6524	0.0012025	2.9199	0.01824
PCo44:3	-3.493	0.0017969	2.7455	0.01824
PCp40:6	-3.4712	0.0018976	2.7218	0.01824
PCo42:6	-3.4682	0.0019118	2.7186	0.01824
PCo40:4	-3.4049	0.0022392	2.6499	0.01824
PC 42:2	-3.368	0.0024548	2.61	0.01824

SM d18:0/20:0	3.3677	0.0024566	2.6097	0.01824
PC 34:1	3.3435	0.0026087	2.5836	0.01824
PC 44:10	-3.3296	0.0027003	2.5686	0.01824
PC 42:10	-3.2993	0.00291	2.5361	0.01824
PCo38:5	-3.2934	0.0029531	2.5297	0.01824
PC 44:2	-3.2546	0.0032494	2.4882	0.01824
PCo38:2	-3.2546	0.0032496	2.4882	0.01824
SM d18:0/22:0	3.2452	0.0033258	2.4781	0.01824
PC 42:1	-3.2325	0.0034313	2.4645	0.01824
PCo36:5	-3.1861	0.0038443	2.4152	0.019414
SM d18:1/14:0	-3.1421	0.0042804	2.3685	0.020587
PCo32:2	-3.071	0.0050874	2.2935	0.023356
PCo42:3	-3.0353	0.0055458	2.256	0.024353
PC 36:2	3.011	0.0058799	2.2306	0.024745
SM d18:2/14:0	-2.9464	0.0068652	2.1633	0.025826
PCo44:5	-2.9444	0.0068986	2.1612	0.025826
PC 42:6	-2.9441	0.006904	2.1609	0.025826
PCo40:6	-2.9218	0.0072801	2.1379	0.02626
SM d18:1/26:0	-2.8838	0.0079675	2.0987	0.026275
PCo40:3	-2.8519	0.0085927	2.0659	0.026275
PC 40:8	-2.8509	0.0086124	2.0649	0.026275
SM d18:0/26:0	-2.8495	0.0086416	2.0634	0.026275
PC 34:6	-2.8392	0.0088554	2.0528	0.026275
PC 40:7	-2.8368	0.0089039	2.0504	0.026275
PCo34:2	-2.8273	0.0091053	2.0407	0.026275
SM d18:1/16:0	-2.81	0.0094845	2.023	0.02631
PC 36:7	-2.8031	0.0096383	2.016	0.02631
PC 36:5	-2.784	0.010081	1.9965	0.026401
PC 42:5	-2.7792	0.010195	1.9916	0.026401
PCo38:6	-2.7621	0.010611	1.9743	0.026778
SM d18:2/18:1	-2.748	0.010964	1.96	0.026778
PCo36:3	-2.7414	0.011135	1.9533	0.026778
PCo36:4	-2.7249	0.011571	1.9366	0.027178
PC 38:9	-2.7141	0.011863	1.9258	0.027232
SM d18:1/12:0	-2.697	0.012342	1.9086	0.027702
PCo36:0	-2.6229	0.014639	1.8345	0.032143
PCo32:0	-2.5693	0.016543	1.7814	0.035066
PC 30:2	-2.566	0.016665	1.7782	0.035066
PCo40:1	-2.5494	0.017306	1.7618	0.035671
PCo32:3	-2.4549	0.021395	1.6697	0.043217
PC 40:1	-2.4015	0.024088	1.6182	0.04695
PC 40:4	-2.3999	0.024172	1.6167	0.04695

Table C.5 Discriminant individual lipids between low-grade and high-grade BAT identified by ROC curve analysis (M1 method)

Lipid	AUC	Pval	FC	clusters
TAG58:3_FA 18:1	0.88888889	0.00014437	-0.028847	2
TAG58:6_FA 18:1	0.87222222	0.00148195	-0.0377835	2
PC 36:1	0.86111111	0.00239809	0.29662813	2
PC 34:0	0.85555556	0.0008573	0.17624053	2
TAG60:4_FA 18:1	0.85	0.00133485	-0.0190851	2
O-arachidonoylcarnitine	0.83888889	0.00392203	-0.0400148	2
O-13-carboxytridecanoylcarnitine	0.83333333	0.00922118	-0.020713	2
TAG58:1_FA 18:1	0.82777778	0.00242299	-0.0282681	2
PCo42:6	0.82777778	0.00327645	-0.0189318	2
PC 36:5	0.81666667	0.01337718	-0.0530289	2
TAG58:2_FA 18:1	0.81666667	0.00375286	-0.0112177	2
TAG54:2_FA 18:2	0.81666667	0.00258917	-0.0135851	2
PCo38:5	0.81111111	0.00640614	-0.0157643	2
TAG50:3_FA 18:2	0.80555556	0.00314216	-0.0138982	2
PC 34:1	0.8	0.00777992	0.69821818	5
2-ethylacryloylcarnitine, Tiglylcarnitine	0.8	0.00491761	-0.1434069	2
TAG56:1_FA 18:2	0.8	0.00232425	-0.019696	2

Table C.6 Discriminant individual lipids between low-grade and high-grade BAT identified by ROC curve analysis (PC method)

Lipid	AUC	Pval	FC	clusters
SM d18:0/16:0	0.92222222	0.0010239	-0.1919695	4
PC 36:1	0.9	0.00068597	0.55944658	5
PC 34:0	0.86666667	0.00120253	0.2540185	5
SM d18:0/12:0	0.86666667	0.00076968	-0.0939628	4
SM d18:0/22:0	0.85	0.00332578	0.2478778	5
PC 36:6	0.84444444	0.00110519	-0.0556481	4
PC 44:10	0.83888889	0.00270032	-0.0591855	4
PC 34:1	0.82777778	0.0026087	0.72367954	1
SM d18:0/20:0	0.82777778	0.00245665	0.53290821	2
PCo42:6	0.82777778	0.0019118	-0.0645083	4
PCo38:2	0.82777778	0.00324965	-0.0524443	4
PCo40:6	0.82222222	0.00728006	-0.1032962	4
PCo36:5	0.82222222	0.00384428	-0.0590017	4
PCo44:3	0.82222222	0.00179692	-0.0598652	4
PCp40:6	0.82222222	0.00189757	-0.0470806	4
PC 34:6	0.81111111	0.00885545	-0.0589162	4
PC 42:6	0.81111111	0.00690399	-0.0512104	4

PCo42:3	0.81111111	0.00554582	-0.0559515	4
PC 42:2	0.81111111	0.00245476	-0.0438227	4
PC 42:10	0.80555556	0.00291	-0.0641397	4
PCo34:2	0.80555556	0.00910529	-0.0443703	4
PC 36:2	0.8	0.00587992	0.16461272	5
PC 36:5	0.8	0.01008057	-0.1555464	4
PCo40:4	0.8	0.00223915	-0.0685826	4

Grade II v. grade III brain around tumor

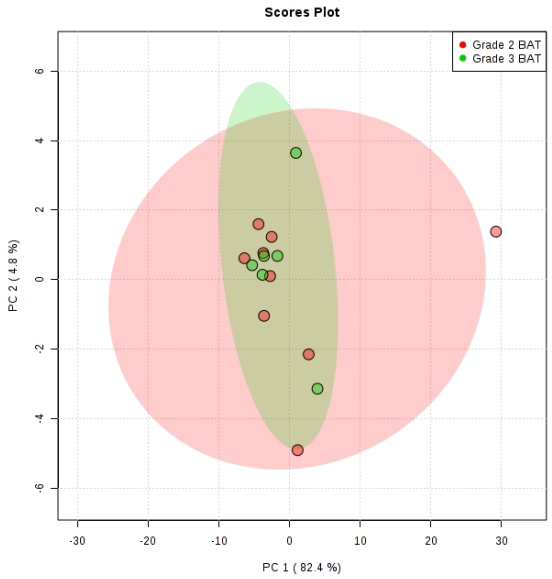

Figure C.7 M2 screening method PCA plot of grade II and grade III BAT identified minimal separation between clusters.

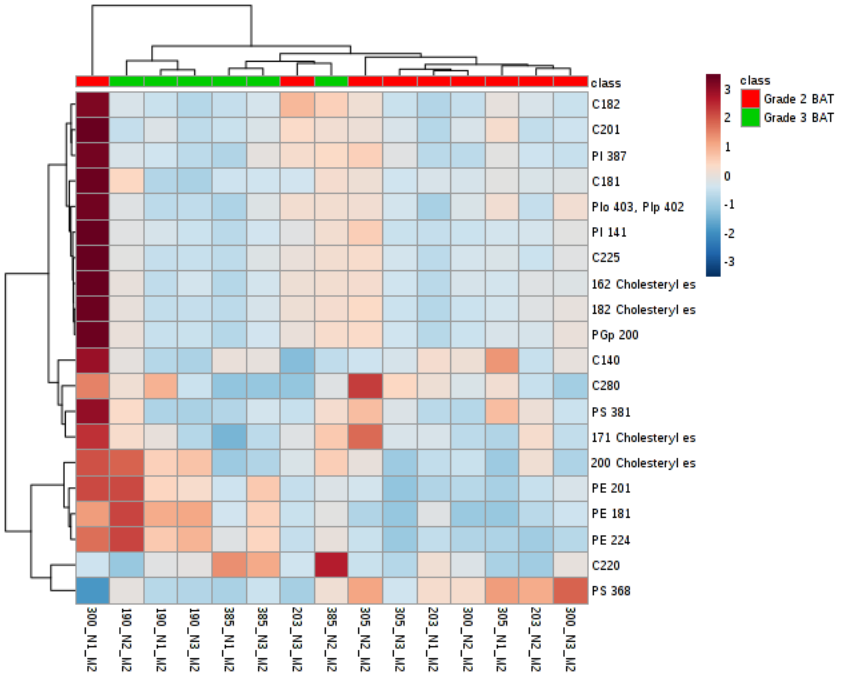

Figure C.8 Cluster analysis showed minor trend in cluster separation between grade II and III groups in top 20 lipids profiled with the M2 method.

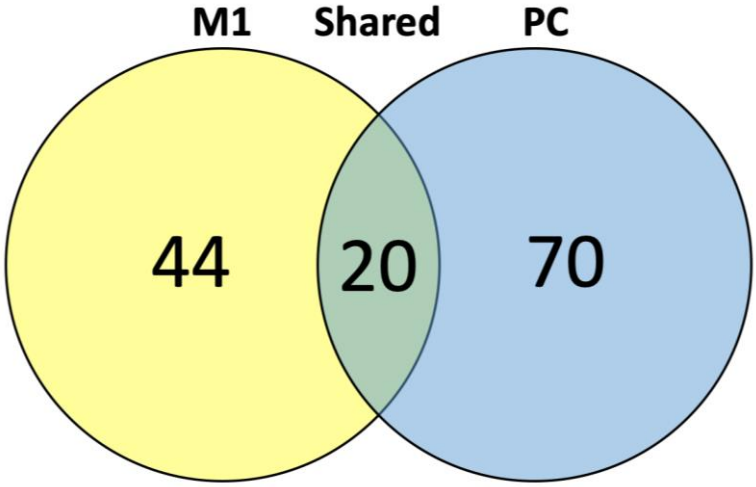

Figure C.9 Lipids with significantly different relative abundance by method between grade 2 an grade 3 BAT.

Table C.7 Significant lipid species identified between BAT grade II and III by t-test (M1 method)

Lipid	t.stat	p.value	-log10(p)	FDR
PC 36:1	-10.579	9.33E-08	7.0303	8.86E-06
SM d18:0/22:0	-8.8715	7.08E-07	6.1497	3.36E-05
PC 38:2	-5.2402	0.00015956	3.7971	0.0032146
PC 36:2	-5.2054	0.00016949	3.7708	0.0032146
PC 34:0	-5.1925	0.00017335	3.7611	0.0032146
TAG58:2_FA 18:1	5.102	0.00020303	3.6924	0.0032146
TAG50:3_FA 18:2	4.828	0.00032987	3.4817	0.0044768
TAG54:5_FA 18:2	4.534	0.00056127	3.2508	0.0062191
PCo34:1	-4.501	0.00059624	3.2246	0.0062191
SM d18:2/24:1	-4.4303	0.00067872	3.1683	0.0062191
PC 36:5	4.3982	0.00072011	3.1426	0.0062191
TAG58:3_FA 18:1	4.3021	0.00085992	3.0655	0.0068077
PC 34:1	-4.1364	0.0011706	2.9316	0.0078488
TAG54:2_FA 18:2	4.1084	0.0012335	2.9089	0.0078488
PCo36:1	-4.1059	0.0012393	2.9068	0.0078488
TAG58:6_FA 18:1	4.0696	0.0013265	2.8773	0.0078764
PCp40:6	4.0237	0.0014462	2.8398	0.0080816
PC 36:8	-3.9791	0.0015729	2.8033	0.0083014
SM d18:1/24:115Z	-3.7848	0.0022721	2.6436	0.010389
PC 384	-3.7839	0.0022757	2.6429	0.010389
SM d18:0/20:0	-3.7792	0.0022964	2.6389	0.010389
SM d16:1/24:0	-3.7244	0.0025488	2.5937	0.010601
TAG56:8_FA 18:1	3.7207	0.0025666	2.5906	0.010601
PC 36:0 PCp38:6	-3.6519	0.0029269	2.5336	0.011544
PCo38:5	3.6324	0.0030379	2.5174	0.011544
O-oleoylcarnitine, Elaidic carnitine	3.5175	0.0037847	2.422	0.013829
PCo42:6	3.4898	0.0039913	2.3989	0.014043
TAG58:1_FA 18:1	3.444	0.0043584	2.3607	0.01449
TAG58:5_FA 18:1	3.4363	0.0044232	2.3543	0.01449
PCo40:6	3.3658	0.0050645	2.2955	0.015949
TAG60:4_FA 18:1	3.3516	0.0052046	2.2836	0.015949
O-arachidonoylcarnitine	3.2472	0.0063621	2.1964	0.018887
Palmitoylcarnitine, 5Z-13-carboxytridec-5-enoylcarnitine	3.1765	0.0072898	2.1373	0.020986
TAG56:1_FA 18:2	3.1314	0.0079509	2.0996	0.022216
2E-hexenedioylcarnitine, O-octanoylcarnitine	3.0541	0.0092271	2.0349	0.025045
Arachidyl carnitine, O-9Z-17-carboxyheptadec-9-enoylcarnitine	2.952	0.011228	1.9497	0.02963

SM d18:1/24:0	-2.9316	0.011677	1.9327	0.029982
12-Hydroxy-12-octadecanoylcarnitine, 3-hydroxyoctadecanoylcarnitine	2.8667	0.013228	1.8785	0.033069
PCo38:6	2.786	0.015438	1.8114	0.037606
PC 38:1	-2.6603	0.019624	1.7072	0.045874
PCo34:2	2.6556	0.019798	1.7034	0.045874
TAG58:2_FA 18:2	2.6382	0.020466	1.689	0.046293
PC 30:2	2.5964	0.022156	1.6545	0.04895
Stearoylcarnitine, hexadecanedioic acid mono-L-carnitine ester	2.5809	0.022818	1.6417	0.049267

Table C.8 Significant lipid species identified between BAT grade II and III by t-test (PC method)

Lipid	**t.stat**	**p.value**	**-log10(p)**	**FDR**
PC 36:1	-14.605	1.92E-09	8.7171	1.94E-07
SM d18:0/22:0	-8.7103	8.71E-07	6.0602	4.40E-05
PCo34:1	-6.0857	3.87E-05	4.4124	0.001002
PC 32:2	6.07	3.97E-05	4.4014	0.001002
PC 34:0	-5.2761	0.00014992	3.8241	0.0030285
SM d18:1/24:115Z	-4.9143	0.00028281	3.5485	0.0047606
PC 36:2	-4.7331	0.00039117	3.4076	0.005644
SM d16:1/24:1	4.4792	0.00062053	3.2072	0.0078342
SM d18:1/24:0	-4.3235	0.00082654	3.0827	0.0079392
PC 34:6	4.2988	0.00086518	3.0629	0.0079392
SM d18:1/14:0	4.2027	0.0010344	2.9853	0.0079392
SM d18:1/12:0	4.1949	0.0010495	2.979	0.0079392
SM d18:0/12:0	4.1553	0.0011299	2.947	0.0079392
PC 34:1	-4.1412	0.0011602	2.9355	0.0079392
PCo40:6	4.1325	0.0011791	2.9285	0.0079392
PCo34:2	4.0517	0.001372	2.8626	0.0081623
PC 36:6	4.0152	0.0014694	2.8329	0.0081623
SM d18:0/20:0	-4.0012	0.0015087	2.8214	0.0081623
PC 36:5	3.9918	0.0015355	2.8138	0.0081623
PCo38:2	3.9241	0.0017447	2.7583	0.0086774
SM d16:1/18:1	3.8692	0.0019358	2.7131	0.0086774
SM d18:1/18:19Z	3.8273	0.002096	2.6786	0.0086774
PC 40:7	3.8135	0.0021515	2.6673	0.0086774
PCo44:5	3.8101	0.0021653	2.6645	0.0086774
PC 42:2	3.7803	0.0022914	2.6399	0.0086774
PCo38:5	3.7697	0.0023382	2.6311	0.0086774
SM d16:1/24:0	-3.7505	0.0024252	2.6153	0.0086774

PC 44:10	3.7138	0.0026006	2.5849	0.0086774
PC 38:9	3.6874	0.0027347	2.5631	0.0086774
PC 42:1	3.6849	0.0027478	2.561	0.0086774
PCo36:5	3.6739	0.0028062	2.5519	0.0086774
PC 42:10	3.6566	0.0029006	2.5375	0.0086774
PC 38:2	-3.6357	0.0030189	2.5202	0.0086774
PCo36:3	3.6232	0.0030914	2.5099	0.0086774
PC 44:2	3.601	0.0032259	2.4914	0.0086774
PC 38:0	3.5957	0.0032588	2.4869	0.0086774
PCo36:4	3.5636	0.0034649	2.4603	0.0086774
SM d18:0/14:0	3.5623	0.0034738	2.4592	0.0086774
SM d18:2/14:0	3.5468	0.0035781	2.4464	0.0086774
PCo38:6	3.5397	0.0036271	2.4404	0.0086774
PCo42:6	3.5276	0.0037124	2.4303	0.0086774
PCo32:3	3.5195	0.0037702	2.4236	0.0086774
PCo44:3	3.5182	0.0037795	2.4226	0.0086774
PCp40:6	3.5118	0.0038261	2.4172	0.0086774
PCo42:3	3.5064	0.0038662	2.4127	0.0086774
PCo32:0	3.4502	0.0043067	2.3659	0.009456
PC 36:7	3.3801	0.0049271	2.3074	0.010436
PC 30:2	3.3767	0.0049599	2.3045	0.010436
PCo32:2	3.3515	0.005206	2.2835	0.010731
SM d18:2/18:1	3.3227	0.0055016	2.2595	0.011113
PC 36:0 PCp38:6	-3.2293	0.006586	2.1814	0.013043
SM d18:1/26:0	3.1924	0.0070706	2.1505	0.013733
PCo40:4	3.0924	0.0085707	2.067	0.016333
PCo34:0	3.0582	0.0091546	2.0384	0.017122
PCo40:0	3.0037	0.010167	1.9928	0.01867
PC 40:8	2.968	0.010889	1.963	0.019638
PCo40:5	2.926	0.011804	1.928	0.020916
PCo40:3	2.8925	0.012589	1.9	0.021922
PC 42:5	2.8825	0.012831	1.8917	0.021965
PC 32:0	2.8009	0.015003	1.8238	0.025254
PC 40:4	2.7768	0.015713	1.8038	0.026016
PC 42:6	2.7668	0.016015	1.7955	0.026088
SM d18:0/26:0	2.7185	0.017563	1.7554	0.028156
PC 38:8	2.6808	0.018873	1.7241	0.029785
PC 36:3	2.6591	0.019667	1.7063	0.03056
SM d18:0/16:0	2.6401	0.020393	1.6905	0.031207
PC 40:6	2.6131	0.021466	1.6682	0.03236
PC 38:6	2.6045	0.02182	1.6612	0.032409
PCo36:0	2.5721	0.023202	1.6345	0.033962
PC 34:2	2.4619	0.028565	1.5442	0.041215

Table C.9 Discriminant individual lipids between grade II and grade III BAT identified by ROC curve analysis (M1 method)

Lipid	AUC	Pval	FC	clusters
PC 36:1	1	9.33E-08	-0.5923702	4
PC 34:0	1	0.00017335	-0.18422	3
SM d18:0/22:0	1	7.08E-07	-0.2847099	3
TAG58:2_FA 18:1	1	0.00020303	0.02040612	3
TAG50:3_FA 18:2	1	0.00032987	0.02387643	3
O-17-carboxyheptadecanoylcarnitine	0.98148148	0.16033204	0.37128493	4
PCo34:1	0.98148148	0.00059624	-0.1487147	3
TAG58:6_FA 18:1	0.98148148	0.00132655	0.04397609	3
TAG58:3_FA 18:1	0.98148148	0.00085992	0.04107039	3
TAG54:5_FA 18:2	0.98148148	0.00056127	0.01821155	3
PC 34:1	0.96296296	0.00117058	-0.9484361	2
PC 36:2	0.96296296	0.00016949	-0.1753969	3
PC 38:2	0.96296296	0.00015956	-0.1407551	3
PC 36:5	0.96296296	0.00072011	0.02256771	3
SM d18:1/24:115Z	0.94444444	0.00227206	-0.290211	3
PC 38:4	0.94444444	0.00227571	-0.056862	3
PC 36:0 PCp38:6	0.94444444	0.0029269	-0.0413937	3
PCo36:1	0.94444444	0.00123929	-0.0355572	3
PCo40:6	0.94444444	0.00506448	0.0403421	3
O-oleoylcarnitine, Elaidic carnitine	0.94444444	0.00378468	0.03347772	3
PCo42:6	0.94444444	0.00399128	0.02198831	3
PCo38:5	0.94444444	0.00303792	0.01711376	3
TAG58:5_FA 18:1	0.94444444	0.00442322	0.02859936	3
TAG54:2_FA 18:2	0.94444444	0.00123347	0.01751857	3
SM d16:1/24:0	0.92592593	0.0025488	-0.0773322	3
PC 36:8	0.92592593	0.0015729	-0.0318124	3
Palmitoylcarnitine, 5Z-13-carboxytridec-5-enoylcarnitine	0.92592593	0.00728981	0.04943576	3
TAG60:4_FA 18:1	0.92592593	0.00520456	0.02697514	3
PCp40:6	0.92592593	0.00144618	0.01530671	3
SM d18:0/20:0	0.90740741	0.00229641	-0.5417386	4
O-arachidonoylcarnitine	0.90740741	0.00636209	0.03626597	3
TAG56:8_FA 18:1	0.90740741	0.00256659	0.03831534	3
TAG58:1_FA 18:1	0.90740741	0.00435842	0.0338615	3
SM d18:2/24:1	0.90740741	0.00067872	-0.0246492	3
3-hydroxylinoleoylcarnitine,	0.88888889	0.02880589	0.11913938	4
TAG58:2_FA 18:2	0.88888889	0.02046628	0.02995858	3
2E-hexenedioylcarnitine, O-octanoylcarnitine	0.88888889	0.00922711	0.04267855	3

TAG56:1_FA 18:2	0.88888889	0.00795092	0.02538176	3
O-13-carboxytridecanoylcarnitine	0.88888889	0.03249303	0.02412591	3
Arachidyl carnitine, O-9Z-17-carboxyheptadec-9-enoylcarnitine	0.87037037	0.0112283	0.25139577	1
Stearoylcarnitine, hexadecanedioic acid mono-L-carnitine ester	0.87037037	0.02281827	0.14312151	4
PCo34:2	0.87037037	0.01979834	0.01208886	3
PC 38:1	0.85185185	0.01962378	-0.0349871	3
11Z-eicoseneoylcarnitine	0.85185185	0.03530399	0.03587902	3
2-ethylacryloylcarnitine, Tiglylcarnitine	0.83333333	0.05483043	0.1628239	3
SM d18:1/24:0	0.83333333	0.01167738	-0.072484	3
PC 30:2	0.83333333	0.02215631	0.01385544	3
PCo38:6	0.83333333	0.01543824	0.01179582	3
7Z,10Z,13Z,16Z-docosatetraenoylcarnitine	0.81481481	0.04970208	0.10985594	4

Table C.10 Discriminant individual lipids between grade II and grade III BAT identified by ROC curve analysis (PC method)

Lipid	**AUC**	**Pval**	**FC**	**clusters**
PC 36:1	1	1.92E-09	-1.018044	1
SM d18:0/22:0	1	8.71E-07	-0.4968263	1
PCo34:1	1	3.87E-05	-0.2142536	1
PC 36:5	1	0.00153548	0.09437974	4
PC 32:2	1	3.97E-05	0.07814507	4
PCo40:6	1	0.00117909	0.15656852	4
PC 34:6	1	0.00086518	0.08992179	4
SM d18:1/12:0	1	0.00104947	0.10950238	4
PC 44:10	1	0.00260063	0.07586034	4
PC 38:0	1	0.00325875	0.06230506	4
PCo42:3	1	0.00386617	0.07228324	4
PCo44:3	1	0.00377952	0.07154516	4
PCo34:2	1	0.00137201	0.07657632	4
PCo36:3	1	0.00309135	0.07875678	4
PCo38:2	1	0.00174473	0.08215937	4
SM d18:2/14:0	1	0.00357808	0.08445028	4
SM d16:1/18:1	1	0.00193581	0.09085165	4
PCo32:2	1	0.00520597	0.07604357	4
SM d18:2/18:1	1	0.0055016	0.07278475	4
PC 34:1	0.98148148	0.00116024	-0.7663815	2
PC 34:0	0.98148148	0.00014992	-0.2033641	1

PC 36:2	0.98148148	0.00039117	-0.2664549	1
SM d18:0/12:0	0.98148148	0.00112989	0.12334921	4
PCo38:5	0.98148148	0.00233825	0.07698982	4
PC 40:7	0.98148148	0.00215145	0.07829333	4
PC 42:10	0.98148148	0.00290056	0.07848621	4
PC 36:6	0.98148148	0.00146939	0.0737693	4
PC 42:2	0.98148148	0.00229141	0.06641848	4
PCo44:5	0.98148148	0.00216535	0.078803	4
PCo36:4	0.98148148	0.00346487	0.07278511	4
SM d18:0/20:0	0.96296296	0.0015087	-0.6230478	5
SM d16:1/24:1	0.96296296	0.00062053	0.08219016	4
PCo40:0	0.96296296	0.0101671	0.05944492	4
PCo42:6	0.96296296	0.00371236	0.08812952	4
PC 42:5	0.96296296	0.01283084	0.0935307	4
PCo38:6	0.96296296	0.00362711	0.09005429	4
PCo36:5	0.96296296	0.00280617	0.09041068	4
PC 30:2	0.96296296	0.00495991	0.08298255	4
SM d18:1/24:115Z	0.94444444	0.00028281	-0.5427728	1
SM d16:1/24:0	0.94444444	0.0024252	-0.1194502	1
SM d18:0/16:0	0.94444444	0.02039252	0.23131656	4
PCo40:5	0.94444444	0.01180401	0.10103093	4
PCo32:3	0.94444444	0.00377017	0.09590602	4
PCp40:6	0.94444444	0.00382613	0.06910364	4
PC 38:9	0.94444444	0.00273474	0.06980517	4
PC 44:2	0.94444444	0.00322589	0.07304576	4
PCo40:3	0.94444444	0.01258871	0.06373731	4
PCo34:0	0.92592593	0.00915455	0.06835228	4
SM d18:1/14:0	0.92592593	0.00103442	0.07870205	4
SM d18:0/14:0	0.92592593	0.00347385	0.07844069	4
SM d18:1/26:0	0.92592593	0.00707061	0.06405059	4
PC 42:1	0.92592593	0.0027478	0.07296382	4
SM d18:1/18:19Z	0.90740741	0.00209599	0.08407234	4
SM d18:1/24:0	0.90740741	0.00082654	-0.0884811	4
PC 40:4	0.90740741	0.01571265	0.06684785	4
PC 42:6	0.90740741	0.01601468	0.06647987	4
PC 36:7	0.90740741	0.00492709	0.0587545	4
PCo40:4	0.90740741	0.00857073	0.0944088	4
PC 40:8	0.90740741	0.01088866	0.06238907	4
SM d18:0/26:0	0.90740741	0.01756255	0.06660565	4
PC 38:6	0.88888889	0.02181963	0.09749179	4
PC 36:0 PCp38:6	0.88888889	0.006586	-0.1303805	1
PCo32:0	0.88888889	0.00430669	0.07596468	4

PC 40:1	0.88888889	0.03625944	0.04705262	4
PC 32:0	0.87037037	0.01500255	0.27580876	3
PC 38:2	0.87037037	0.00301888	-0.1887198	4
PCp42:6	0.87037037	0.04907868	0.21611401	1
PCo40:1	0.87037037	0.03798415	0.04220499	4
PC 36:3	0.85185185	0.01966718	0.07833136	4
PCo36:0	0.85185185	0.02320203	0.05247886	4
PC 40:0	0.83333333	0.04643559	0.20230737	1
PCp36:5	0.83333333	0.05603771	0.10657919	4
PC 40:6	0.83333333	0.0214664	0.05434046	4
PC 38:8	0.83333333	0.01887349	0.04843102	4
PCo38:0	0.81481481	0.07365033	0.33532636	3
PC 40:2	0.81481481	0.04390634	0.03701403	4

APPENDIX D. CHAPTER 5 SUPPLEMENTAL FIGURES

Low-grade glioma v. low-grade BAT

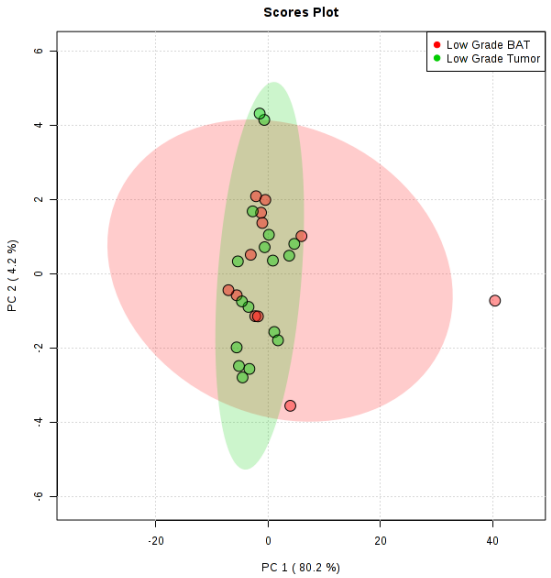

Figure D.1 Multivariate analysis identified similar lipid composition between low-grade glioma and low-grade BAT in the M2 method.

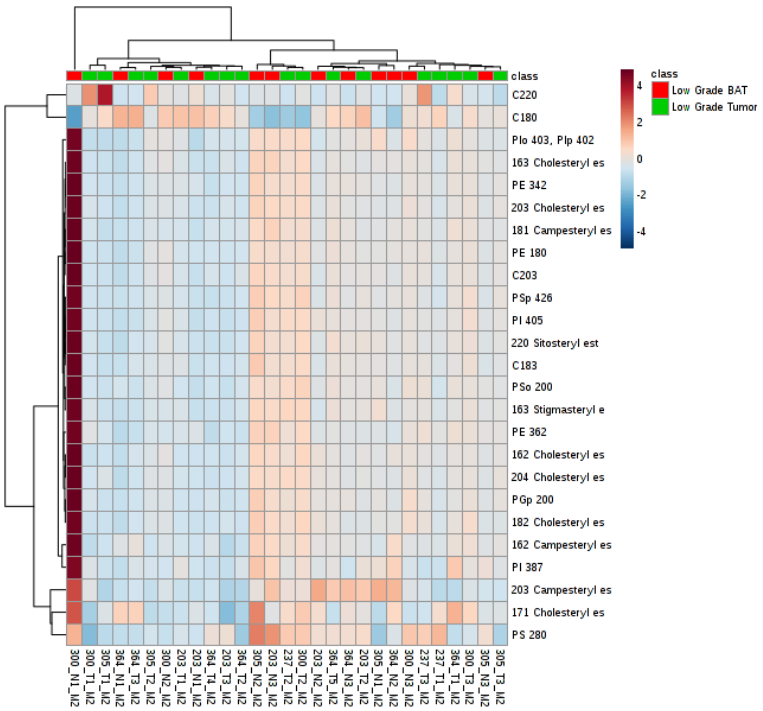

Figure D.2 Cluster analysis of top 25 lipids indicated indiscriminate separation between low-grade glioma and BAT groups in the M2 method.

High-grade glioma v. high-grade BAT

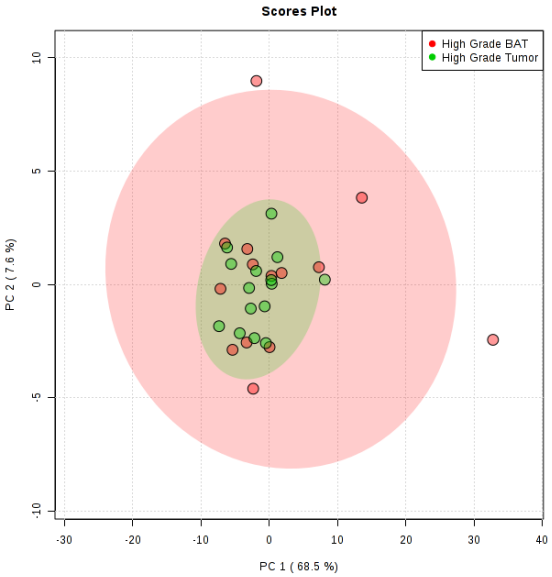

Figure D.3 M2 method PCA plot comparing high-grade glioma and BAT identified limited point separation suggesting comparable lipid composition between groups.

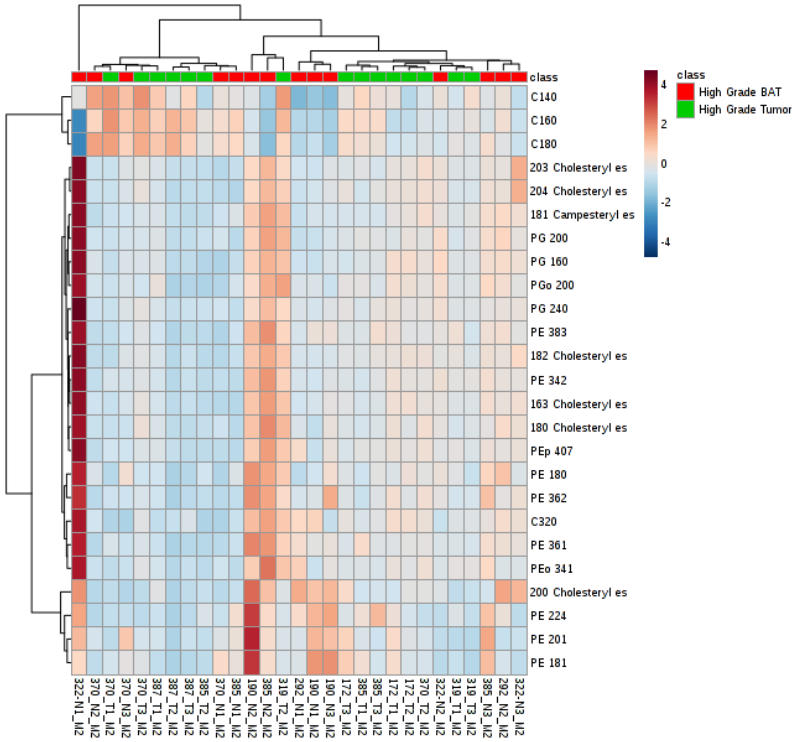

Figure D.4 M2 method heatmap of top 25 lipids displayed minimally distinct clusters between high-grade glioma and BAT groups.

Glioma v. BAT

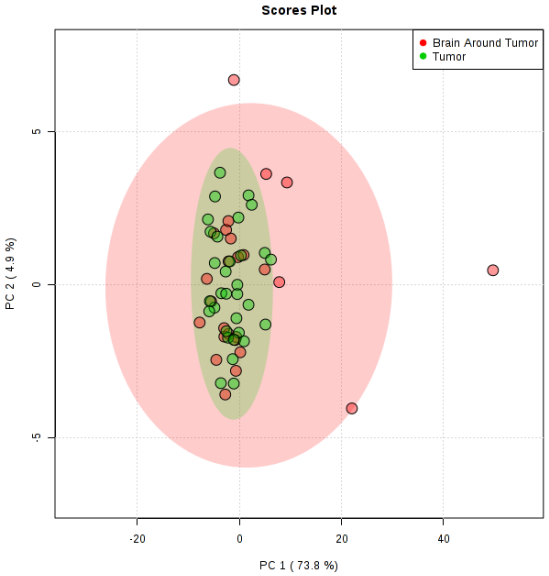

Figure D.5 PCA plot indicated highly similar lipid profiles in glioma and BAT noted by proximal clustering within the plot.

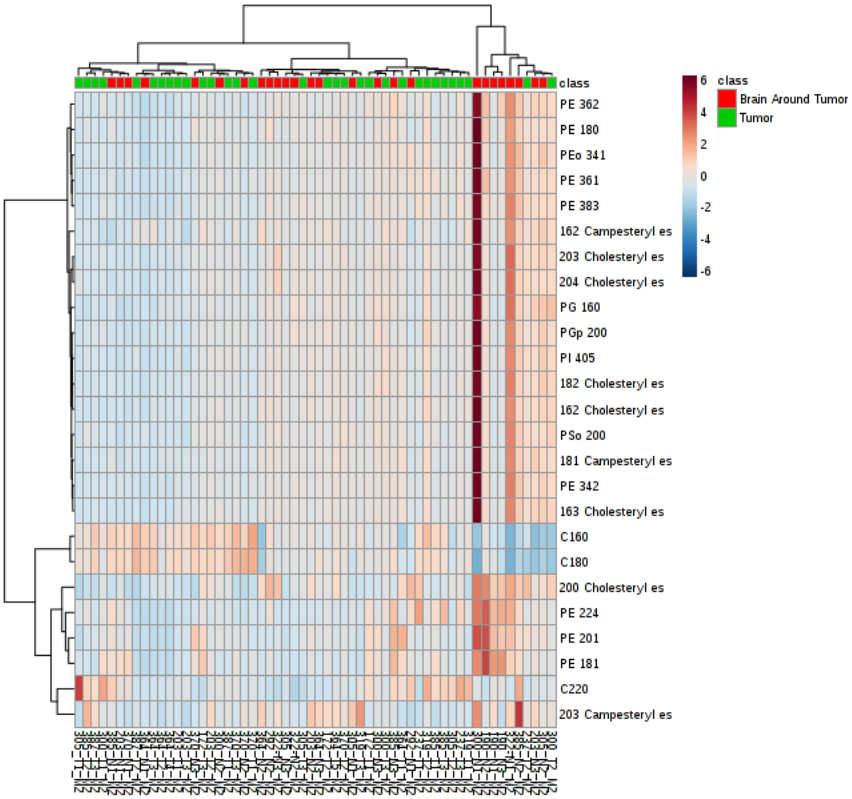

Figure D.6 Cluster analysis of top 25 lipid demonstrated glioma and BAT shared comparable relative abundances of M2 screened lipids.

VITA

Stephen Miloro graduated Summa Cum Laude from Quinnipiac University in 2013 with a B.Sc. in Behavioral Neuroscience. In 2014, Stephen worked as a lab technician at UCLA for the Brain Cancer working group where he worked under Dr. Linda Liau, Dr. Robert Prins, and Dr. Carol Kruse. During his time at UCLA, he worked collaboratively on two clinical trials using dendritic cell and allosteric cytotoxic t-lymphocytes to treat glioblastoma patients. In 2015, Stephen enrolled into the Purdue University's Interdisciplinary Life Sciences (PULSe) Ph.D. program where she worked under Dr. Jenna Rickus and Dr. Kari Clase. During his first year, Stephen earned the Lynn Fellowship geared toward students working in interdisciplinary fields. His Ph.D. project under Dr. Rickus and Dr. Clase focused on defining lipid profiles in human glioma and bran around tumor tissue using multiple reaction monitoring-based lipidomics. To perform this research, he worked collaboratively with Dr. Tiffany Lyle and Purdue Histology Research Lab, Dr. Tim Kwok and the laser capture microdissection system in the Birck Nanotechnology Center, and Dr. Christina Ferreira and the Bindley Metabolomics Profiling Facility. Stephen's primary interests include 1) integration of histology, laser capture microdissection, and MRM-profiling to investigate lipid profile differences between glioma and brain around tumor tissue, 2) investigation of glioma-grade related changes to lipid composition driving disease progression, 3) definition of lipid composition changes to brain around tumor throughout glioma progression, and 4) characterization of lipid synthesis pathways driving alterations to glioma lipid profiles. In 2018, Stephen was awarded second place at the Purdue Agricultural and Biological Engineering Department Graduate Research Symposium. In 2019, he was awarded second place at the Purdue Health and Disease Research Symposium. For his excellence in teaching, Stephen was awarded the Magoon Teaching Award for the Agricultural and Biological Engineering Department and was also the recipient of the Purdue Departmental Teaching Academy Graduate Teaching Award. He was also active in leadership roles through his Ph.D. career. Stephen was a chair for PULSe Science in Schools from 2016-19, which organized events teaching elementary school children about different areas of science. He was also an undergraduate student mentor for both the Purdue Cancer Prevention Intern and Summer Undergraduate Research Fellowship Programs, advising undergraduates to organize and carry out all stages of research projects. Stephen also helped found a student support

group and acted as a student liaison aiding fellow PULSe students during the preliminary exam period of the program.